

Distribution Agreement

In presenting this thesis or dissertation as a partial fulfillment of the requirements for an advanced degree from Emory University, I hereby grant Emory University and its agents the non-exclusive license to archive, make accessible, and display my thesis or dissertation in whole or in part in all forms of media, now or hereafter known, including display on the world wide web. I understand that I may select some access restrictions as part of the online submission of this thesis or dissertation. I retain all ownership rights to the copyright of the thesis or dissertation. I also retain the right to use in future works (such as articles or books) all or part of this thesis or dissertation.

Signature:

_____ Anna K. Kania _____

_____ 1/12/21 _____

Date

The role of H3K27me3 demethylases in B cell differentiation

By

Anna Karolina Kania
Doctor of Philosophy

Graduate Division of Biological and Biomedical Science
Genetics and Molecular Biology

Jeremy M. Boss, PhD
Advisor

William G. Kelly, PhD
Committee Member

Roger B. Deal, PhD
Committee Member

Lawrence H. Boise, PhD
Committee Member

Joshy Jacob, PhD
Committee Member

Accepted:

Kimberly Jacob Arriola, PhD, MPH
Dean of the James T. Laney School of Graduate Studies

Date

The role of H3K27me3 demethylases in B cell differentiation

By

Anna Karolina Kania

B.S., University of Mary Washington, 2015

Advisor: Jeremy M. Boss, PhD

An abstract of

A dissertation submitted to the Faculty of the

James T. Laney School of Graduate Studies of Emory University

in partial fulfillment of the requirements for the degree of

Doctor of Philosophy

in

Graduate Division of Biological and Biomedical Science

Genetics and Molecular Biology

2022

Abstract

The role of H3K27me3 demethylases in B cell differentiation

By: Anna Kania

B cell differentiation into antibody-secreting plasma cells (PC) requires substantial metabolic, transcriptional, and epigenetic reprogramming, including changes in the distribution of the histone modification H3 lysine 27 trimethylation (H3K27me3). This histone modification is associated with repressive chromatin state and gene silencing. While the role of EZH2, the H3K27me3 methyltransferase, in B cells has been well established, little is known about the role of active demethylation of this histone modification by UTX and JMJD3. Here, the role of the two H3K27me3 demethylases in B cell differentiation was investigated using chemical inhibition and genetic deletion of these enzymes. Pharmacological inhibition of these enzymes in *ex vivo* cultured B cells led to an increase in PC, which was associated with upregulation of cell cycle genes and increased proliferation. The findings were further investigated using mice with conditional deletion of *Utx* and *Jmjd3* in B cells (dKO). Similar to what has been observed with the inhibitor, loss of both enzymes led to an increase in PC following stimulation with TI antigens. This phenotype occurred in a UTX-dependent manner as UTX single knockout mice mimicked the dKO mice. Loss of *Utx* and *Jmjd3* also resulted in an increase in marginal zone B cells; however, increased differentiation was also observed in follicular B cells, suggesting a common mechanism by which H3K27me3 demethylases regulate B cell differentiation. UTX and JMJD3-deficient PC upregulated genes associated with OXPHOS and showed increased spare respiratory capacity. Furthermore, loss of *Utx* and *Jmjd3* led to vast changes in chromatin accessibility and resulted in an increase in H3K27me3 levels at pro-apoptotic genes, which corresponded to reduced apoptosis of dKO PC. Analysis of B cell responses following infection with PR8 influenza virus revealed that UTX and JMJD3 regulated germinal center (GC) response in a cell-intrinsic manner. Loss of *Utx* and *Jmjd3* led to an increase in GC B cells, which downregulated genes associated with signaling and chemotaxis. Taken together, this work identified UTX as a novel epigenetic regulator restraining B cell responses.

The role of H3K27me3 demethylases in B cell differentiation

By

Anna Karolina Kania

B.S., University of Mary Washington, 2015

Advisor: Jeremy M. Boss, PhD

A dissertation submitted to the Faculty of the
James T. Laney School of Graduate Studies of Emory University
in partial fulfillment of the requirements for the degree of
Doctor of Philosophy

in

Graduate Division of Biological and Biomedical Science

Genetics and Molecular Biology

2022

Acknowledgments

First, I would like to thank my advisor, Dr. Jerry Boss, for his rigorous training and mentorship that helped me become the scientist I am today. Second, I would like to thank Dr. Chris Scharer for his support, mentorship, and help in steering my project forward.

I would like to thank my fellow graduate students Dillon Patterson, Madeline Price, and Bob Haines for always being there for me, whether to commiserate, provide an extra pair of hands, or celebrate the rare successes and achievements. Being together in the lab not only made the time much more enjoyable but also made our science stronger. Special thanks to Dillon Patterson for his sticky notes with words of encouragement and smiley faces ☺.

I would like to thank members of the dissertation committee Drs. Bill Kelly, Roger Deal, Larry Boise, Joshy Jacob for their time and valuable suggestions on my project.

Thanks to Muyao Guo for her time in training me in the techniques and assays routinely utilized in the lab and most importantly for her support.

I would like to thank all the members of Boss lab with whom I interacted during my time at Emory: Bagde Akdogan, Ben Barwick, Lex Bally, Royce Butler, Bhanu Gandham, Lou-Ella George-Alexander, Mansi Gupta, Sakeenah Hicks, Joshua Lee, Parimal Majumder, Jeff Maurer, Tian Mi, Raven Mims, Dennis Neeld, Herbey Padilla-Quirarte, Mike Powell, Andrew Rahmberg, Jim Rose, Qing Wang, Keenan Wiggins, and Zhihong Zuo.

I would like to thank Rebecca Masel and Jennifer O'Neil for taking care of the behind-the-scenes administrative duties, such as organizing department events and processing reimbursements. Additionally, I would also like to thank Rebecca for her support, hugs, and keeping common areas neat and well-decorated.

Most importantly, I would like to thank my parents, Bozena and Artur Kania, for their unconditional love and support throughout my entire life, but especially during my time at Emory. Their love and positive energy could be felt even from several states away. I would like to thank my sister, Justyna Wilson, for her support and our weekly phone calls, which were always the highlight of my week. Thank you to my brother-in-all, Ian Wilson, for his support and his great cooking. Thank you to my niece, Jane Wilson, for being the source of great joy for the entire family.

TABLE OF CONTENTS

Chapter 1. Introduction	1
I. The role of B cells in health and disease.....	2
a. The good: immunity and vaccines.....	2
b. The bad: cancer and autoimmunity.....	3
II. B cell development and differentiation.....	4
a. B cell development.....	4
b. B cell differentiation.....	6
III. Unique biology of a plasma cell*.....	8
a. Metabolic adaptations to manufacture and secrete antibodies.....	8
b. Antibody-secreting cell survival and homing.....	10
IV. Cellular and molecular reprogramming accompanying PC formation.....	11
a. B cell differentiation is associated with extensive cell proliferation.....	12
b. Transcriptional regulation of B cell differentiation.....	13
c. Changes in chromatin accessibility accompany B cell differentiation	14
V. Epigenetic control of B cell differentiation*.....	15
a. DNA methylation.....	15
b. Enhancer of zeste homolog 2 (EZH2).....	17
c. Lysine-specific histone demethylase 1A (LSD1).....	18
d. Disruptor of telomeric silencing 1- like (DOT1L).....	19
e. 3D architecture during b cell differentiation.....	20
VI. The role of UTX and JMJD3 in health and disease.....	23
a. The biochemical function of UTX and JMJD3.....	23
b. Role of H3K27me3 demethylase in mammalian development.....	24
c. Role in the adaptive immune system.....	26
d. Role in disease	31
VII. Rational and overview.....	32
Chapter 2. Inhibition of H3K27me3 demethylase promotes plasmablast formation	33
I. Abstract	34
II. Introduction	35
III. Results	38
IV. Discussion	50
V. Supporting data	55
VI. Methods	56
Chapter 3. H3K27me3 demethylase UTX restrains plasma cell formation	60
I. Abstract	61
II. Introduction	62
III. Results	65
IV. Discussion	82
V. Supporting data	88
VI. Methods	92
Chapter 4. Work in progress: The role of UTX and JMJD3 in response to TD antigens	100

Chapter 5. Discussion.....	113
References	123

List of Figures and Tables

Chapter 1

Figure 1-1. B cell development

Figure 1-2. B cell differentiation

Figure 1-3. B cell differentiation to PC requires epigenetic reprogramming.

Figure 1-4. Active demethylation of H3K27me3 is mediated by UTX and JMJD3.

Chapter 2

Figure 2-1 - H3K27me3 demethylases are upregulated during B cell differentiation

Figure 2-2 – GSK-J4 treatment leads to an increase in the frequency of CD138+ plasmablasts.

Figure 2-3 – Inhibition of UTX and JMJD3 leads to global changes in gene expression.

Figure 2-4 – Inhibition of UTX and JMJD3 promotes cell proliferation

Figure 2-5 – DEGs are enriched for genes regulated by H3K27me3 levels.

Supplemental Figure 2-1. UTX and JMJD3 are upregulated in PC.

Supplemental Figure 2-2. Representative gating strategies.

Chapter 3

Figure 3-1. Deletion of Utx and Jmjd3 promotes PC formation.

Figure 3-2. UTX- and JMJD3-deficient MZB generate more PC

Figure 3-3. Loss of UTX alone leads to increases in PC formation.

Figure 3-4. Deletion of Utx and Jmjd3 results in upregulation of genes associated with cell growth and proliferation.

Figure 3-5. UTX- and JMJD3-deficient MZB have a proliferative advantage.

Figure 3-6. UTX- and JMJD3-deficient PC upregulate OXPHOS.

Figure 3-7. UTX and JMJD3 regulate H3K27me3 enrichment and chromatin accessibility.

Supplemental Figure 3-1. Efficient deletion of Utx and Jmjd3 by CD19^{cre}.

Supplemental Figure 3-2. Phenotypic analysis of B cell development in dKO mice.

Supplemental Figure 3-3. Magnetic enrichment and FACS sorting of B cells and PC.

Supplemental Figure 3-4. Validation of differentially expressed genes in dKO PC.

Chapter 4

Figure 4-1. Loss of Utx and Jmjd3 leads to an increase in GC B cells.

Figure 4-2. UTX and JMJD3 regulate GC B cell response in a cell-intrinsic manner.

Figure 4-3. UTX and JMJD3 regulate GC B cells transcriptome.

Figure 4-4. LLPC formation in UTX and JMJD3-deficient mice.

Figure 4-5. UTX and JMJD3 single knockout mice exhibit distinct GC phenotypes.

Chapter 5

Figure 5-1. The importance of balanced levels of H3K27me3 in B cells.

Figure 5-2. UTX and JMJD3 are negative regulators of B cell responses.

Chapter 1. Introduction

Anna K. Kania¹, Dillon G. Patterson¹, Zhihong Zuo¹, Christopher D. Scharer¹, and Jeremy M. Boss¹

¹Department of Microbiology and Immunology, Emory University School of Medicine, Atlanta, GA 30322, USA

Chapter Notes

Components of this chapter were previously published in *Immunological Reviews* and have been modified for the purposes of this chapter. These sections are indicated by an asterisk (*) after the title.

.

Originally published in *Immunological Reviews*:

Dillon G. Patterson, Anna K. Kania, Zhihong Zuo, Christopher D. Scharer, and Jeremy M. Boss. 2021. Epigenetic gene regulation of plasma cells. *Immunol Rev. Sep;303(1):8-22*.

I. The role of B cells in health and disease

The good: immunity and vaccines

B cells are part of the adaptive immune system and provide us with long-lasting immunity by differentiating into antibody-secreting plasma cells (PC) and memory B cells. In an event of reinfection with a previously encountered pathogen, the secreted antibodies promote clearance of the pathogen via multiple mechanisms: 1) direct neutralization and inactivation of viruses and toxins, 2) opsonization and activation of other immune cells, 3) antibody-dependent cellular cytotoxicity (ADCC) to promote the lysis of the pathogen by natural killer cells, and 4) activation of complement to facilitate the destruction of the pathogens via formation of membrane pores (1, 2). While antibodies provide the first wave of protection upon reinfection, their levels are not always sufficient to clear the pathogen. When that is the case, memory B cells can rapidly respond to previously encountered antigens by rapidly differentiating into a new wave of antibody-secreting PC to control the infection (3, 4).

This ability of our immune system to “remember” and rapidly clear previously encountered antigens serves as the basis for vaccine development (5, 6). Furthermore, the levels of antigen-specific antibody titers induced by vaccines are typically used as a correlate of protection during the development of new vaccines and clinical trials, thus illustrating the clear correlation between antibody and immune protection (6). In fact, the protective antibody titers against mumps and measles have estimated half-lives of over 200 years, thus providing life-long protection against reinfection (5). However, in other cases, boosters of the vaccine, which rely on the activation of memory B cells, are necessary to maintain immunity (6). Taken together, PC and memory B cells provide us with long-lasting immunity against pathogens.

The bad: cancer and autoimmunity

While B cell differentiation is meant to provide protection against pathogens, when dysregulated, it can also lead to the development of B cell malignancies and autoimmunity. As described in more detail below, the generation of high-affinity antibodies involves iterative rounds of somatic hypermutation of B cell receptor (BCR) followed by affinity selection (7, 8). However, this process can also lead to chromosomal translocations and mutations in non-immunoglobulin genes and ultimately result in the development of B-cell lymphomas (9). Furthermore, while PC are non-proliferating, the genomic alterations acquired during the GC response combined with additional mutations can promote PC proliferation and expansion resulting in the development of multiple myeloma (10).

The ability of B cells to respond to a wide range of pathogens is driven by a diverse repertoire of the BCR. The theoretical number of potential BCR sequences is estimated to be 10^{18} thanks to a process referred to as somatic rearrangement (11). While most B cells recognizing self-antigens are eliminated during B cell development, in certain cases the cells persist and differentiate into PC leading to the production of autoantibodies that either directly bind to self-antigen or activate the complement cascade (12). Regardless of the nature and localization of the target antigen, autoimmune diseases are characterized by sustained inflammation, which is the major focus of current therapeutic interventions (13). One of the autoimmune diseases with a strong B cell component is systemic lupus erythematosus (SLE). This disease is characterized by an expansion of the naïve B cells with an activated phenotype referred to as DN2 (IgD⁻CD27⁻CXCR5⁻CD11c⁺), which are primed to differentiate into PC (14). A better understanding of B cells responses during healthy states will likely aim in the development of novel treatment options aimed at augmenting pathogenic B cell responses.

II. B cell development and differentiation

B cell development

The process of B cell development begins in the bone marrow (BM) with hematopoietic stem cells (HSC) differentiation into multipotent progenitor cells, which in turn differentiate in the common lymphoid progenitors (CLP) (15). The transition from CLP to pro-B cells requires the induction and activity of transcription factors such as EBF, E2A, and PAX5, which promote the expression of the B cell transcriptome. Loss of *Pax5* results in a developmental block at the pro-B cell stage and reverts the cells back to their multipotent stage (16). Furthermore, under proper stimulation conditions, PAX-deficient cells can differentiate into one of the other hematopoietic lineages, thus illustrating the essential role of PAX5 in the commitment to the B cell fate (17). The following stages of B cell development are accompanied by a stepwise rearrangement of the variable (V), diversity (D), and junction (J) regions of the immunoglobulin (Ig) genes to generate a functional BCR (18, 19). Successful rearrangement to the V, D, and J segments of the heavy chain (IgH) occurs at the pro-B cell stage and allows the cells to transition into the large pre-B stage of B cell development (**Figure 1-1**). At this stage, the rearranged IgH containing the μ constant regions joins a surrogate light chain and is displayed at the cell membrane to test the function of the IgH (20). Signaling through the pre-BCR prevents the arrangement of the second IgH and promotes B cell proliferation and initiation of the next stage of B cell development, small pre-B cell (21, 22). At this stage, the V and J regions of the light chain (IgL) are rearranged and then join the IgH to form the final IgM BCR thus initiating the immature B cell stage of B cell development (19, 23).

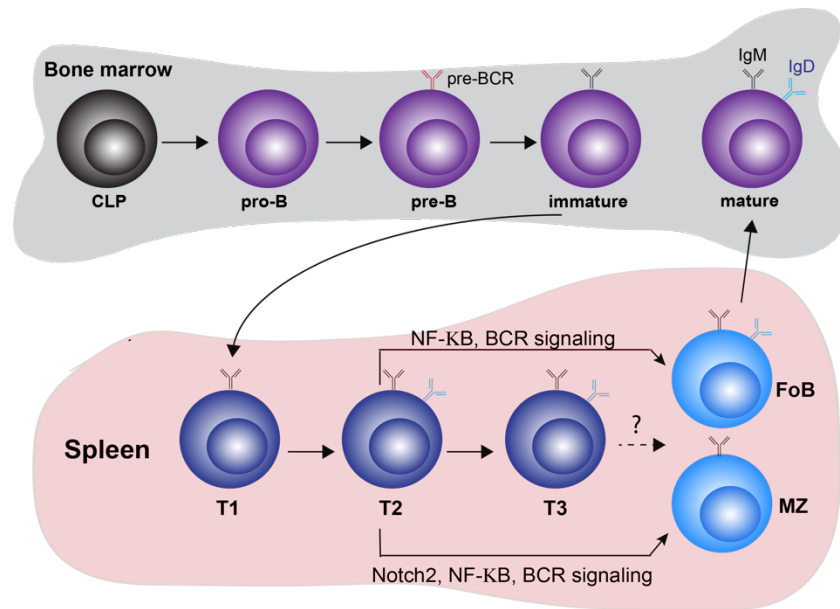


Figure 1-1. **B cell development.** B cell formation begins in the bone marrow with differentiation of the common lymphoid progenitor into pro-B cells. These cells continue their development process in the bone marrow through the immature B cell stage and then migrate to the spleen, where they mature into marginal zone B cells or follicular B cells.

The newly formed immature B cells upregulate sphingosine-1-phosphate receptor 1 (S1PR1), which allows them to respond to the sphingosine-1-phosphate (S1P) gradient in the blood and migrate to the spleen to finish their maturation process (24, 25). B cells that arrive in the spleen are referred to as transitional 1 (T1) B cells (26, 27). Once the cells acquire the expression of CD23 and IgD, they enter the T2 stage of B cell development (28). At this point, the cells mature either into T3 B cells, marginal zone B cells (MZB), or follicular B cells (FOB) depending on external stimuli received (26, 27). The T3 B cell pool predominantly consists of anergic and self-reactive B cells that are unlikely to give rise to mature B cells (28, 29). Weak BCR signaling and engagement of the NOTCH2-ligand Delta-like 1 (DL1) drive T2 B cell maturation into MZB (30, 31); whereas, strong BCR signaling and lack of NOTCH2 signaling promotes the FOB fate. Survival and maturation of both cell types is mediated by NF-κB signaling downstream of BAFFR (26, 27). Mature MZB reside in the marginal zone of the spleen between the red pulp and marginal

sinus (32); whereas, FOB occupy B cell follicles or recirculate via blood and lymph to other lymphoid organs such as lymph nodes (LN) and BM (26, 27).

B cell differentiation

B cell differentiation into PC is the cornerstone of humoral immunity and relies on the ability of B cells to respond to a wide range of antigens (**Figure 1-2**) (33, 34). In this dissertation, B cell differentiation and PC formation will be used interchangeably unless stated otherwise. Stimulation with T-cell independent (TI) antigens, such as lipids and polysaccharides, leads to the formation of short-lived PC (SLPC). Type I TI antigens activate a polyclonal pool of B cells by stimulation of Toll-like receptors (TLR), which are pattern recognition receptors that recognize conserved characteristics of pathogens. These responses are predominately driven by MZB, which rapidly respond to blood-borne pathogens such as lipopolysaccharides (LPS) (35, 36). Type II TI antigens contain highly repetitive structures that activate the cells by crosslinking BCR and as such result in antigen-specific responses (37).

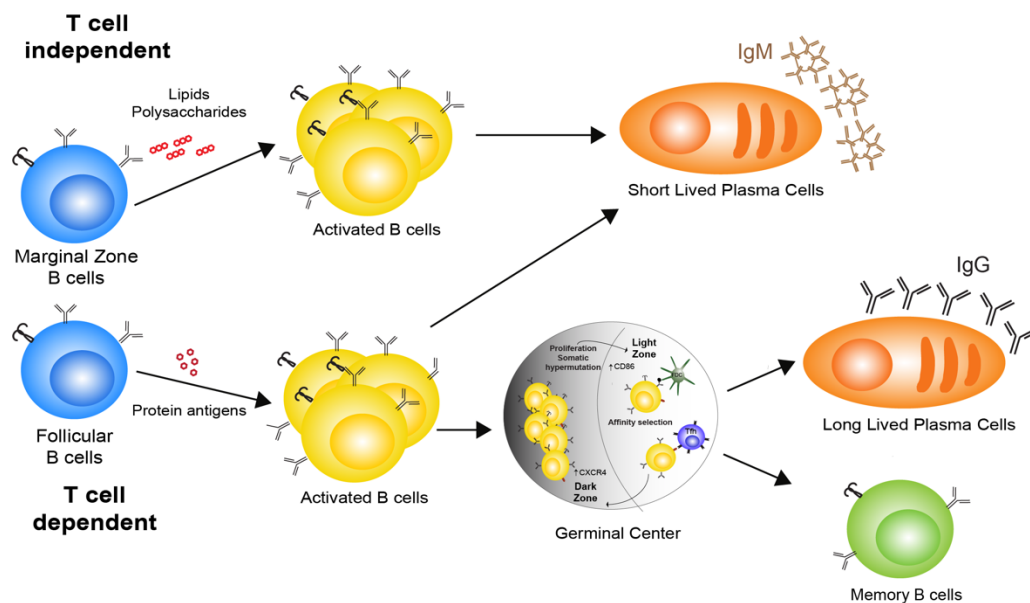


Figure 1-2. **B cell differentiation.** The response to T-cell independent antigens is predominately driven by marginal zone B cells and leads to the generation of short-lived plasma cells (PC). Protein antigens induce a T-cell dependent B cell differentiation with ultimately leads to the formation of long-lived PC and memory B cells.

Protein antigens induce a T-cell dependent (TD) B cell response, which is driven mostly by FOB as B cell follicles are located in close special proximity to the T cell zone within secondary lymphoid tissues (**Figure 1-2**) (7, 38). Following BCR-mediated activation, FOB migrate to the border of the B and T cell zones to present the antigen to CD4 T cells and to receive costimulatory signals. These activated B cells either differentiate into short-lived extrafollicular PC or early memory B cells, or migrate to the germinal centers (GC) (39, 40). Germinal centers are anatomical structures divided into the light zone (LZ) and the dark zone (DZ) where B cells undergo affinity maturation of their BCR (8). Responding B cells enter the DZ where they rapidly proliferate and mutate the immunoglobulin genes in a process referred to as somatic hypermutation. Following several rounds of cell division, B cells enter the LZ, where they compete for binding to the antigen displayed by follicular dendritic cells (FDC) (7). Following antigen engagement and internalization, B cells present the antigen to CD4 follicular helper cells and receive costimulatory signals (41). BCR affinity correlates with the ability of the B cell to bind to the antigen and strength of the co-stimulatory signals received from T cells. As a result, high-affinity B cells are selected to return to the DZ to undergo another round of rapid proliferation and somatic hypermutation (8, 42, 43). Classically, class-switch recombination (CSR) was thought to also occur in the DZ; however, a recent study demonstrated that this process occurs prior to GC formation, thus allowing for a more diverse response of early PC and memory B cells (44). This iterative process of somatic hypermutation and affinity selection ultimately leads to the formation of long-lived PC (LLPC) and memory B cells, which together provide long-lasting protection against future infections (45).

Taken together, stimulation with either TI- and TD-antigens ultimately leads to the formation of antibody-secreting PC. While SLPC and LLPC differ in their longevity, localization, and affinity, they share a unique transcriptional signature suggesting that the reprogramming required to become a PC is likely similar (46). Furthermore, both PC populations play an important role in the overall immune response. While LLPC provide long-lasting immunity, SLPC contribute to the early protection from pathogens (47).

III. Unique biology of a plasma cell*

Metabolic adaptations to manufacture and secrete antibodies

The primary function of PC is the manufacturing and secretion of antibodies. Remarkably, PC are capable of secreting up to 10,000 antibodies per second (48). To support the high rate of antibody secretion, nB undergo significant morphological and bioenergetic changes as they differentiate from a quiescent B cell that does not secrete antibody to antibody-secreting PC (49). This change in metabolism is essential to meet the energy demands required for the rapid proliferation of responding B cells and the translational requirements of PC (50, 51). Responding activated B cells (actB) utilize both glycolysis and oxidative phosphorylation (OXPHOS), whereas GC B cells also utilize fatty acid oxidation (52, 53). As actB divide and differentiate towards PC, they gradually increase their capacity to perform OXPHOS (52). This shift towards OXPHOS is in part due to an increase in the transcription of more than 100 components of the electron transport chain, tricarboxylic acid cycle (52), as well as Protein Kinase C β (PKC- β), which is induced in actB following antigen stimulation (54, 55). PKC- β was shown to promote mTORC1 signaling to facilitate mitochondrial remodeling and heme biosynthesis, which is necessary for PC formation. While PKC- β -deficient cells accumulated reactive oxygen species and failed to differentiate, these

phenotypic changes were reversed by treatment with hemin suggesting a mechanistic link between PKC- β and heme biosynthesis (56). PC primarily rely on OXPHOS to support antibody secretion, and this metabolic switch is dependent on BLIMP1, one of the master transcriptional regulators of PC fate (52). Experimentally, promoting OXPHOS metabolism in responding B cells using dichloroacetate (57-59) results in increased PC formation, suggesting a role for OXPHOS in promoting differentiation (52). However, within the PC lineage there appear to be differences in oxygen consumption. While SLPC consume oxygen nearly at their maximal possible levels, bone marrow LLPC exhibit high spare respiratory capacity (60).

Another difference specific to LLPC is the high surface level expression of the glucose transporter GLUT1 (60). Interestingly, despite PC reliance on glucose to support their metabolic demands, genetic deletion of GLUT-1 does not completely block PC formation, indicating that glucose uptake depends on additional transporters or pathways (61, 62). Furthermore, differences in glucose uptake and subsequent pyruvate import into the mitochondria have been attributed to differences in the longevity of SLPC versus LLPC, thus pointing to cross-talk between metabolism and cell survival (60). Therefore, while LLPC use glucose for various processes, OXPHOS is still an important source of energy. Additionally, the unique metabolic features of LLPC might also serve as physiological adaptations to the hypoxic BM environment (63). Taken together, these studies highlight the unique bioenergetic adaptations of PC metabolism and how distinct modes may be utilized to promote differentiation and support the demands of antibody generation.

The high rate of antibody production also requires substantial adaptations of the secretory apparatus and unfolded protein response (UPR), which is normally induced during stress and initiated by the accumulation of misfolded proteins in the endoplasmic reticulum (ER) (64). The response initiated by inositol-requiring enzyme 1 α (IRE1 α) is best understood in PC. IRE1 α is a

ribonuclease and splicing factor that promotes the splicing of X-box protein 1 (XBP1) mRNA to a more stable *Xbp1* isoform (65). Once generated, XBP1 promotes the expression of genes necessary for the expansion of the secretory apparatus (66, 67). The importance of XBP1 is highlighted by *in vivo* studies, where deletion of *Xbp1* impeded the ability of PC to secrete antibodies. XBP1-deficient PC exhibited normal protein folding but altered glycosylation and lipid synthesis, leading to the failure to mount a proper UPR (68). These findings indicate that XBP1 is not required for PC formation but rather for antibody secretion (67, 69). While XBP1 is typically thought of as the master transcription factor regulating the UPR response initiated due to the high antibody secretion, a recent study demonstrated that actB upregulate UPR-related genes prior to becoming a PC (70). Upregulation of the actB UPR program was regulated by mTORC1 signaling and the adaptor protein Raptor and occurred prior to XBP1 activity (70). This important finding indicates that part of the actB program is to prepare for subsequent antibody synthesis by initiating and building the transcriptional networks to deal with the stress of protein production and secretion.

Antibody-secreting cell survival and homing

PC are able to survive in multiple niches in mammals. Both SLPC and LLPC can reside in secondary lymphoid organs, such as the spleen and BM (71, 72), and in tissues such as the gut (72-74). Since PC are generated in secondary lymphoid organs, migration of PC to their survival niche is facilitated by the expression of chemokine receptors. This process is initiated by upregulation of S1PR1, which allows for entry into the bloodstream (7), followed by expression of specific chemokine receptors that direct PC to their niche. Expression of CXCR4 promotes homing to the BM (75). Blocking the CXCR4-CXCL12 axis diminished PC homing to and retention in the BM

(76), resulting in obvious accumulation of PC in the spleen and a concordant decrease in BM (77). CXCR3 promotes homing to inflamed tissues (78), while CCR10 and CCR9 promote the migration of IgA⁺ PC to the gut, with CCR9 being restricted to the small intestine (79).

Lasting humoral immunity relies on the long-term survival of PC. However, not all PC are created equally. TI responses predominantly generate SLPC that die within a few days. On the other hand, PC formed following stimulation with TD antigens are able to home to the BM and persist for decades (5, 7, 80). Thus, understanding the factors regulating PC survival is crucial to the improvement and development of successful vaccines. The BM is the primary niche of LLPC owing in part to the presence bone marrow stromal cells and cytokines, such as APRIL and BAFF, which promote the expression of the anti-apoptotic gene *Mcl1* and thus promoting PC survival (81, 82). A recent study identified two novel factors, fibronectin and YWHAZ, secreted by stromal cells to promote survival of human LLPC *in vitro* (83). Treatment with antibodies targeting these proteins reduced PC survival in the culture. Furthermore, the combination of mesenchymal stromal cells secretome (including fibronectin and YWHAZ), APRIL, and hypoxic conditions improved the long-term survival of LLPC *in vitro* and likely *in vivo* (83). However, even within the BM, there is heterogeneity in the lifespan of PC, suggesting that other factors, including cell-intrinsic differences, are at play.

IV. Cellular and molecular reprogramming accompanying PC formation

B cell differentiation is associated with extensive cell proliferation

Early work demonstrated that treatment of peripheral blood mononuclear cells with a cell cycle inhibitor impeded PC formation, suggesting that cell division is required for B cell differentiation (84). The development of carboxyfluorescein succinimidyl ester (CFSE) (85) and CellTraceViolet

(CTV) (86) dyes allowed for an extensive analysis of the relationship between cell division and B cell differentiation. Evaluating B cell proliferation and PC formation revealed a strong correlation between the strength of stimuli, cell division, and B cell differentiation *ex vivo* (87-90). The relationship between cell division and PC formation *in vivo* was examined using an adoptive transfer model. In this system, CTV-labelled naïve B cells (nB) were transferred into B-cell deficient μ MT (91) host mice followed by stimulation with LPS (92). This approach revealed that 8 or more cell divisions were required for PC formation (92, 93). Importantly, this observation held true following stimulation with NP-Nicoll or influenza virus or an adoptive transfer into MYD88-deficient (94) hosts, suggesting a cell-intrinsic requirement of 8 or more cell divisions for PC formation (93, 95). However, following an adoptive transfer into wild-type host, PC were observed as early as division 5, suggesting that cell-extrinsic factors can alter the kinetics of B cell differentiation (93).

Interestingly, a recent study demonstrated that cell division is not required for all differentiating B cells. Stimulation of CTV-labelled MZB and FOB *ex vivo* with CpG (TLR9 agonist), IL-4, and IL-5 revealed that the former were able to differentiate into PC without undergoing any cells divisions. In fact, MZB generated PC even after treatment with cell cycle inhibitors (96). Further experiments illustrated that this unique ability of MZB to rapidly differentiate was driven by NOTCH2 signaling, which promoted the expression of *Myc* and its targets as well as genes associated with the mammalian target of rapamycin complex 1 (mTORC1) (96). Together, the data suggest that the relationship between cell division and PC formation is more complex than previously thought.

Transcriptional regulation of B cell differentiation

The nB and PC fates are regulated by distinct sets of mutually antagonist transcription factors (TF); therefore, B cell differentiation into PC requires substantial transcriptional reprogramming. As mentioned above, PAX5 plays a crucial role in the commitment to the B cell lineage. In addition, PAX5 is also necessary for the maintenance of the nB fate by promoting the expression of many other transcription factors associated with nB such as *Bach2*, *Spib*, *Irf8*, and repression of *Prdm1* (BLIMP1), the PC master regulator (97-100). Interestingly, a recent study suggests that downregulation of *Pax5* might not be necessary for PC formation as an enforced expression of *Pax5* did not impede PC formation (101). BACH2 also inhibits the PC fate by directly repressing the expression of *Prdm1* resulting in increased B cell differentiation following loss of *Bach2* (102-104). SPIB and PU.1 (encoded by *Spi1*) are two closely related ETS family TF that regulate gene expression either by directly binding to DNA or by heterodimerizing with IRF family members, IRF4 or IRF8 (105). The high homology between SPIB and PU.1 is illustrated by a redundant function of these TF during B cell development and GC formation (106, 107). Furthermore, loss of *Spib* and *Spi1* resulted in an increase in PC following *in vitro* stimulation despite reduced expression of the genes involved in BCR and TLR signaling (107). Additionally, PU.1 and IRF8 negatively regulate B cell differentiation by directly binding to and promoting the expression of *Pax5* and *Bcl6*, both of which are repressors of *Prdm1* (108-110).

The transition to the PC fate is initiated by the progressive upregulation of *Irf4* following B cell activation, which at high concentrations promotes the expression of *Prdm1* (111, 112). Once expressed, BLIMP1 represses the expression of the *Pax5*, *Spib*, and *Id3* thus leading to extinguishing of the nB transcription program (110, 113). In addition, BLIMP1 promotes the expression of genes involved in the unfolded protein response, including *Xbp1* and *Atf6*, necessary

to promote antibody secretion (114, 115). Intriguingly, despite the essential role of BLIMP1 in PC formation, this TF is dispensable for the survival of mature PC (114), suggesting BLIMP1 is only required for the initiation of the PC transcriptional program.

Changes in chromatin accessibility accompany B cell differentiation

The activity of a TF relies on its ability to bind to its DNA motif, thus requiring that the chromatin is open and accessible (116). As a result, chromatin accessibility can be used to identify regulatory elements and TF networks that function within a given cell type to regulate gene expression. In fact, this approach has proven to provide novel insights into the regulation of B cell differentiation (117). Assessment of chromatin accessibility in differentiating B cells at distinct cell divisions using the adoptive transfer approach described above revealed a hierarchy of TF that regulate B cell differentiation. Regions with increased accessibility were enriched for NF- κ B family TF and AP1:IRF (AICE) motifs in dividing B cell followed by strong enriched for IRF4, IRF:IRF homodimers (ISRE), and E2A motifs at regions that become accessible in CD138⁺ PC (117). This study also revealed the presence of primed promoters that were accessible in undivided B cells and were not expressed until the PC stage, suggesting that other factors must be regulating the activity of these genes. In fact, a subset of those genes was enriched for the repressive histone modification H3K27me3 in nB (117). The presence of primed chromatin regions is not unique to nB as it has also been observed in memory T cells and memory B cells (118, 119). Taken together, while chromatin accessibility is a useful tool for identifying regulatory regions, it does not always correlate with gene expression as transcription is also be influenced by various epigenetic mechanisms.

V. Epigenetic control of B cell differentiation*

As described above, the transcription factor networks regulating plasma cell fate have been well established. In addition, there is also a growing body of evidence suggesting the crucial role of epigenetics in fine-tuning the magnitude of the immune response (120, 121). Epigenetics is the study of heritable mechanisms that alter gene expression without changes in the DNA sequence. Although multiple epigenetic modifications exist (116, 122), here we will discuss the consequences of deletion of some epigenetic modifiers that control DNA methylation and histone modifications (**Figure 1-3**).

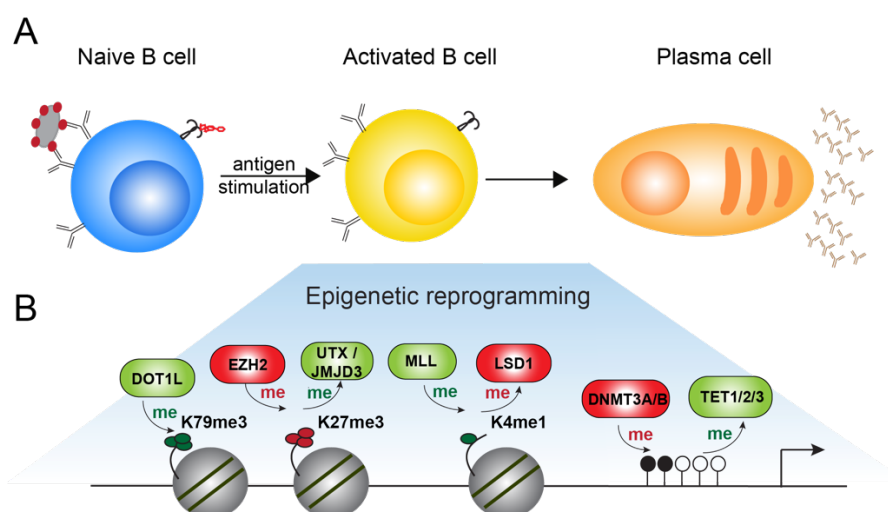


Figure 1-3. B cell differentiation to PC requires epigenetic reprogramming. (A) Following stimulation with T-cell independent or T-cell dependent antigens, naïve B cells become activated and differentiate into plasma cells. (B) The process of naïve B cell reprogramming requires substantial changes to the epigenome. Enzymes that catalyze the addition or removal of DNA methylation and various histone modifications are depicted in the shaded box. Enzymes that promote gene expression are colored in green, while enzymes promoting gene repression are colored in red.

DNA methylation

The methylation of cytosine at CpG dinucleotides is a central epigenetic modification that controls gene expression by recruiting proteins involved in gene repression or by inhibiting the binding of TF to DNA (123). DNA methylation localized to promoters or enhancers results in gene

repression. Alternatively, methylation across the gene body coupled with loss of methylation at promoters or enhancers supports gene expression (124). DNA methylation is mediated by one of three DNA methyltransferases (DNMT). DNMT3A and DNMT3B promote *de novo* DNA methylation (125), while DNMT1 maintains DNA methylation during cell division (126). Loss of DNA methylation can occur either via passive loss of methylation during cell division or an active process mediated by Ten-eleven translocation methylcytosine dioxygenases (TET1, TET2, TET3). TET enzymes promote DNA demethylation in a step wise manner by conversion of mCpG into 5-hydroxymethylcytosine (5hmC), 5-formylcytosine (5fC) and 5-carboxylcytosine (5caC), which leads to DNA repair and unmethylated DNA (127).

B cell differentiation is associated with a progressive loss of DNA methylation with only a small number of loci gaining *de novo* DNA methylation at the PC stage (92, 128). DNA demethylation occurs predominately at enhancers and corresponded to the changes in transcription factor binding and gene expression at each cell division. Importantly, the loss of DNA methylation occurred at many genes known to play a crucial role in PC formation such as *Prdm1*, *Irf4*, *Xbp1* (92), suggesting that a targeted demethylation is critical during B cell differentiation.

Examination of (5hmC), an intermediate step during active demethylation, suggests that active demethylation contributes to PC formation (128). Indeed, deletion of the genes encoding TET2 or TET2 and TET3 in HSC or class-switched B cells led to a reduction in PC and antibody titers with a corresponding expansion of GC B cells due to a failure to induce the transcriptional program necessary for GC exit (129, 130). While deletion of *Tet2* and *Tet3* using inducible Cre-ER^{T2} followed by *ex vivo* stimulation did not alter the frequency of PC generated, there was a significant defect in class switch recombination due to a failure to demethylate the *Aicda* (AID) locus (131). Furthermore, inhibition of DNA methylation (92) or enhancement of TET enzymes

via ascorbic acid (vitamin C) (132) led to an increase in PC, thus providing functional evidence for the essential role of DNA demethylation in PC formation.

Despite the fact that *de novo* DNA methylation occurs only at a small number of loci, those changes are necessary for restraining the commitment to the PC fate. B cell conditional deletion of *Dnmt3a* and *Dnmt3b* led to an increase in GC B cells and PC, which exhibited an aberrant transcriptional profile. DNMT3A/B-deficient PC upregulated genes associated with lysosome function, transcription, as well as various metabolic pathways (133). However, despite the well-established role of DNA methylation in PC formation, it is yet to be determined how these enzymes are recruited to the specific loci. Additionally, more work is needed to uncouple passive and active demethylation events and determine the timing in which these processes occur.

Enhancer of zeste homolog 2 (EZH2)

Enhancer of zeste homolog 2 (EZH2) is the catalytic component of the Polycomb Complex 2 that mediates histone 3 lysine 27 trimethylation (H3K27me₃), which is associated with gene silencing (134-136). Mutations in *EZH2* are frequently found in diffuse large B-cell lymphoma and follicular lymphoma, which led to a great interest in understanding its role in B cells. In fact, EZH2 was shown to function at multiple stages of B cell development and differentiation (137-139). EZH2 is necessary for GC formation and was shown to cooperate with BCL6 and the CBX8-BCOR complex to repress genes associated with PC fate and cell cycle inhibitors, such as *Cdkn1a*, to allow for the rapid proliferation of GC B cells (137). Furthermore, gain of function EZH2 mutant proteins contribute to follicular lymphoma by allowing the mutant B cells to persist and expand in the light zone of the GC in a manner independent of T cell help (140). In addition, EZH2 has been shown to directly interact with BLIMP1 to mediate gene repression (115). Consistent with these findings, deletion of *Ezh2* led to an upregulation of BLIMP1 target genes and failure to repress the

B cell transcriptome. Phenotypically, EZH2-deficiency led to a decrease in PC formation *in vivo*, and a profound proliferation defect, with EZH2-deficient B cells accumulating in cell divisions 3-5 (141). Furthermore, deletion of *Ezh2* led to a failure to upregulate genes associated with the UPR, glycolysis, and OXPHOS, which correlated with reduced ability of the cells to secrete antibodies and perform glycolysis, as well as lower basal respiration rate. Thus, EZH2-dependent gene repression is necessary to repress the B cell program and initiate metabolic and secretory reprogramming during PC formation.

Lysine-specific histone demethylase 1A (LSD1)

Histone H3K4 methylation is associated with gene expression, with monomethylation (H3K4me1) associated with enhancers, dimethylation (H3K4me2) with enhancers and gene bodies, and trimethylation (H3K4me3) with RNA polymerase engaged promoters (142). Demethylation of H3K4me1/2 (as well as H3K9me1/2) is mediated by the monoamine oxidase lysine-specific histone demethylase 1A (LSD1) (143, 144), which has been shown to physically interact with BLIMP1 (145) and regulate PC formation (146). Deletion of *Lsd1* led to a failure to decommission nB enhancers, resulting in reduced differentiation of LSD1-deficient B cells into PC. Furthermore, LSD1-deficiency led to downregulation of genes associated with cell cycle and proliferation, including E2F and MYC target genes, which corresponded with impaired proliferation (146). In the context of the GC, LSD1 was shown to physically interact with BCL6 to repress enhancers of BCL6 target genes, including nB enhancers that are normally either lost or poised in GC B cells (143). Interestingly, the function of LSD1 in the GC was independent of its catalytic activity as pharmacological inhibition of the catalytic domain did not impede GC formation seen in the genetic knockout (143). In fact, the Tower domain of LSD1, which interacts with the corepressor complex CoREST, was necessary for the survival of lymphoma cell lines (143). While deletion of

Lsd1 led to a reduction in GC B cells, the opposite was true for the H3K4 methyltransferase KMT2D (147). The increase in GC B cells was attributed to increased proliferation of KMT2D-deficient follicular B cells, as the phenotype was not observed when *Kmt2d* was conditionally deleted in GC B cells (147). The role of H3K4 methyltransferases in PC formation remains to be elucidated. However, evaluating the role of the specific H3K4 methyltransferases is complicated by the existence of four partially redundant H3K4 methyltransferases (142).

Conditional deletion of *Lsd1* during B cell development resulted in a significant decrease in MZB but not FOB (148). Loss of MZB was due to the reprogramming of cells towards the FoB compartment, as the top 200 FoB genes were upregulated in LSD1-deficient MZB. Moreover, chromatin accessibility data indicated that NF- κ B-like motifs were affected. Further analyses showed that the non-canonical NF- κ B family member p52 interacted with LSD1. As a result, LSD1 activity through the BAFF signaling pathways during transitional B cell development to MZB, was diminished in LSD1-deficient cells (148).

Disruptor of telomeric silencing 1-like (DOT1L)

Disruptor of telomeric silencing 1-like (DOT1L) facilitates methylation of H3K79, which is associated with gene expression and has been of interest in B cells due to its role in leukemias characterized by translocation of the mixed lineage leukemia (*MLL*; also known as *KMT2A*) gene. In the tumor setting, *MLL* frequently forms fusion complexes with DOT1L-interacting proteins such as AF10, AF4, and ENL. As a result, DOT1L is recruited by *MLL* fusion complexes to promote malignant gene expression and therefore is a target for drug development (149). In the context of B cell differentiation, DOT1L deficiency impaired GC and PC formation in response to TI and TD antigens *in vivo* (149-151). The failure to mount a robust response following stimulation

in vivo was attributed to a failure of DOT1L-deficient B cells to upregulate genes associated with cell movement and migration, resulting in aberrant cell localization within secondary lymphoid organs (151). Interestingly, differentiation of DOT1L-deficient B cells or inhibition of DOT1L *ex vivo* resulted in an increase in PC. However, while DOT1L-deficient B cells expressed key PC genes (CD138 and BLIMP1), these *ex vivo* generated PC failed to fully downregulate B220 or CD19 suggesting incomplete differentiation. Additionally, *ex vivo* cultured DOT1L-deficient B cells failed to upregulate the expression of *Bach2*, *Myc*, MYC-target genes, and *Ezh2*. Consistent with downregulation of *Ezh2*, DOT1L-deficient B cell upregulated EZH2-target genes, including *Cdkn1a*, suggesting a mechanistic link between the two epigenetic enzymes (150).

3D architecture during B cell differentiation

In addition to changes in transcription factor networks, DNA methylation, and histone modifications, B cell differentiation is also associated with substantial 3D reorganization of the genome (152). The advent of chromatin conformation capture techniques allowed for a closer examination of DNA architecture, which coupled with whole genome sequencing (Hi-C), revealed the presence of topologically associated domains (TAD). TAD are regions of the genome that tend to frequently interact with each other compared with regions outside of TAD (153, 154). Although this field is young and rapidly progressing, there have been important observations regarding the stage-specific reorganization of the 3D genome and the key enhancer-promoter interactions that mediate B cell differentiation and function.

A comparison of the genomic profiles of nB, actB, or PC revealed substantial differences in their genomic architecture. B cell differentiation leads to a significant increase in the number of DNA loops and a shift from long-range to mostly short-range interactions (155, 156). These changes are also associated with alterations in the epigenetic landscape, such as gains in the active

histone modification H3K27ac at regions surrounding key genes critical for PC, including *Prdm1*, *Atf4*, *Ell2* (156). Fine scale mapping of chromatin architecture changes by time and cell division *ex vivo* revealed that the first wave of chromatin reorganization occurred just prior to the first cell division (152), a process that is likely driven by MYC (155). Genome organization remained largely unchanged in dividing actB until PC formation, at which a second wave of changes was observed (152). The essential role of rewiring the 3D architecture and DNA loop formation was further exemplified by studies investigating the role of *Smc3*, the catalytic component of the cohesion complex, in GC formation and B cell differentiation (157). Genetic deletion of *Smc3* impeded GC formation; however, haploinsufficiency of *Smc3* resulted in expanded GC and a block in PC formation (157). This indicates that the final step of PC differentiation requires major reorganization of the genome architecture compared to other differentiation stages and is sensitive to changes in SMC3 levels.

Furthermore, the study of 3D architecture revealed the presence of multi-enhancer genes and multi-gene enhancers in actB. The multi-enhancer genes were enriched for gene ontology pathways, such as MHC-II antigen processing and ER-associated degradation, while the latter group included genes associated with metabolism and DNA replication (158). The important role of such multi-gene enhancers in regulating cell fate decisions was illustrated by another study, which evaluated the 3D architecture in GC B cells. This work revealed the presence of an enhancer that functioned as a locus of region control (LRC; a GC-specific enhancer cluster) by interacting with many GC signature genes. Deletion of this region using CRISPR led to abolished GC formation (159).

In addition to the global genome architecture studies mentioned above, local enhancer-promoter interactions are also important and dynamic during B cell differentiation. Analysis of the

MHC-II locus in mice and humans has revealed the complex interplay between TF, cis-regulatory elements, and genetic variation in the regulation of antigen presentation and potentially adaptive immunity (160-162). The entire MHCII locus contains a set of loops that are orchestrated by the CCCTC-binding factor (CTCF), which is known to regulate 3D interactions (163), and the cohesion complex (164-166). CTCF is required for maximal MHC-II gene expression (161), and in murine cells, the MHC-II locus is reorganized into distinct compartments when MHC-II gene expression is repressed in PC (167). In the era of genomics, a new set of super enhancers that are enriched for multiple transcription factor binding sites, active histone modifications, the Mediator complex, and cover large domains greater than 10kb in size have been described (168). A super enhancer located between the *HLA-DRB1* and *HLA-DQA1* genes (termed *DR/DQ-SE*) is one of the most acetylated regions of the B cell genome and contains the highest density of genetic polymorphisms in the human genome (162). Deletion of the *DR/DQ-SE* led to significant changes in 3D loops, enrichment of histone modifications and ultimately lower levels of MHC-II gene expression that impaired the ability of B cells to stimulate allogeneic T cell proliferation in a mixed lymphocyte reaction assay (162). These studies highlight how genetic variation within a super enhancer can impact the 3D architecture of a single locus and ultimately result in variation in MHC-II gene expression across a population. This indicates that non-coding genetic variation may be as important as HLA allelic variation within a population. Further work will help delineate the factors controlling MHC-II enhancer-promoter interactions and how variation impacts the adaptive immune response.

VI. The role of UTX and JMJD3 in health and disease

As described earlier, epigenetic modifiers play a critical role in fine-tuning B cell differentiation and PC function. However, a complete understanding of the role of epigenetics, and in particular histone modifications, in this process is still lacking. In particular, while the role of EZH2, H3K27me3 methyltransferase, in B cell has been well established (137-139, 141), little is known about the role of active demethylation of the histone modification.

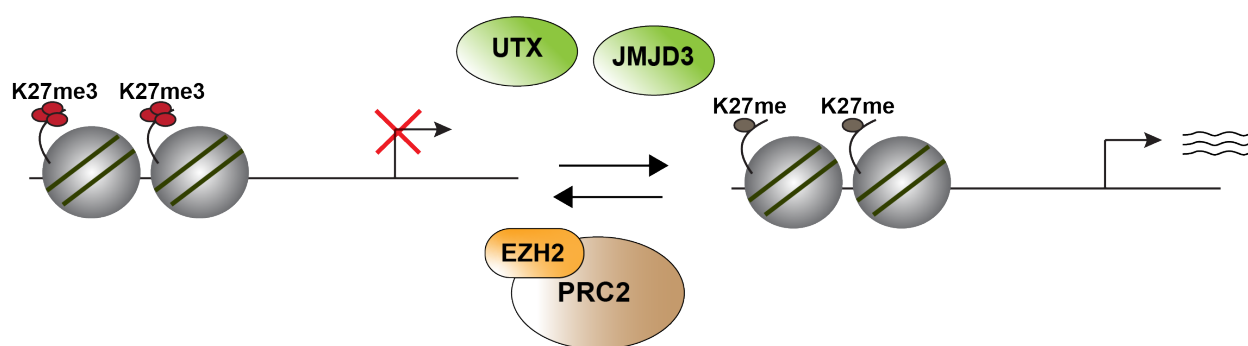


Figure 1-4. Active demethylation of H3K27me3 is mediated by UTX and JMJD3.

UTX and JMJD3 enzymatically remove methyl groups from H3K27me_{2/3} to promote gene expression. In doing so, these enzymes counteract the activity of EZH2, the H3K27me₃ methyltransferase.

The biochemical function of H3K27me3 demethylases

The active loss of H3K27me₃ is mediated by two demethylases: ubiquitously transcribed tetratricopeptide repeat, X chromosome (UTX) and JmjC Domain-Containing Protein 3 (JMJD3), which were first identified in 2007. The enzymes are also referred as KDM6A and KDM6B (**Figure 1-4**) (169-171). Both enzymes facilitate the removal of methyl groups from H3K27me₃ and H3K27me₂, but not H3K27me₁ (169-171). Demethylation of H3K27me₁ is mediated by KDM7A, which has been also shown to also act on H3K27me₂ and H3K9me_{2/1} (172, 173). It is important to note that UTX is encoded on the X-chromosome and escapes X-inactivation (174).

Additionally, the Y chromosome encodes a UTX homolog, UTY, which shares high homology with UTX, but has very little, if any, catalytic activity due to point mutations in the demethylase domain (169, 171, 175).

UTX and JMJD3 facilitate the removal of H3K27me_{2/3} via the Jumonji C (JmjC) domain, which requires oxygen and alpha-ketoglutarate as substrates and iron as a co-factor. This process occurs via direct hydroxylation of a methyl group resulting in a formation of a hydroxymethyl intermediate, which is then released as formaldehyde (176-178). Structural studies of UTX revealed that its specificity towards H3K27me_{3/2} is mediated by the interaction of the JmjC domain with H3 residues 25-33 and a novel zinc-binding domain with residues 17-21 (176). Additionally, UTX and UTY also contain six tetratricopeptide repeat domains, which facilitate protein-protein interactions (179, 180).

In addition to their catalytic activity described above, UTX and JMJD3 have also been shown to regulate gene expression in a demethylase-independent manner by promoting the assembly of protein complexes (181-184). Examples of both demethylase-dependent and independent functions of the two H3K27me₃ demethylases will be discussed below in the context of mammalian development and the adaptive immune system.

Role of H3K27me₃ demethylase in mammalian development

Full body deletion of the two H3K27me₃ demethylases in mice revealed a crucial role of these enzymes in embryogenesis and directly after birth. Loss of *Jmjd3* resulted in perinatal lethality due to respiratory failure (185); whereas, deletion of *Utx* led to severe defects in the formation of mesoderm derived tissues midgestation and resulted in embryonic lethality at embryonic days 10.5-13.5 (186-189). Intriguingly, sex-specific differences were observed. A subset of UTX-

deficient male embryos survived until birth, albeit they were born smaller and had reduced lifespan (186, 187, 189). Moreover, males lacking both *Utx* and *Uty* phenocopied UTX-deficient females (189) and embryonic stem cells (ESC) containing catalytically inactive UTX developed normally (186). Together, the data suggest that the demethylase activity of UTX is dispensable for its function during embryonic development.

Mechanically, UTX has been shown to regulate ESC differentiation in concert with MLL4, an H3K4me1/2 methyltransferase also known as KMT2D, and P300, a histone acetyltransferase. Together, these epigenetic modifiers promoted enhancer activation and subsequent transcription of their target genes, including retinoic acid response genes (182). Consistent with the previous studies, UTX regulated enhancer activation in a demethylase-independent manner. Here, UTX functioned as a scaffolding protein required to recruit and enhance the activities of MLL4 and P300 (182). In addition to their role in embryogenesis, UTX and JMJD3 have also been demonstrated to regulate later stages of development or function of specific tissues, including the heart (190), the nervous system and brain (191-193), retina (194), bones (195, 196).

Furthermore, a recent study revealed that UTX regulates cell fate decisions by directly sensing oxygen levels (197). Low oxygen levels or knockdown of UTX, but not JMJD3, in C2C121 murine myoblasts impaired differentiation of these cells into myotubes due to increased levels of H3K27me3 and failure to upregulate myogenic genes (197). The differences in the response of UTX and JMJD3 to hypoxia could largely be explained by the differences in oxygen affinity between these two enzymes. In fact, overexpression of UTX engineered to possess higher oxygen affinity partially rescued the differentiation block of C2C121 cells (197).

Role in the adaptive immune system

The critical role of UTX in hematopoiesis can be illustrated by the fact that inducible deletion of this enzyme resulted in reduced levels of white blood cells in the peripheral blood and impaired erythropoiesis (198). Furthermore, UTX-deficient HSC exhibited reduced migration towards stromal cell-derived factor-1 (SDF-1), which is known to regulate HSC proliferation and trafficking (198, 199). Interestingly, these phenotypes occurred in a sex-specific manner, suggesting a demethylase-independent role of UTX in the early hematopoiesis (198).

The demethylase-independent function of UTX in hematopoiesis was corroborated by a later study using a mouse model with a conditional deletion of this enzyme in HSC. Loss of *Utx* resulted in an expansion of cells in the myeloid lineage leading to the development of spontaneous acute myeloid leukemia (200). However, UTX-deficient males resembled the wild-type control and overexpression of catalytically inactive UTX or UTY compensated for *Utx* loss; thus, once again suggesting that demethylase activity is not required for its role in early hematopoiesis (200). These phenotypic observations corresponded with the results of the molecular analyses, which revealed a minor effect of UTX on H3K27me3 in HSC. Instead, UTX-deficiency resulted in vast changes in the enrichment of H3K27ac and H3K4me1 as well as chromatin accessibility (200). Beyond early hematopoiesis, numerous studies have revealed a role of UTX and JMJD3 in the development and function of specific immune cell types (201-204). The remainder of this section will focus on the role of H3K27me3 demethylases in the adaptive immune system.

UTX and JMJD3 were found to play a redundant function in T cell development in the thymus, where they regulated the egress of newly formed CD4 and CD8 T cells from the thymus (205). Deletion of these enzymes during T cell development resulted in increased levels of H3K27me3 and reduced expression of *Slpr1*, which is required for entry into the bloodstream, as

well as *Klf2*, a transcription factor that regulates *Slpr1* expression (205). These findings were corroborated by a later study that evaluated the role of JMJD3 in cell trafficking. In addition to *Slpr1*, this study also identified *Pdlim4* as a direct target of JMJD3 (206). PDLIM4 is a known modifier of actin filaments and was shown to physically interact with S1PR1 to regulate cell migration (206, 207). At the molecular levels, JMJD3 interacted with KLF2 and members of the MLL complex to modulate the H3K27me3 and H3K4me3 enrichment and ultimately control the expression of *Pdlim4* (206). Together, the results provided a mechanistic insight into how H3K27me3 demethylases modulate the late stages of T cell development in the thymus by regulating the expression of *Slpr1* and *Pdlim4* (205, 206).

The central role of CD4 T cells is to modulate the functions of other immune cell types, including B cells, CD8 T cells, and macrophages (208, 209). Naïve CD4 T helper cells become activated through their T cell receptor and differentiate into distinct subsets with unique roles in the overall immune response in a process driven largely by the cytokine microenvironment. These subsets include: T-helper 1 cells (Th1), T-helper 2 cells (Th2), T-helper 17 cells (Th17), T follicular helper cells (Tfh), and T regulatory cells (Treg) (208, 209). This differentiation process is associated with substantial transcriptional and epigenetic remodeling (210, 211), which has led to an interest in studying the roles of UTX and JMJD3 in this process.

Deletion of *Utx* during early T cell development impaired the formation of Tfh during an chronic viral infection thus impeding the eventual clearance of the virus (212). At the molecular level, UTX-deficient Tfh cells showed reduced expression of genes associated with Tfh fate and increased expression of Th1-related genes, suggesting a role for UTX in regulating the fate decisions (212). Furthermore, loss of *Utx* resulted in increased levels of H3K27me3 at a subset of the downregulated genes, including *Il6ra*, which is known to play an important role in the Tfh

development (212). Thus, UTX is required to promote the expression of the Tfh transcriptional program.

The role of JMJD3 in CD4 T cell differentiation has also been evaluated. Stimulation of JMJD3-deficient CD4 T cells *in vitro* with polarizing and non-skewing cytokines showed that loss of *Jmjd3* resulted in an increased propensity of the cells to differentiation into Th2 and Th17 and reduction in Th1 (213). The findings were also validated *in vivo* using Th1-dependent colitis model, where an adoptive transfer of JMJD3-deficient cells led to an expansion of Th2 and reduced the disease burden (213). Functionally, JMJD3 cooperated with TBET and MLL complex to regulate H3K27me3 and H4K4me3 enrichment at Th1 and Treg lineage defining factors, such as *Ifng* and *Foxp3* (213). However, another study showed that loss of *Jmjd3* impaired Th17 differentiation (214). The discrepancy likely stems from the differences in the Th17-inducing stimulation conditions, suggesting that the role of JMJD3 during CD4 differentiation might depend on the external stimuli. Furthermore, while loss of *Utx* impaired Tfh formation in response to a chronic, but not an acute LCMV infection, deletion of *Jmjd3* led to a reduction in Tfh following an acute infection (212, 215), thus highlighting a context-specific activity of these enzymes.

The role of UTX and JMJD3 has also been investigated in CD8 T lymphocytes, which primary role is to eliminate pathogen-infected cells. Loss of *Utx* led to an expansion of the memory CD8 T cell pool following infection with *Listeria monocytogenes* expressing OVA (Lm-OVA) and resulted in a more robust response following a secondary infection (216). The increase in memory CD8 T cells was associated with downregulation of genes associated with the effector CD8 T cells, including *Prdm1*. UTX directly bound to *Prdm1* promoter to modulate the levels of H3K27me3 at that locus and ultimately gene expression (216). A separate study revealed even more profound effect of *Utx* deletion following infection with LCMV variant A-22, which

promotes chronic infection. Loss of *Utx* resulted in an expansion of activated CD8 T cells (217). Interestingly, these UTX-deficient CD8 T cells failed to upregulate effector-associated genes and exhibited impaired effector functions leading to increased viral load and disease burden. Furthermore, UTX-deficient cells were more resistant to apoptosis and had higher expression of inhibitory receptors (217). Interestingly, however, CD8 T cells with catalytically-inactive UTX phenocopied the results of a complete loss of *Utx*. Together, the data suggest that the demethylase activity of UTX is required during an acute (216), but not a chronic viral infection (217).

The role of JMJD3 in CD8 T cells has also been evaluated. Similar to the above-mentioned studies on UTX, loss of *Jmjd3* led to an expansion of the early effector and memory precursor CD8 T cells. However, despite the increase in memory compartment and, unlike UTX-deficient CD8 T cells, JMJD3-deficient memory CD8 T cells generated a poor response following a secondary challenge. Loss of *Jmjd3* resulted in a reduced number of antigen-specific cells and a failure to reacquire the characteristics of an effector cell, such as expression of KLRG1 (215). However, similar to what was observed following deletion of *Utx* (216, 217), loss of *Jmjd3* resulted in downregulation of genes associated with effector CD8 T cells and impaired effector functions, suggesting a redundant role of these enzymes in regulating a subset of the effector genes (215).

Despite the extensive studies on the role of UTX and JMJD3 in various immune cell types, little is known about their role in B cell differentiation. One study demonstrated that deletion of *Utx* in HSC significantly impaired the commitment to the B cell lineage during hemopoiesis (218). Furthermore, overexpression of JMJD3 in human GC B cells was reported to alter the expression of genes associated with PC and memory B cells (219), suggesting that H3K27me3 demethylases might be critical regulators of B cell differentiation. Further evidence for the putative role of UTX

and JMJD3 in B cell fate decisions comes from the fact that mutations in these enzymes have been reported in human diseases.

Role in disease: Kabuki syndrome

Kabuki syndrome is a rare congenital disorder that affects multiple organs. Patients are characterized by distinct craniofacial features, skeletal abnormalities, cardiac defects, delayed development and/or intellectual disability (220, 221). Furthermore, patients also exhibit immunological defects characterized by recurrent infections and reduced serum antibody titers (222, 223). The vast majority of Kabuki syndrome cases are caused by loss of function mutations in *KMT2D*, an H3K4 methyltransferase and the catalytic component of the MLL complex (224, 225). However, 5-10% of patients harbor mutations in *KDM6A* (UTX) (226, 227). As mentioned above, UTX has been described to interact with KMT2D and other members of the MLL complex to promote gene expression (228). Thus, given the common clinical features of patients with Kabuki syndrome regardless of the causative mutation, it is likely that UTX and KMT2D regulate the same group of genes.

Role in disease: B-cell malignancies

Mutations in *UTX* and *JMJD3* have been reported in various human cancers including B-cell malignancies, suggesting that these enzymes are critical regulators of the B cell fate (229, 230). Interestingly, depending on the type of cancer, UTX and JMJD3 act either as tumor suppressors or oncogenes, thus highlighting the context dependent activity of these enzymes (229, 230).

Loss of function mutations in *UTX* have been reported in B cell lymphomas and multiple myeloma (MM) (231, 232). Mouse studies revealed that loss of *Utx* accelerated E μ -Myc-induced B cell

lymphomagenesis and led to more severe disease (232). UTX-deficient tumors altered the expression of genes associated with antigen processing and presentation as well as early B cell development, such as *Vpreb1*, *Igll1*, *Rag1*, *Blk* (232). Furthermore, loss of *Utx* resulted in upregulation of *Efnb1* encoding Ephrin B, which has previously been shown to play a role in tumor metastasis and angiogenesis (232, 233). In MM cell lines, loss of *UTX* resulted in increased proliferation *in vitro* and increased tumorigenesis in mice implanted with the tumor cells. UTX was shown to regulate the expression of genes associated with cell growth and survival as well as cell-cell interactions (231). Importantly, a subset of differentially expressed genes in UTX-deficient MM cells corresponded to genes previously defined as PRC2 target genes. Furthermore, loss of *UTX* sensitized the cells to treatment with EZH2-inhibitor, thus highlighting a critical role of maintaining balanced levels H3K27me3 in PC biology (231).

Intriguingly, while *UTX* mutations in B cell malignancies are typically loss of function, overexpression of *JMJD3* has been reported in diffuse large B cell lymphoma (DLBCL), where higher expression of *JMJD3* was associated with poor survival (234, 235). Reciprocally, deletion or inhibition of *JMJD3* in DLBCL cell lines induced apoptosis, suggesting a role of this enzyme in promoting tumorigenesis (235).

VII. Rationale and overview

As described above, B cell differentiation is the cornerstone of humoral immunity that provides us with long-standing immunity and serves as the basis behind vaccine development (5, 33). However, when misregulated, this process can also lead to the development of B-cell malignancies or autoimmunity (9, 12); thus, a full understanding of B cell and PC biology is necessary to facilitate the development of more potent vaccines and novel therapeutics for B-cell mediated

diseases. The study of the epigenetic reprogramming that occur during B cell differentiation provides a novel avenue for therapeutic interventions. In fact, inhibitors of various epigenetic modifiers are either already used in the clinic or currently in clinical trials as treatments of various cancers (236).

In addition to substantial metabolic and transcriptional reprogramming, B cell differentiation is also associated with vast changes in the distribution of DNA methylation and histone modifications, including H3K27me3. This histone modification is deposited by EZH2 and removed by UTX and JMJD3. However, while the role of EZH2 in B cell development and differentiation has been well established and led to the use of EZH2 inhibitors in the clinic (137, 139, 141, 237, 238), little is known about the role of active demethylation of H3K27me3 during B cell differentiation. In this dissertation, UTX was identified as a critical epigenetic modifier required to fine-tune B cells responses.

Collectively, we identified that H3K27me3 demethylases are negative regulators of B cell differentiation. Through the use of pharmacological inhibition in chapter 2 and genetic deletion of both enzymes in chapter 3, we showed that inhibition or loss of *Utx* and *Jmjd3* led to an increase in PC. Our *in vivo* studies revealed that these enzymes regulated cell proliferation, metabolism, and apoptosis. In chapter 4, we demonstrated that H3K27me3 demethylases are also required to fine-tune the GC response as loss of these enzymes led to an increase in GC B cells. Taken together, our data add to our growing understanding of the epigenetic regulation of B cell differentiation.

Chapter 2. Inhibition of H3K27me3 demethylase promotes plasmablast formation

Anna K. Kania[†], Muyao Guo^{†‡}, Christopher D. Scharer[†], and Jeremy M. Boss^{† *}

[†] Department of Microbiology and Immunology, Emory University School of Medicine, Atlanta, GA 30322, USA

[‡] Currently at Department of Rheumatology and Immunology, Xiangya School of Medicine, Central South University, Changsha, 410008, China

* Correspondence: jmboss@emory.edu; 404-727-5973

Author contributions

A.K.K. designed and performed experiments, analyzed, and interpreted the data, and wrote the manuscript; C.D.S. designed experiments and interpreted the data. J.M.B designed experiments, interpreted the data, and wrote the manuscript.

This manuscript was originally published in *Immunohorizons*.

Kania AK, Guo M, Scharer CD, Boss JM. 2021. Inhibition of H3K27me3 demethylases promotes plasmablast formation. *Immunohorizons*, 5(12):918-930.

I. ABSTRACT

B cell differentiation into antibody-secreting plasma cells requires transcriptional, metabolic, and epigenetic remodeling. H3K27me3, a histone modification associated with gene silencing, is dynamically regulated during B cell differentiation. Although several studies have focused on mechanisms involving the gain of this modification in plasmablasts (PB), the role of active demethylation of H3K27me3 by UTX and JMDJ3 during B cell differentiation has not been examined. Here, this process was assessed using a pharmacological inhibitor of UTX and JMJD3, GSK-J4. Treatment of *ex vivo* stimulated mouse B cells with GSK-J4 led to an increase in plasmablast frequency without affecting the ability of the newly formed plasmablasts to secrete antibodies. Consistent with the role of UTX and JMJD3 in promoting gene expression, the majority of differentially expressed genes were downregulated upon GSK-J4 treatment. GSK-J4-treated cells downregulated genes associated with signaling and P53 pathways. Inhibitor treated cells upregulated genes associated with cell cycle and proliferation, which correlated with an increase in actively proliferating cells. Unexpectedly, a majority of the downregulated transcripts corresponded to genes that in the wild-type setting were genes that gain H3K27me3 and downregulated in PB. Together, our results show that UTX and JMDJ3 are required to restrain B cell differentiation and suggest that they function as a rheostat for H3K27me3 to control this process.

II. INTRODUCTION

Humoral immunity relies on the ability of naïve B cell (**nB**) to differentiate into antibody secreting short-lived plasmablasts (**PB**) or long-lived post-mitotic plasma cells (**PC**). To allow for robust antibody secretion and differentiation, B cells undergo substantial changes in their transcriptional profile as well as metabolism (33, 49, 80, 239). nB and PC fates are regulated by distinct sets of transcription factors. Whereas PAX5 (17, 113, 240, 241) and BACH2 (102, 104) promote the nB stage, BLIMP1 (242-244) and high levels of IRF4 (112, 245) promote PC formation. In addition, there is a growing appreciation for the epigenetic reprogramming that occurs during B cell differentiation (246, 247). This is well exemplified by the fact that differentiating B cells undergo cell-division coupled reprogramming of their accessible chromatin landscape and progressive DNA hypomethylation of their genome following stimulation with T-cell independent antigens (92, 117).

In addition to changes in DNA methylation to facilitate cell fate decisions, the distribution of histone modification also changes during B cell differentiation (115, 117, 141). Of particular note is the status of histone H3 lysine 27 trimethylation (H3K27me3) modifications at nB- and PB-specific genes. This histone modification is associated with a repressed chromatin state and gene silencing (134). H3K27me3 is deposited by EZH2 (135, 136, 248), a component of the PRC2 complex, and is enzymatically removed by two demethylases UTX (Ubiquitously transcribed tetratricopeptide repeat, X chromosome) and JMJD3 (Jumonji Domain-Containing Protein 3) (169, 171). UTX and JMJD3 are also termed KDM6A and KDM6B, respectively. In a recent study, H3K27me3 was shown to be dynamically regulated during B cell differentiation with roughly equal number of promoter regions that gain and lose this histone modification as B cells differentiate to PB (141). Deposition of H3K27me3 by EZH2 has been shown to play an important

role during B cell development (139, 249), germinal center formation and maintenance (137, 138, 250), as well as PB formation in response to T-independent antigens (141). However, a significant gap in knowledge persists concerning the role of UTX and JMJD3 in the epigenetic regulation of B cell differentiation and PC formation.

UTX and JMJD3 facilitate H3K27me3 demethylation via their Jumonji C domain in an iron and alpha-ketoglutarate dependent manner (176, 177). This process occurs via direct hydroxylation of the methyl group resulting in a formation of a hydroxymethyl intermediate, which is then released as a formaldehyde (178). UTX is X linked with a homolog, UTY, encoded on the Y chromosome. The demethylation activity of UTY is extremely low compared to UTX (169, 171, 175). In addition to their catalytic activity, UTX and JMJD3 influence gene expression through interactions with a host of chromatin regulators, including BRG1 (184, 200) and CHD4 (200, 251), p300 (182), and most notably the MLL complex, which promotes H3K4 methylation (228, 252). The tumor suppressor p53 also interacts with UTX and JMJD3 (253). UTX and JMJD3 have been shown to function in various biological processes, including early embryonic development (185, 187, 189). The H3K27me3 demethylases were shown to facilitate resolution of bivalent promoters at retinoic acid-inducible genes (254) and derepression of inactive enhancers (182). Other roles have included cardiac development (190), hematopoiesis (198), M2 following GSK-J4macrophages differentiation (255), and regulation of various T cell subsets (184, 203-205, 213, 214, 216).

In a clinical setting, mutations in *UTX* lead to a rare, congenital disorder characterized by distinct facial features, developmental delay, intellectual disability, and multi-organ malfunctions (221, 224). Furthermore, mutations in *UTX* have been identified in Diffuse Large B-cell Lymphoma (DLBCL) (232) and multiple myeloma (231, 256, 257). Mutations in JMJD3 have

been described in Hodgkin's Lymphomas (219) and DLBCL (234, 235). Together, this suggests that these enzymes are important regulators of B cell fate. Furthermore, changes in the expression of genes associated with PC and memory B cells have been reported following overexpression of JMJD3 in human germinal center B cells (219). However, the role of UTX and JMJD3 in B cell differentiation has not been fully examined, thus leaving a significant gap in our knowledge of epigenetic regulation of PC formation.

In this study, we utilized a pharmacological inhibitor for UTX and JMJD3 to examine their role in regulating B cell differentiation using an *ex vivo* model system. The results showed that the demethylation enzymes are involved in controlling cell cycle, proliferation, and ultimately the frequency of B cells that differentiate into PB and are therefore critical for PB reprogramming and function.

III. RESULTS

H3K27me3 demethylases are upregulated during B cell differentiation

Previous work (141) described significant gains and losses in H3K27me3 modifications as B cells differentiated to PB in response to LPS, pointing to a potential role for the removal of these marks by histone demethylases. The expression of the two H3K27me3 demethylases (UTX and JMJD3) was examined in a previously published data set (146), which quantified gene expression during *in vivo* differentiation of nB following LPS stimulation. Analysis of this data revealed that compared to nB, *Utx* was upregulated several fold in newly formed plasmablasts (PB), while *Jmjd3* expression showed a modest albeit statistically significant increase in expression (**Figure 2-1A**). Expression of UTX and JMJD3 was also examined in a second LPS-induced *in vivo* B-cell differentiation model dataset that correlated gene expression as a function of cell division (92). In that system, PB form after division 8 and are phenotypically recognized by expression of the plasma cell maker CD138 (termed division 8+). Again, *Utx* expression was significantly higher in the division 8+ cells, which represent the newly formed PB compared to control earlier divisions (**Figure 2-1B**). Furthermore, consistent with the changes in gene expression, the protein levels of UTX and JMJD3 were higher in PB derived from *ex vivo* cultures compared to nB and not altered in expression by GSK-J4 treatment (**Supplemental Figure 2-1A**). In a similar manner, other histone modifiers that are known to be functionally affected by GSK-J4 were not altered in expression by the inhibitor (**Supplemental Figure 2-1A**). To determine whether change in H3K27me3 during B cell differentiation correlated with transcriptional differences, the change in promoter H3K27me3 enrichment (141) was plotted against the change in gene expression between nB and PB (146). Consistent with the repressive role of H3K27me3, the analysis revealed two major sets of genes: 1) genes that had high expression and low H3K27me3 levels in PB (**Figure**

2-1C; green quadrant); and 2) genes that had low expression and high H3K27me3 in PB compared to nB (**Figure 2-1C; blue quadrant**). H3K27me3 enrichment at the abovementioned gene groups was quantified (**Figure 2-1D**). This analysis also revealed a group of genes that were upregulated in PB but exhibited a higher level of promoter H3K27me3 (**Figure 2-1C; gray shade**) and are therefore not likely to be regulated by this histone modification but rather by other epigenetic or transcriptional mechanisms.

To study the role of UTX and JMDJ3 during B cell differentiation, a pharmacological inhibitor, GSK-J4, known to inhibit the activity of these enzymes was utilized (258). In this system, naïve B cells were differentiated *ex vivo* with LPS, IL-2, and IL-5 as previously described (259).

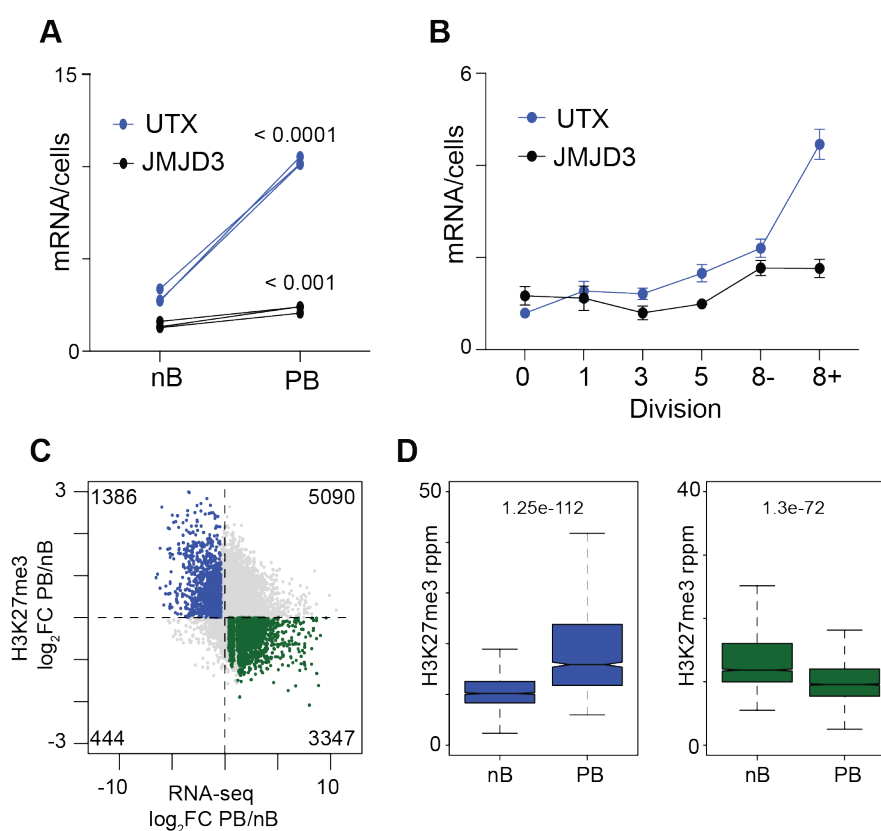


Figure 2-1. H3K27me3 demethylases are upregulated during B cell differentiation.

(A) Expression in mRNA/cell of *Utx* and *Jmjd3* in control nB and PB (Haines *et al.* 2018). (B) Expression in mRNA/cell of *Utx* and *Jmjd3* per division (Barwick *et al.* 2016). (C) The log₂FC change in gene expression between PB and nB (Haines *et al.* 2018) was plotted against the log₂FC

change in H3K27me3 between PB and nB (Guo et al. 2018). The total number of unique genes in each quadrant is indicated. **(D)** Quantification of H3K27me3 levels in PB and nB

Treatment with GSK-J4 promotes PB formation

To examine the effect of the inhibitor-mediated loss of UTX and JMJD3 catalytic activity on B cell differentiation, nB were isolated and stimulated *ex vivo* with LPS, IL-2, and IL-5 in the presence of 250nM GSK-J4 or DMSO control. After three days of culture, flow cytometry analysis revealed a significant increase in the frequency of CD138⁺ PB in the GSK-J4 treated cultures (**Figure 2-2A**) with a small but significant increase in the B220⁺GL7⁺ activated B cells (**ActB**) (**Figure 2-2B**). Importantly, an increase in PB following GSK-J4 treatment was also observed when compared to the inactive control compound, GSK-J5 (**Figure 2-2C**). To determine whether the observed phenotype was specific to TLR signaling, the effect of inhibitor treatment on PB formation was examined following stimulation with CD40L, IL-4, and IL-5 that mimic T-cell dependent B cell activation (260). Enhanced B cell differentiation was also observed following this mode of stimulation (**Figure 2-2D**).

To determine whether the UTX/JMJD3 inhibition affected the ability of cells to secrete antibodies, CD138⁺ PB from the LPS cultures were magnetically enriched after three days of *ex vivo* culture and an equal number of cells was plated in fresh media. Antibody secretion was then analyzed by ELISA and revealed no difference in the IgM antibody titers between the GSK-J4 and DMSO treated PB (**Figure 2-2E**), suggesting that UTX/JMJD3 regulate the process of B cell differentiation but not the antibody-secreting function of PB.

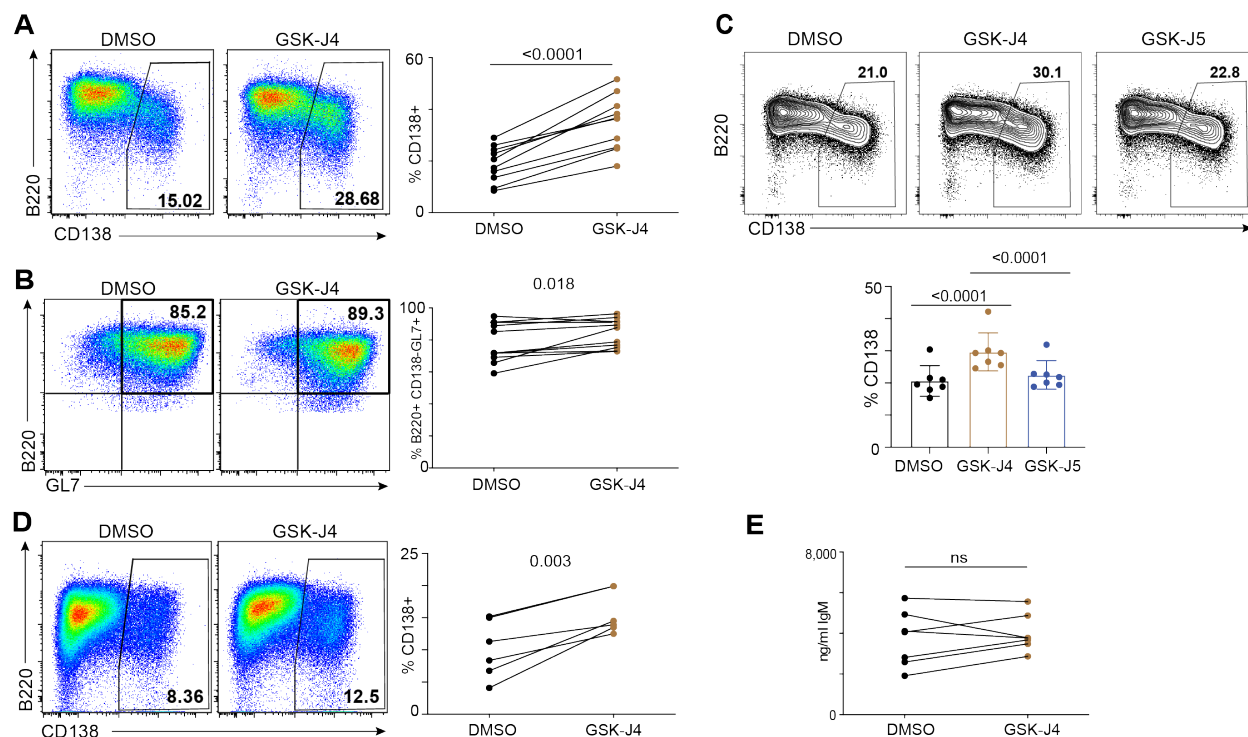


Figure 2-2. GSK-J4 treatment leads to an increase in the frequency of CD138+ plasmablasts. Representative plots and quantitation of the frequency of (A) CD138+ PB and (B) CD138-B220+GL7+ ActB after 3 days of *ex vivo* stimulation with LPS, IL-2, IL-5 in the presence of 250 nM GSK-J4 or DMSO control. (C) Representative plots and quantitation of the frequency of CD138+ PB after 3 days of *ex vivo* stimulation with LPS, IL-2, IL-5 in the presence of 250 nM GSK-J4, 250 nM GSK-J5 (inactive compound), or DMSO. (D) Frequency of CD138+ PB at day four of *ex vivo* culture with CD40L, IL-4, IL-5 in the presence of 250 nM GSK-J4 or DMSO. (E) IgM antibody titers after 2.5 hr incubation of magnetically enriched PB from DMSO or 250 nM GSK-J4 treated cultures. Data are from two independent experiments with 3-4 mice each. Significance was determined by paired two-tailed Student's *t* test.

Inhibitor treatment alters B cell transcriptome

To define the mechanism by which treatment with GSK-J4 promotes B cell differentiation, RNA-seq was performed on magnetically enriched nB, as well ActB and PB derived from GSK-J4 or DMSO cultures at day 3 post LPS, IL-2, and IL-5 stimulation (**Supplemental Figure 2-2B**). Principal component analysis (PCA) revealed that the activation status was the major source of variation as principal component (PC) 1 separated nB from ActB and PB. PC2 separated ActB from PB, while PC3 stratified cells based on GSK-J4 treatment status (Figure 2-3A). Consistent

with results of PCA, hierarchical clustering of samples and differentially expressed genes (DEG) between GSK-J4 and DMSO revealed that samples stratified based on cells type rather than treatment status (**Figure 2-3B**). Differential expression analysis of GSK-J4 and DMSO treated cells (1.5-fold change, FDR <0.05) revealed a skewing towards genes downregulated following drug treatment. In the ActB comparison, 253 genes were downregulated (downDEG) and 106 were upregulated (upDEG). In the PB comparison, there were 352 downDEG and 84 upDEG (**Figure 2-3C; Supplemental Table 1**). Furthermore, a common set of 113 genes was downregulated in both comparisons (**Figure 2-3D**). The observed enrichment for downregulated genes is consistent with inhibition of UTX and JMJD3, which in the wild-type setting promote gene expression. GSK-J4 has been shown to act, although with weaker activity, on KDM5B and KDM5C, the H3K4me_{2/3} demethylases (258, 261). However, inhibition of H3K4me₃ demethylases would be predicted to result in gene upregulation. Thus, this observation suggests that the inhibitor primarily acts on the UTX and JMJD3 demethylase pathway rather than others.

To identify the pathways altered following GSK-J4 treatment, gene set enrichment analysis (GSEA) (262) was performed on a ranked gene list for the ActB GSK-J4 v ActB DMSO comparison. This analysis revealed downregulation of genes associated with hypoxia, TNF signaling, P53 pathways, and apoptosis (**Figure 2-3E**). Examples of genes downregulated following inhibitor treatment included *Cdkn2a*, encoding p16^{Ink4a} and p19^{Arf}, which inhibit the G1/S cell cycle transition (263) and regulate p53 stability (264), respectively. Other examples of down regulated DEG include *Bnip3l*, which promotes apoptosis (265), and *Pdk1*, which inactivates pyruvate dehydrogenase, thereby inhibiting the conversion of pyruvate into acetyl-CoA (266, 267) (**Figure 2-3F**). Despite dysregulation of several apoptotic factors, there was no difference in the frequency of apoptotic cells following inhibitor treatment. A small but significant increase in

necrotic cells at 48hr post stimulation was observed (**Supplemental Figures 2-1B and 2-1C**), but this difference does not explain differences observed in the number of plasmablasts formed (**Figure 2-2A and 2-2C**).

Additionally, cell cycle and proliferation genes were upregulated following inhibitor treatment (**Figure 2-3G**). Some of the pathways dysregulated have been previously shown to be downregulated in the absence of EZH2 (141) and are upregulated as B cells progress through cell division and differentiate to PB (92). This suggested that the PB program may be initiated early or more strongly in GSK-J4 treated cells. To test this, expression of genes that were previously described to constitute a PC transcriptional signature was examined in inhibitor treated cells (46). GSEA analysis revealed upregulation of PC-signature genes in inhibitor treated ActB and PB (**Figures 2-3H 2-3I, Supplemental Figure 2-1D**). Taken together, GSK-J4 led to global changes in the B cell transcriptome, indicating a role for H3K27 demethylation in regulating the PB transcriptome.

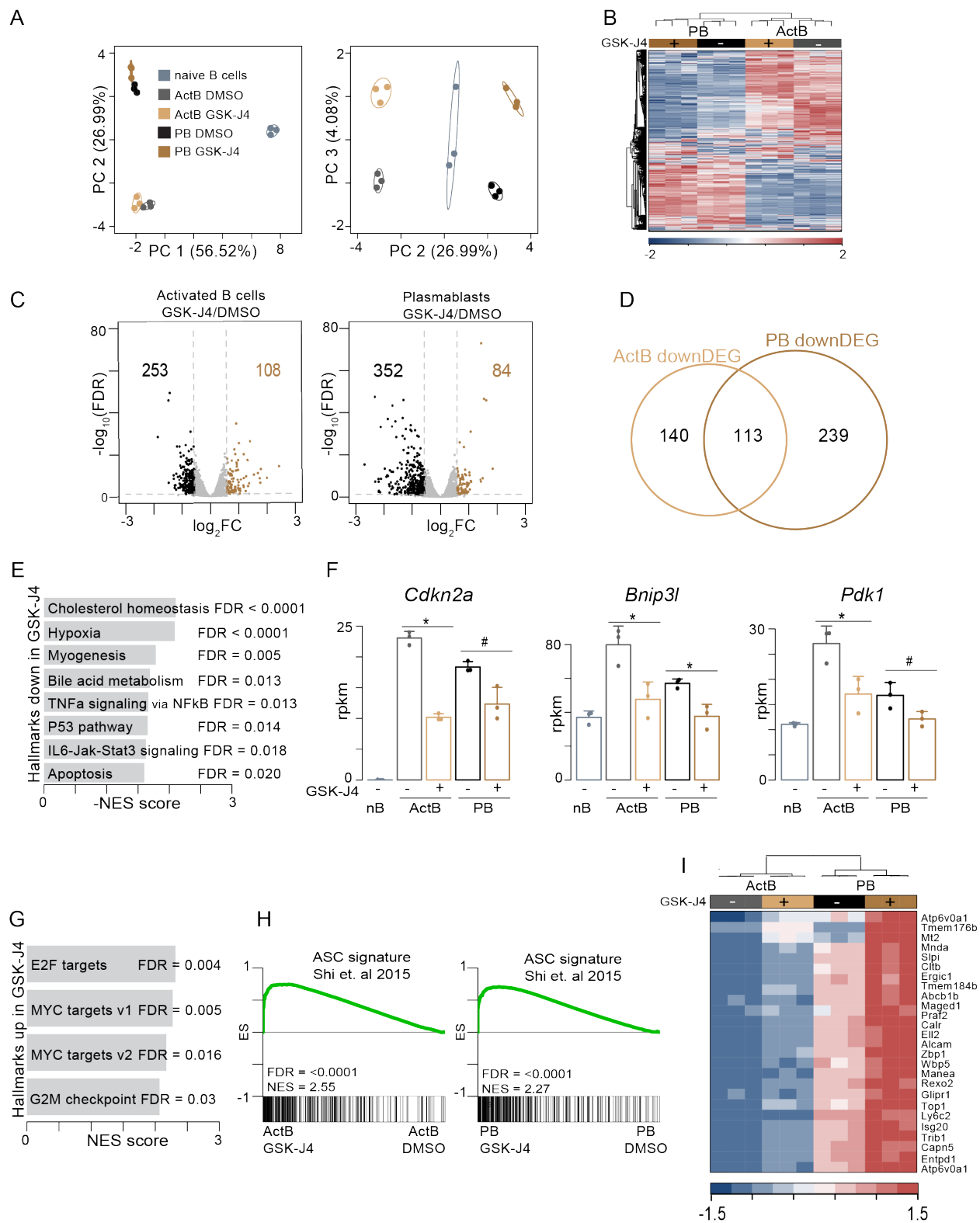


Figure 2-3. Inhibition of UTX and JMJD3 leads to global changes in gene expression.

RNA sequencing was performed on magnetically enriched ActB and PB from DMSO or 250 nM GSK-J4 treated cultures as well as naïve B cell controls. (A) Principal component analysis of 10,031 genes differentially expressed in a least one comparison RNA-seq data. The percentage in parentheses is the proportion of variation explained by each component and circles represent 99% confidence intervals for each group. (B) Hierarchical clustering of samples and DEG (FDR < 0.05, 1.5-fold change) between inhibitor GSK-J4 and DMSO cells. (C) Volcano plots of DEG (FDR < 0.05, 1.5-fold change) between GSK-J4 and DMSO treated ActB (left) and PB (right). (D) Venn diagram representing the overlap of ActB and PB downDEG between inhibitor and DMSO treated cells. (E) Hallmark gene sets downregulated upon treatment with GSK-J4 treated ActB. GSEA was performed on a ranked gene list comparing ActB GSK-J4 vs DMSO treated cells. (F) Examples of genes downregulated in GSK-J4 treated cells. (G) Hallmark gene sets upregulated in GSK-J4 treated ActB. (H) GSEA for a previously defined ASC-signature genes (Shi *et al.* 2015) in GSK-J4 treated ActB (left) and PB (right) versus control. (I) Heatmap showing the expression of the top 25 DEG from the ASC-signature gene set from (H) in GSK-J4 and DMSO treated ActB and PB. Data represent the mean of three biological replicates per group. * FDR < 0.05 and >1.5 fold change, # FDR < 0.05 with <1.5 fold change

Inhibitor treated cells exhibit increased proliferation

The downregulation of *Cdkn2a* and the p53 pathway combined with an upregulation of genes associated with cell cycle and proliferation following GSK-J4 treatment, led to the hypothesis that inhibitor treatment results in enhanced proliferation. To examine whether treatment with GSK-J4 altered cell division kinetics, nB were stained with CellTrace Violet (CTV) and stimulated *ex vivo* with LPS, IL-2, IL-5 in the presence of GSK-J4 or DMSO. Irrespective of treatment, cultured B cells underwent six cell divisions after three days of culture. However, analysis of PB frequency at each division revealed a significant increase in PB per division following inhibitor treatment, with PB increasing as early as division four (**Figure 2-4A**). To examine whether inhibitor treatment altered cell cycle distribution in treated cells, at day 3 post LPS stimulation, B cell cultures were pulsed with bromodeoxyuridine (**BrdU**) for 2 hours and analyzed by flow cytometry. GSK-J4 treatment led to a significant increase in the frequency of cells in the S phase of the cell cycle (**Figure 2-4B**). Further, analysis of BrdU by cell division revealed a significant increase in the frequency of BrdU⁺ cells at the early cell divisions (**Figure 2-4C**). Overall, while GSK-J4

treatment does not alter the total number of cell divisions, it does lead to an increase in actively proliferating cell (S phase cell cycle) with a proportional reduction of cells in the G1 phase.

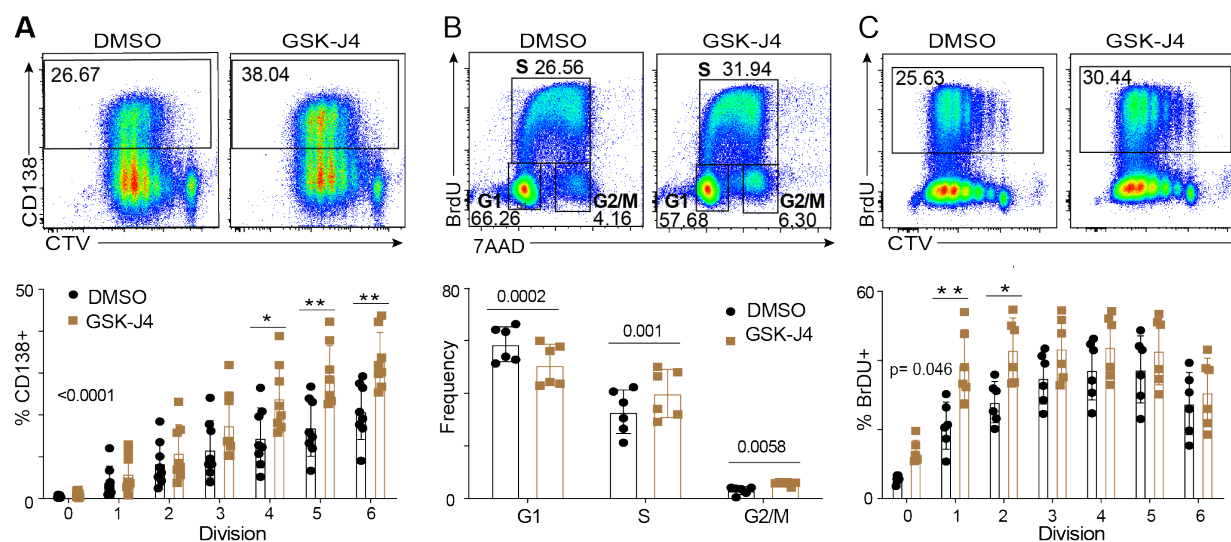


Figure 2-4. Inhibition of UTX and JMJD3 promotes cell proliferation

(A) Representative plots of CD138 versus CTV after three days of *ex vivo* culture (top) and quantification of the frequency of CD138+ plasmablasts per cell division (bottom) at day 3 of *ex vivo* stimulation. (B) Frequency of cells at G1 (2N, BrdU-), S (BrdU+), and G2/M (4N, BrdU-) phases of the cell cycle following two-hour incubation with BrdU at day 3 of *ex vivo* stimulation in the presence of GSK-J4 or DMSO. (C) Representative plots of BrdU versus CTV for GSK-J4 and DMSO treated cells (top) with quantification of BrdU+ cells per division (bottom). Data are summary of two independent experiments with 3-4 mice each. Significance was determined by paired two-tailed Student's *t* test (B) and two-way ANOVA followed by Sidak's multiple comparisons test (A,C). * p-value < 0.05, ** p-value < 0.001.

DEG are enriched for genes regulated by H3K27me3

To determine whether inhibition of UTX and JMJD3 predominately affects genes regulated by H3K27me3 during B cell differentiation, genes downregulated in PB following GSK-J4 treatment were overlaid on the scatterplot comparing PB/nB gene expression vs change in H3K27me3 enrichment in Figure 2-1. Consistent with the hypothesis that UTX and JMJD3 promote demethylation of H3K27me3 at genes upregulated in PB, several of GSK-J4 downDEG fell in the “green” quadrant described above. This group includes genes such as *Slc7a3*, which encodes a

sodium-independent transporter of cationic amino acids (268, 269) (**Figure 2-5A, 2-5D**). Other genes included *Cth* (270), *Lars2* (271), *Ddt* (272), *Fut1*, *Tmed6* (273), *Galk1*(274), *Gstt1* (275), *Abcb8* (276), that are involved in various aspects of protein synthesis or protein modification, secretion, vesicular trafficking and metabolism. Unexpectedly, the majority of the genes downregulated following inhibitor treatment correspond to genes that in the wild-type setting gain promoter H3K27me3 and are downregulated in PB (“blue” quadrant) (**Figure 2-5A**). H3K27me3 levels at GSK-J4 downDEG in the respective quadrants was quantified (**Figure 2-5B**). Thus, genes downregulated by inhibition of UTX and JMJD3 are predominately enriched for regions that in the wild-type setting gain H3K27me3 during B cells differentiation. Due to the gain in H3K27me3, these genes are likely regulated in part by EZH2, which is the counterpart to UTX/JMJD3. In fact, GSK-J4 downDEG genes in the “blue” quadrant corresponded to genes that were significantly upregulated in EZH2-deficient PB and 29% were defined as DEG (141) (**Figure 2-5C**).

Examples of genes that are downregulated following GSK-J4 treatment and have high levels of H3K27me3 in wild-type PB include *Id3* (inhibitor of DNA-binding/differentiation 3), which forms heterodimers with E box proteins to inhibit their DNA binding (277), is normally repressed during plasma cell formation with concomitant accumulation of H3K27me3. Following GSK-J4 treatment, *Id3* expression is super repressed in the PB (**Figure 2-5E top**). *Spib*, which regulates the ability of B cells to respond to external stimulation and inhibits germinal center B cell and PB formation (107), followed a similar path, normally accumulating H3K27me3 in PB and was super repressed in GSK-J4 treated PB (**Figure 2-5D bottom**). Together, these data suggest that inhibition of UTX and JMJD3 leads to enhanced repression of a subset of B cell fate genes that gain H3K27me3, thus promoting PB formation.

To evaluate whether genes upregulated following inhibitor treatment were enriched for genes regulated by H3K4me3, we overlaid genes upregulated in PB following inhibitor treatment on a scatterplot comparing PB/nB gene expression (146) versus change in H3K4me3 enrichment (117) in a manner similar to Figure 5A. A majority of the GSK-J4 upDEG corresponded to genes that exhibited minimal, if any, change in H3K4me3 methylation during B cell differentiation (Figures 2-5F and 2-5G). Thus, the data strongly suggest the genes upregulated following inhibitor treatment are the result of inhibiting H3K4me3 demethylases.

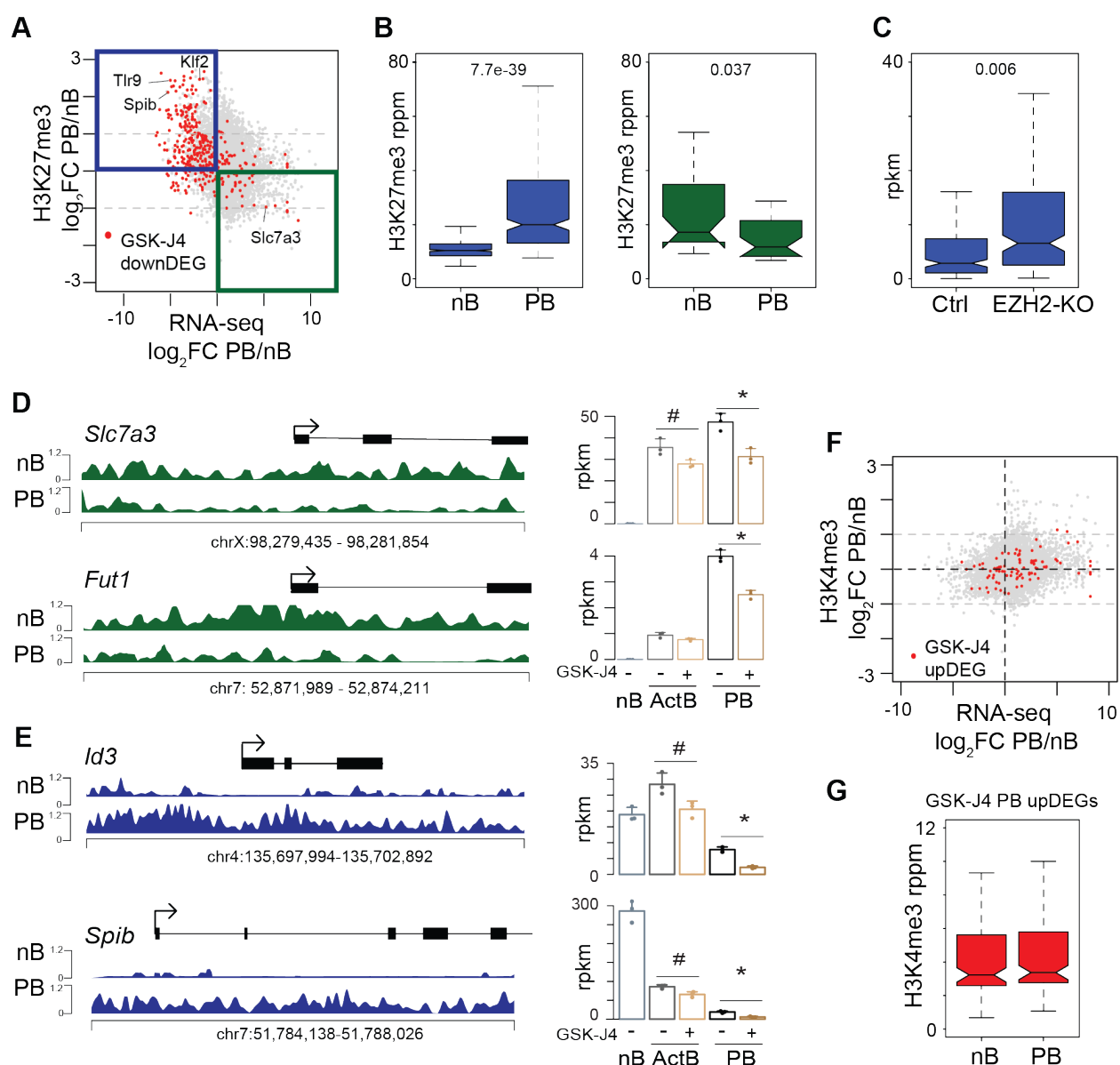


Figure 2-5. DEGs are enriched for genes regulated by H3K27me3 levels.

(A) The \log_2 FC change in gene expression between PB and nB (Haines *et al.* 2018) was plotting against the \log_2 FC change in H3K27me3 between PB and nB (Guo *et al.* 2018) as in Figure 1. GSK-J4 downDEG between GSK-J4 and DMSO treated PB were represented by red dots. (B) Quantification of H3K27me3 levels in wild type nB and PB at GSK-J4 downDEG. (C) Average expression of GSK-J4 downDEG in the “blue” quadrant in A in EZH2-sufficient and -deficient PB (Guo *et al.* 2018). (D, E) Examples of GSK-J4 downDEG regulated by H3K27me3 levels. * FDR < 0.05 and >1.5 fold change, # FDR < 0.05 with <1.5 fold change. (F) The \log_2 FC change in gene expression between PB and nB (Haines *et al.* 2018) was plotting against the \log_2 FC change in H3K4me3 between PB and nB (Scharer *et al.* 2018). GSK-J4 upDEG between GSK-J4 and DMSO treated PB PB comparison were represented by red dots. (G) Quantification of H3K4me3 levels in wild type nB and PB at GSK-J4 upDEG.

IV. DISCUSSION

This study investigated the role of histone H3K27me3 demethylation by UTX and JMJD3 on B cell differentiation through the use of GSK-J4, a pharmacological inhibitor that functions as a competitor for their substrate α -ketoglutarate (258). GSK-J4 was previously shown to display high specificity for UTX and JMJD3 and H3K27me3 demethylation and acted at a lower specificity towards H3K4me3 demethylases (258, 261). GSK-J4 treatment of nB cells stimulated with LPS, IL-2, and IL-5 led an increase in the frequency of PB and dysregulation in gene expression. Despite promoting PB formation, GSK-J4 treatment had no influence on the ability of treated cells to secrete antibodies. At the molecular level, GSK-J4 treatment during the differentiation process led to more genes being down regulated than expected. This observation suggests that the changes are likely driven by inhibition of UTX and JMJD3, which by removal of the inhibitory histone mark H3K27me3 normally promote gene expression. Some of these dysregulated genes included those associated with hypoxia, signaling, apoptosis, and P53 pathways, including cell cycle inhibitor *Cdkn2a* (263). The transcription factors SPIB and ID3, which are known PB repressors (107, 260), were also downregulated and may account for the upregulation of PC-signature genes. Other genes found to be upregulated by GSK-J4 treatment during the differentiation process were associated with cell cycle and proliferation. These changes in gene expression were correlated with an increase of actively proliferating BrdU⁺ cells following GSK-J4 treatment of *ex vivo* differentiated nB. Thus, targeting cell cycle inhibitors and PB repressors are in part responsible for the increases in PB appearing following inhibition of these demethylases.

Epigenetic remodeling is necessary during B cell differentiation (115, 117, 141), and the histone modification H3K27me3 shows dynamic changes at thousands of loci with sites both gaining and losing the mark. A majority of GSK-J4 down modulated DEG were associated with

changes in promoter localized H3K27me3 – although other changes can be observed in the gene body – during the differentiation process. This observation is consistent with the active and direct demethylase activities of UTX and JMJD3 in which a subset of GSK-J4 downDEG corresponded to genes that normally lose promoter H3K27me3 and gain expression as B cells differentiate. Surprisingly, a number of GSK-J4 down modulated DEG matched genes that normally gain promoter H3K27me3 and are downregulated as B cells differentiate to PB. This included transcription factors known to repress the PB fate. Thus, UTX and JMJD3 might function as the rheostat or counterbalance for H3K27me3 by counteracting the activity of EZH2, the H3K27 methyltransferase. Taken together, these data suggest that the level of promoter H3K27me3 and gene expression during B cell differentiation is modulated by three distinct mechanisms: 1) direct control of a gene by either UTX/JMJD3 or EZH2; 2) a balanced control in gene expression in which both UTX/JMJD3 and EZH2 compete for the same genes, resulting in fine tuning of gene expression; or 3) indirect control of gene expression through passive loss of H3K27me3 through cell division in which EZH2 is no longer recruited to a locus.

There is growing evidence that the balance in the levels of histone modifications are necessary for proper B cell differentiation. Methylation of H3K4 is associated with gene activation and has been shown to play a critical role in B cells (120). Deletion of *Kmt2d*, the H3K4 methyltransferase, led to an increase in germinal center B cells as a result of enhanced proliferation capacity of follicular B cells lacking *Kmt2d* (147). Deletion of LSD1, the H3K4me1/2 demethylase, resulted in the opposite phenotype. B cells lacking LSD1 showed reduced proliferation and differentiation following T cell independent stimulation (146), as well as reduced germinal center B cells (278). In a similar scenario, deletion of EZH2 resulted in reduction in germinal center and plasma cell formation and reduced proliferation (137, 138, 141); whereas,

here, inhibition of UTX and JMJD3 led to increased PB formation and enhanced cell proliferation. Together, these results suggest that balanced level of opposing histone modifications is necessary for maintaining B cell fate and controlling cell proliferation.

The importance of balanced levels of histone modification is well exemplified by the fact that mutations in various epigenetic modifiers are frequently found in cancer (236). In particular, gain of function mutations in *EZH2* have been identified in various human malignancies, including DLBCL, which results in increased promoter H3K27me3 methylation at cell cycle checkpoint genes including *CDKN1A* and genes associated with germinal center exit (137). However, mutations in *UTX* are typically loss-of-function or deletion, which leads to a failure to demethylate H3K27me3. This results in increased levels of H3K27me3, possibly mimicking *EZH2* hyperactivation (229, 257). Furthermore, attempts to re-establish a homeostatic level of this histone modification have proved to be an effective therapeutic avenue for human cancers as *EZH2* inhibitors are in clinical use and ongoing trials (237). A recent study has also proposed the use of *EZH2* inhibitors for malignancies with *UTX* loss-of-function mutations. Treatment with *EZH2* inhibitors led to reduced viability and cell cycle arrest of multiple myeloma cell lines lacking *UTX* and resulted in reduced tumor burden *in vivo* (231). Taken together, the balanced level of H3K27me3 is necessary to maintain homeostatic and prevent development human malignancies.

The role of UTX and JMJD3 has been examined in various cells types, including the hemopoietic lineage. Interestingly, several studies revealed demethylase independent roles for these enzymes in addition to their known role in active demethylation. The demethylase activity of UTX is required for the formation of invariant natural killer T cells; however, in mouse embryonic stem cells UTX cooperates with MLL4 complex and p300 to convert enhancers from an inactive to active state. This action occurs in the absence of the demethylase activity of UTX.

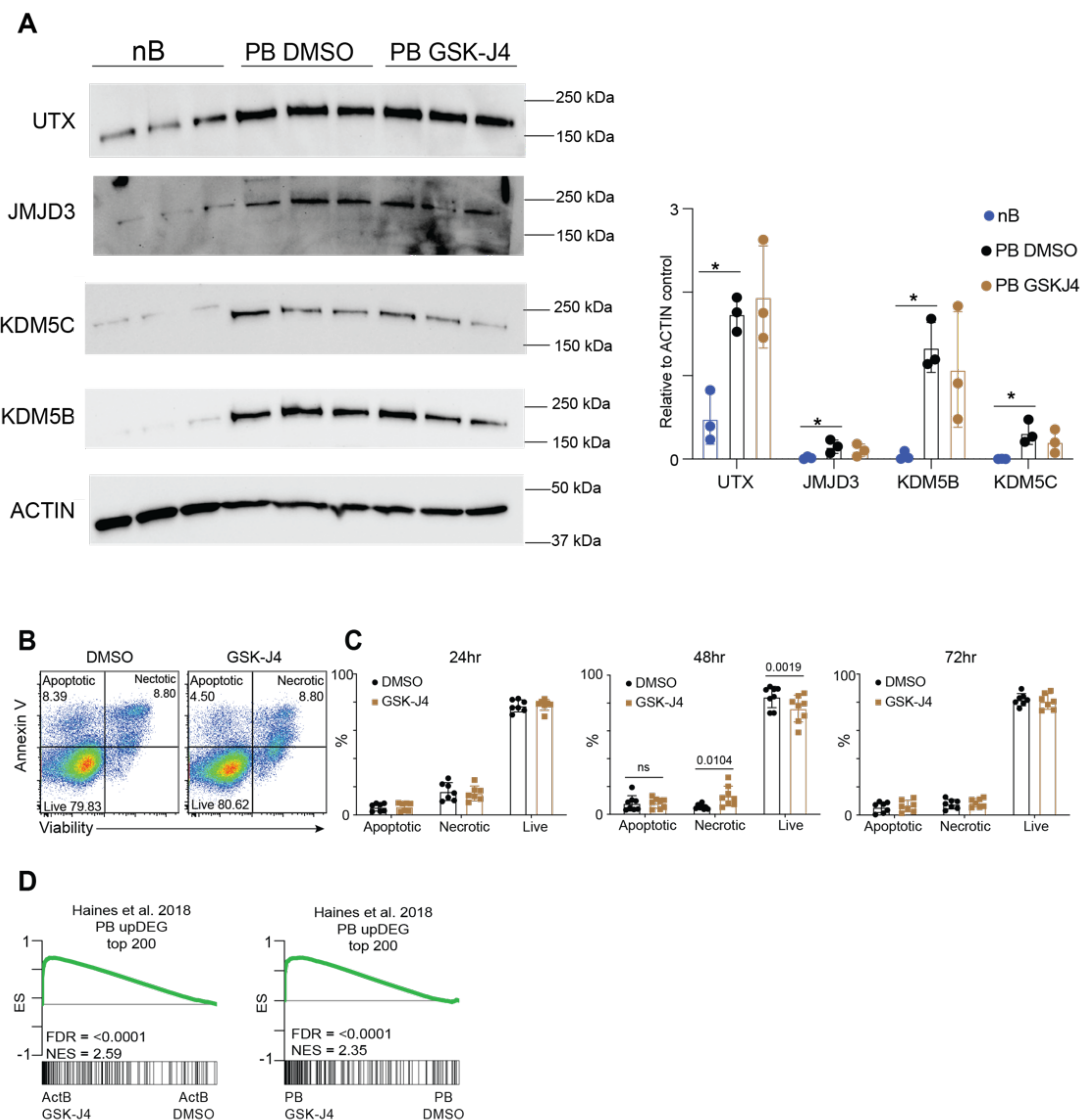
In this setting, UTX promotes and enhances the activity of its binding partners to promote H3K4me1 and H3K27ac at enhancers (182). The inhibitor utilized in this study targets the catalytic activity of UTX and JMJD3 thus allowing for a targeted analysis of active H3K27me3 demethylation by both enzymes during B cell differentiation.

While the presented data strongly suggest that the observed increase in PB is the result of the inhibition H3K27me3 demethylases, the GSK-J4 has also been shown to act on other histone demethylase (258, 261). As such, it remains possible that the observed increase in PB following GSK-J4 treatment is a cumulative effect of inhibiting multiple demethylases, including UTX and JMJD3. The development of new compounds specifically targeting the H3K27me3 demethylases is necessary to more definitely address the role of inhibition of UTX and JMJD3 in B cell differentiation.

Mutations in *UTX* and *JMJD3* have been reported in various cancers and several studies identified GSK-J4 as a potential therapeutic treatment for a subset of malignancies driven by gain of function mutations in these genes (235, 279, 280). Despite the promising effects of GSK-J4 as a cancer treatment, this drug is not currently used in any clinical trials, likely due to its non-specific activity towards other demethylases. The work presented here would suggest that targeted UTX/JMJD3 inhibition could result in increased PB and PC formation that may exacerbate normal immune responses in treated patients.

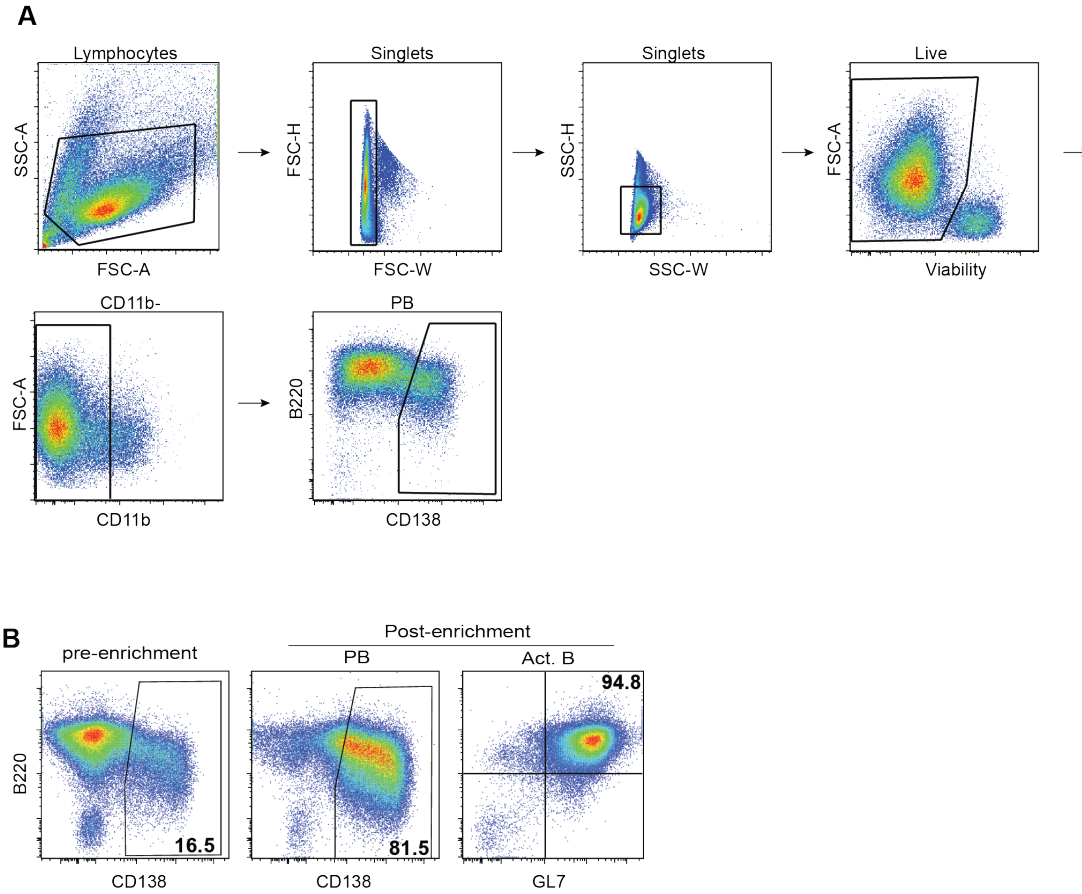
In summary, the work described here demonstrates an important balance in the control of gene expression potentially regulated by the placement and removal of repressive histone modifications at histone H3K27. The dynamic changes in this histone modification at the targeted loci are likely critical for maintaining the cell fates as a B cell or as plasma cells following their complex differentiation process.

V. SUPPORTING DATA



Supplemental Figure 2-1. UTX and JMJD3 are upregulated in PC.

(A) Representative western blot and quantitation of KDM5C, KDM5B, UTX, and JMJD3 protein levels in naive B cells and plasmablasts from DMSO or GSK-J4 treated ex vivo cultures (left). Normalized to Actin control (right). (B) Representative plots of Annexin V versus Viability in DMSO and 250nM GSK-J4 treated cultures after three days of ex vivo stimulation. (C) Frequency of apoptotic, necrotic, and live cells in DMSO and 250nM GSK-J4 treated cells at 24hr (left), 48hr (middle), and 72hr (left) of ex vivo stimulation. (D) GSEA for top 200 gene upregulated in PB (Haines et al. 2018) in GSK-J4 treated ActB (left) and PB (right) versus control. (E) The log₂FC change in H3K4me₃ between PB and nB (Scharer et al. 2018) was plotted against the log₂FC change in gene expression between PB and nB (Haines et al. 2018). GSK-J4 upDEG in PB comparison were represented by red dots. (F) Quantification of the levels of H3K4me₃ at GSK-J4 upDEG in wild type nB and PB from E.



Supplemental Figure 2-2. Representative gating strategies.

(A) General gating strategy use for FLOW cytometry analyses to assess PB formation. (B) Representative FLOW cytometry plots for ActB and PB enrichments performed at day 3 of ex vivo culture. Purity is indicated as the frequency of single cells.

VI. METHODS

Mice

C57BL/6J mice (Stock# 000664) were purchased from Jackson Labs and bred on site. All animals were housed by the Emory Division of Animal Resources following protocols approved by the Emory Institutional Animal Care and Use Committee.

Ex vivo differentiation

Naïve splenic B cells were magnetically enriched by negative selection using CD43 (Ly-48) MicroBeads (Miltenyi Biotec 130-097-148) with >95% purity. Unless otherwise stated, purified B cells were cultured at 0.5×10^6 cells/ml of B cell media (RPMI 1640, 10% heat-inactivated FBS, 0.05 mM 2-ME, 1X nonessential amino acids, 1X penicillin/streptomycin, 10 mM HEPES, and 1 mM sodium pyruvate) supplemented with 20 μ g/ml LPS (Sigma L2630), 20 ng/ml IL-2 (Biolegend 575406), and 5 ng/ml IL-5 (Biolegend 581504). LPS and cytokines were supplemented with half the above dose at 24 and 48hr of *ex vivo* culture as previously described (259). In some experiments, naïve B cells were stained with 5 μ M Cell Trace Violet (Life Technologies C34557) prior to culturing. GSK-J4 (Sigma SML0701) and GSK-J5 (Cayman Chemical, 12074) were dissolved in DMSO and diluted in B cell media. Cells were treated daily with 250nM GSK-J4 or DMSO. For CD40L stimulation, cells were seeded at 10^5 cells/ml in the above B-cell media containing CD40L (100 ng/ml, R&D Systems), IL-5 (5 ng/ml) and IL-4 (20 ng/ml, R&D Systems). Cultures were supplemented with the cytokines at each subsequent day of culture. For bromodeoxyuridine (BrdU) cell cycle analysis, cells were washed, resuspended in fresh media containing 10 μ M BrdU, and incubated at 37°C for two hours. Cell proliferation analysis then

performed using Phase-Flow FITC BrdU Kit following the manufacturer's protocol (Biolegend 370704).

Flow Cytometry

Cells were resuspended at 10^6 per 100 μ l of FACS buffer (1X PBS, 1%BSA, and 2mM EDTA) and blocked with anti-Fc (anti-CD16/CD32) (Tonbo Biosciences, 2.4G2). The following antibodies were used to for staining: B220-PE-Cy7 (Tonbo Biosciences RA3-6B2), CD138-BV711 (BD, 281-2), GL7 eFluor660 (eBioscience, GL-7), CD11b-FITC (Tonbo Biosciences, M1/70), and Ghost Dye™ Red 780 (Tonbo Biosciences 13-0865) to asses viability. The Annexin V FITC Apoptosis Detection Kit (eBioscience BMS500FI-100) was used to assess cell death. Cells were stained for 40 min and fixed using 1% paraformaldehyde.

Enrichment of CD138+ PB was performed by staining with CD138-APC (BD, 281-2), followed by magnetic enrichment using anti-APC MicroBeads (Miltenyi # 130-090-855). For RNA-seq, GL7+ cells were further enriched from the CD138-depleted fractions using GL7-PE (Biolegend #144608) and anti-PE MicroBeads (Miltenyi #130-105-639).

Flow cytometry was performed on a BD LSRII using FACSDiva (v6.2) and analyzed using FlowJo software. The following gating strategy preceded all flow cytometry analyses presented. Cells were gated on 1) lymphocytes (forward light scatter [FSC]–area by side scatter [SSC]–area), 2) singlets (FSC-height by FSC- width), 3) singlets (SSC- height by SSC-width), 4) live cells (Viability Dye negative), with 5) the exclusion of contaminating macrophages bearing CD11b (Supplemental Figure2A).

Western Blot

Ex vivo cultured B cells were lysed on ice in RIPA buffer (150mM NaCl, 0.5% sodium deoxycholate, 0.1% SDS, 1% IGEPAL, 20% glycerol, 50mM Tris pH 8.0) for 20 min. Protein concentration was determined by a Bradford assay (BioRad Inc.). Primary antibody incubation was conducted at 4° C overnight, followed by several washes and a one-hour incubation with the secondary antibody. The following antibodies were used: anti-UTX (Cell Signaling, 33510S), anti-JMJD3 (LSBio, C96528), anti-KDM5B (Abcam, ab181089), anti-KDM5C (Proteintech 14426-1-AP), and anti-ACTIN (Santa Cruz, sc69877). Blots were developed using the Immunobilon Crescendo HRP Substrate (Sigma, WBLURO100) and visualized on Biorad ChemiDoc MP Imaging System.

Enzyme-Linked Immunosorbent Assay (ELISA)

Equal numbers of DMSO- or GSK-J4-treated plasmablasts were cultured in fresh B cell media. After 2.5hr, the supernatant was collected and used to perform ELISA. ELISA plates (Sigma M9410) were coated with goat anti-mouse Ig (Southern Biotechnology 5300-05B) overnight at 4° C and blocked with 3% nonfat dry milk. Standard IgM antibody (Southern Biotechnology 5300-01B) and collected media supernatants were incubated for 2 hr at room temperature, followed by washes, and incubation with HRP-conjugated goat anti-mouse secondary antibody (Southern Biotechnology 1021-05) for 2 hr at room temperature. The plates were developed using the TMB ELISA peroxidase substrate (Rockland 800-666-7625) and the reaction was stopped using 0.2M sulfuric acid. Plates were read using a Synergy HT Multi-Mode Microplate Reader (BioTek).

RNA-seq

RNA was isolated from magnetically enriched PB and ActB using Zymo Quick-RNA MicroPrep

Kit (11-328M). Sequencing libraries were generated using mRNA HyperPrep Kit (KAPA Biosystems KR1352) with 500ng input RNA per sample. Final libraries were quality checked on a bioanalyzer, quantitated by quantitative PCR (qPCR), pooled at equimolar ratio, and sequenced on a HiSeq2500 using paired- end, 50-bp sequencing chemistry. TopHat2²⁷ was used to map the raw sequencing reads to the mm9 mouse genome. For each sample, reads that overlapped exons of unique ENTREZ genes were annotated using the GenomicRanges (v1.22.4) package in R/Bioconductor. Differential expression analysis was performed using Bioconductor package edgeR using $FDR \leq 0.05$ and 1.5-fold change ($\log_2 = 0.58$) (Supplemental Table 1). PCA was performed using vegan package and the indicated z-score normalized gene list. For gene set enrichment analysis (GSEA)(262), all detected genes were ranked by multiplying the sign of fold change by the $-\log_{10}$ (P value).

Data and Code Availability

All sequencing data have been deposited in NCBI Gene Expression Omnibus (GEO) under the accession codes GSE158139. Code and data processing scripts are available from the corresponding author upon request and at <https://github.com/cdschar/>.

Chapter 3. H3K27me3 demethylase UTX restrains plasma cell formation

Anna K. Kania, Madeline J. Price, Lou-Ella George-Alexander, Dillon G. Patterson^{*}, Sakeenah L. Hicks, Christopher D. Scharer, and Jeremy M. Boss[#]

Department of Microbiology and Immunology, Emory University School of Medicine, Atlanta, GA 30322, USA

[#] Correspondence: Jeremy M. Boss; phone: 404-727-5973; email: jmboss@emory.edu

^{*} Current address: Department of Immunology, Blavatnik Institute, Harvard Medical School, Boston, MA 02115, USA

Author Contributions

A.K.K. designed and performed experiments, analyzed, and interpreted the data, and wrote the manuscript; M.J.P. and D.G.P. performed experiments. L.G.A. performed CUT&Tag and helped with experiments. S.L.H generated sequencing libraries. C.D.S. designed experiments and interpreted the data. J.M.B designed experiments, interpreted the data, and wrote the manuscript.

This manuscript was submitted to *The Journal of Immunology*.

I. ABSTRACT

B cell differentiation is associated with substantial transcriptional, metabolic, and epigenetic remodeling, including redistribution of histone H3 lysine 27 trimethylation (H3K27me3), which is associated with a repressive chromatin state and gene silencing. While the role of the methyltransferase EZH2 in B cell fate decisions has been well established, it is not known whether H3K27me3 demethylation is equally important. Here, we showed that simultaneous genetic deletion of the two demethylases UTX and JMJD3 (dKO) led to a significant increase in plasma cell (PC) formation following stimulation with the T cell independent antigens LPS and NP-Ficoll. This phenotype occurred in a UTX-dependent manner as UTX single KO (sKO) mice, but not JMJD3 sKO, mimicked the dKO. While UTX- and JMJD3-deficient marginal zone B cells showed increased proliferation, dKO follicular B cells also showed increased PC formation. In fact, dKO PC upregulated genes associated with oxidative phosphorylation and exhibited increased spare respiratory capacity. Mechanistically, deletion of *Utx* and *Jmjd3* resulted in higher levels of H3K27me3 at proapoptotic genes and resulted in reduced apoptosis of dKO PC *in vivo*. Furthermore, UTX regulated chromatin accessibility at regions containing ETS and IRF transcription factors motifs, including motifs of known repressors of PC fate. Taken together, these data demonstrate that the H3K27me3 demethylases restrain B cell differentiation.

II. INTRODUCTION

Robust differentiation of naïve B cells (nB) into antibody secreting plasma cells (PC) and memory B cells is the cornerstone of a long lasting humoral immune response (5, 33). The nB compartment in the spleen consists of marginal zone B cells (MZB) and follicular B cells (FOB) (26, 27). The former predominately respond to T-cell independent (TI) antigens such as lipids and polysaccharides and differentiate into short-live PC (SLPC). In contrast, FOB facilitate the response to protein antigens in a T cell dependent (TD) manner. TD responses lead to the formation of germinal centers (GC), where B cells undergo somatic hypermutation and affinity maturation, followed by differentiation into long-lived plasma cells (LLPC) or memory B cells (7, 80). While SLPC and LLPC differ in their longevity, location, and affinity, they share a common transcriptional signature, suggesting that aspects of B cell differentiation are conserved across both responses (46).

The transition from quiescent nB to antibody secreting PC requires significant transcriptional, metabolic, and epigenetic rewiring (7, 34). At the transcriptional levels, the nB and PC are regulated by distinct sets of mutually antagonist transcription factors (80, 281). Whereas PAX5 (17, 97, 113, 241) and BACH2 (102, 104) promote the nB stage, BLIMP1 (242-244) and IRF4 (112, 245) promote PC fate. The transcriptional and physiological adaptations are accompanied by changes in chromatin accessibility, chromatin organization as well as the distribution of histone modifications and DNA methylation (34, 120, 246, 247).

Histone 3 lysine 27 trimethylation (H3K27me₃) is an epigenetic modification associated with a repressed chromatin state and gene silencing (134). Addition of this histone modification is catalyzed by EZH2 (Enhancer of zeste homolog 2), a member of the PRC2 complex (135, 136, 248). The two demethylases UTX (Ubiquitously transcribed tetratricopeptide repeat, X

chromosome; KDM6A) and JMJD3 (Jumonji Domain-Containing Protein 3; KDM6B) facilitate the removal of H3K27me_{2/3} (169-171, 202). UTX has a homolog on the Y chromosome, UTY, which exhibits very little, if any, catalytic activity (169, 171, 175). Previous studies revealed that H3K27me₃ is dynamically regulated during B cell differentiation (141), suggesting that redistribution of H3K27me₃ might be necessary for plasma cell formation. In fact, EZH2 has been shown to play a critical role in B cell development (139, 249), GC formation (137, 138, 250), and B cell differentiation into PC (141). However, less is known about the role of UTX and JMJD3 in B cells.

UTX and JMJD3 regulate gene expression in a demethylase-dependent manner by modulating the levels of H3K27me₃ or in a demethylase-independent manner via interaction with proteins complexes containing BRG1 (181), CHD4 (251), and MLL (228, 252). These enzymes have been shown to play critical roles in embryonic development (187, 189, 190) and within the hemopoietic lineage (200, 201, 203, 212, 216, 217). Furthermore, mutations in these enzymes occur in various malignancies (282), including diffuse large B cell lymphoma (232, 234) and multiple myeloma (231, 256) suggesting a potential role of UTX and JMJD3 in regulating B cell fate. In fact, overexpression of *Jmjd3* in human germinal centers has been reported to induce changes in the expression of genes associated with PC and memory B cell fate (219). Moreover, B cell specific deletion of *Utx* has been shown to accelerate lymphoma development in mice (232), while deletion of this enzyme in all hematopoietic cells impaired the commitment to the B cell lineage, hindering B cell development (218). However, little is known about the role of these enzymes in terminal B cell differentiation, thus leaving a significant gap in our understanding of the epigenetic regulation of PC formation.

This study aimed to examine the role of UTX and JMJD3 in B cell differentiation. Deletion of these enzymes led to a significant increase in PC formation, with a corresponding increase in serum antibody titers following stimulation with TI antigens. Intriguingly, loss of *Utx*, but not *Jmjd3*, was sufficient to drive PC differentiation. UTX- and JMJD3-deficient MZB upregulated genes associated with cell growth and proliferation and exhibited proliferative advantage. Further differences were observed at the PC stage, as UTX- and JMJD3-deficient PC exhibited higher spare respiratory capacity and reduced apoptosis, which correlated with enrichment of H3K27me3 at proapoptotic genes. Collectively, this study places UTX as an epigenetic factor restraining B cell differentiation into PC.

III. RESULTS

Deletion of *Utx* and *Jmjd3* leads to an increase in PC

To examine the role of UTX and JMJD3 in B cell differentiation, floxed *Utx* and *Jmjd3* alleles (205) were crossed to *Cd19^{Cre/+}* mice (283) to obtain B cell specific deletion of both enzymes (**dKO**). Efficient deletion of both enzymes was observed in nB with a corresponding reduction of *Utx* and *Jmjd3* mRNA levels (**Sup. Fig. 3-1C-E**). To understand the role of H3K27me3 demethylases in B cell differentiation, the steady-state levels of PC were assessed in naïve *Cd19^{Cre/+}* (**Ctrl**) and dKO mice. Although the total numbers of PC in a naïve animal were substantially lower than in immunized animals, the loss of *Utx* and *Jmjd3* resulted in higher basal levels of PC in the spleen but not in the bone marrow (**Fig. 3-1A, Sup. Fig. 3-1F**). Moreover, this difference in PC corresponded to higher basal IgM antibody titers in the serum of dKO mice (**Fig 3-1B**). To assess whether deletion of *Utx* and *Jmjd3* affects PC formation following a challenge with an antigen, Ctrl and dKO mice were stimulated with LPS and PC formation was examined 3 days later by flow cytometry. A significant increase of splenic CD138⁺ PC was observed in dKO mice which correlated with higher serum IgM antibody titers in dKO mice 3 days after LPS stimulation (**Fig. 3-1C and 3-1D**). An increase in the frequency of PC was also observed after three days of *ex vivo* culture of naïve Ctrl and dKO B cell cells with LPS alone or LPS supplement with IL-2, and IL-5 as described previously (259) (**Sup. Fig. 3-1G and 3-1H**). Additionally, an increase in splenic CD138⁺ PC and NP-specific antibody titers was also observed following stimulation with the type II TI antigen NP-Ficoll. (**Fig. 3-1E and 3-1F**). These data suggest that UTX and JMJD3 are negative regulators of PC formation.

To assess whether the H3K27me3 demethylases also regulate B cell differentiation in response to TD antigens, Ctrl and dKO were infected with PR8 influenza virus and sacrificed ten

days later to evaluate PC formation. A significant increase in the PC frequency but not cell number was observed in the draining lymph nodes of dKO mice (**Fig. 3-1G**). Unlike the responses to TI antigens, this phenotype occurred in a sex-specific manner, with the significant differences observed only in the female dKO mice. This suggests that the UTX Y chromosome homologue UTY, which may possess low catalytic activity (175), may compensate for the loss of *Utx* under these infection conditions.

To examine whether deletion of *Utx* and *Jmjd3* impacted the composition of the naïve B cell compartment, B cell development in Ctrl and dKO mice was assessed.. The frequency of total B cells and immature B cells in the spleen were similar between the groups; however, the absolute numbers of cells were higher in dKO due to the overall increase in the number of splenocytes and spleen size. (**Sup. Fig. 3-2A-C**). However, a significant increase in CD93⁻CD21⁺CD23⁻ MZB, CD93⁻IgM⁺CD21⁺CD23⁺ MZB precursors, and CD93⁺IgM⁺CD23⁺ T2 transitional B cells was observed (**Fig. 3-2A, Sup. Fig. 3-2D and 3-2E**). Analysis of early B cell development in the bone marrow revealed an increase in pro/pre-B cells and a reduction in the frequency of mature recirculating B cells (**Sup. Fig. 3-2F**).

The increase in MZB, which predominately respond to TI antigens, raised the possibility that the increase in PC following LPS stimulation resulted from the altered composition of the mature B cell compartment in the spleen. To address this possibility, Ctrl and dKO MZB were magnetically enriched (**Sup. Fig. 3-3A**), plated in equal numbers, and cultured *ex vivo* with LPS, IL-2, and IL-5 to promote PC formation. Flow cytometry analysis of the cultured cells was performed three days later. A significant increase in PC was observed in the dKO cultures (**Fig. 3-2B**), suggesting that the increase in MZB frequency in naïve animals alone does not fully explain the increase in PC following *in vivo* stimulation.

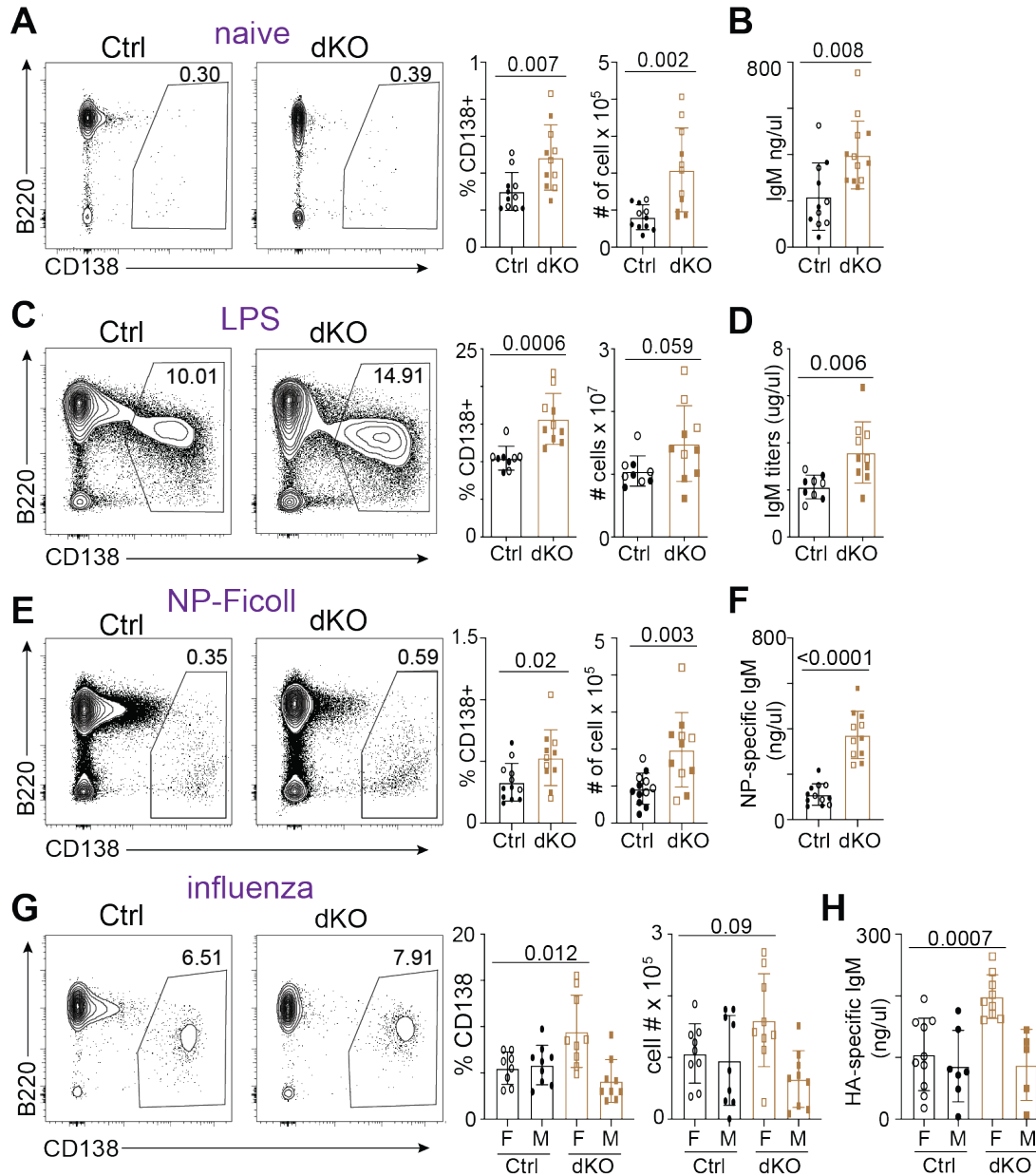


Figure 3-1. Deletion of *Utx* and *Jmjd3* promotes PC formation.

(A) Representative plots of B220 and CD138 expression (left) and quantification of splenic CD138⁺ PC from the highlighted gates (right) in naïve Ctrl and dKO mice. (B) Serum IgM antibody titers of Ctrl and dKO from (A). (C) Representative plots of B220 and CD138 expression (left) and quantification of splenic CD138⁺ PC three days later after stimulation with 50 μ g LPS. (D) Serum IgM antibody titers of Ctrl and dKO from (C). (E) Representative plots of B220 and CD138 expression (left) and quantification of splenic CD138⁺ PC (right) seven days after stimulation with 50 μ g NP-Ficoll. (F) Serum NP-specific IgM antibody titers of Ctrl and dKO mice from (E). (G) Representative plots of B220 and CD138 expression (left) and quantification of CD138⁺ PC in the draining lymph nodes (right) ten days after infection with 150,00 vfu of PR8

influenza virus. (H) Hemagglutinin (HA)-specific serum IgM antibody titers of Ctrl and dKO from (G). Females are designated with open symbols and males with closed symbols. The data represent combined results of at least two independent experiments with a minimum of 3 mice per group. Significance was determined by Student's *t* test with *p*-values ≤ 0.05 considered significant.

The increase in MZB, which predominately respond to TI antigens, raised the possibility that the increase in PC following LPS stimulation resulted from the altered composition of the mature B cell compartment in the spleen. To address this possibility, Ctrl and dKO MZB were magnetically enriched (**Sup. Fig. 3-3A**), plated in equal numbers, and cultured *ex vivo* with LPS, IL-2, and IL-5 to promote PC formation. Flow cytometry analysis of the cultured cells was performed three days later. A significant increase in PC was observed in the dKO cultures (**Fig. 3-2B**), suggesting that the increase in MZB frequency in naïve animals alone does not fully explain the increase in PC following *in vivo* stimulation.

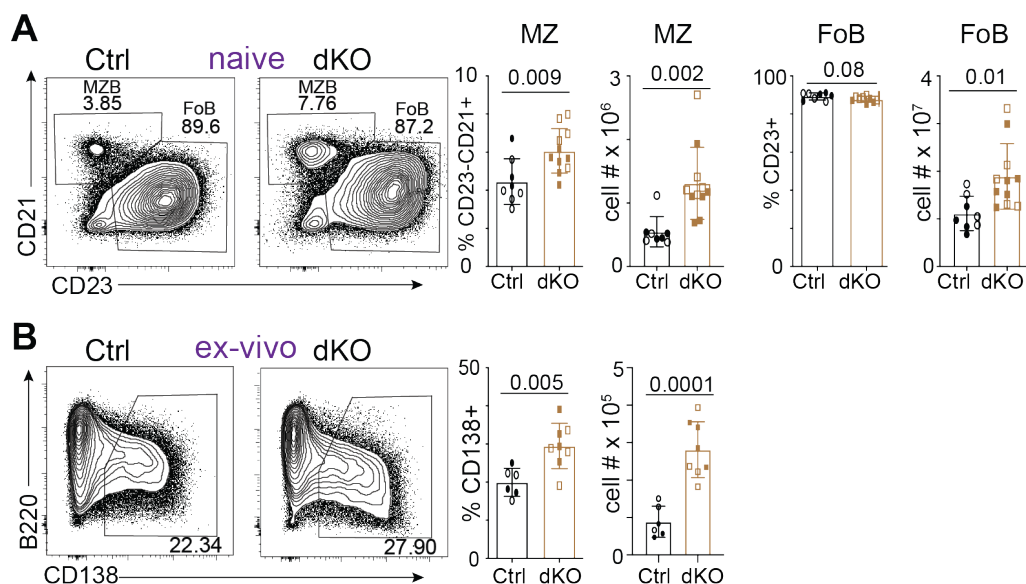


Figure 3-2. UTX- and JMJD3-deficient MZB generate more PC

(A) Representative plots and of CD21 and CD23 expression in B220⁺CD93⁻ naïve Ctrl and dKO mice and quantification of splenic B220⁺CD93⁻CD21⁺ MZB and B220⁺CD93⁻CD21^{mid/low}CD23⁺ FoB. (B) Magnetically enriched splenic Ctrl and dKO MZB were cultured *ex vivo* with LPS, IL-2, IL-5. Representative plots of B220 and CD138 expression (left) and quantification of CD138⁺

PC (right) after three days of ex vivo culture. Each point represents samples from individual mice. Females are designated with open symbols and males with closed symbols. The data represent combined results of at least two independent experiments with a minimum of 3 mice per group. Significance was determined by Student's *t* test with *p*-values ≤ 0.05 considered significant.

Loss of UTX alone leads to increases in PC formation

To evaluate whether UTX and JMJD3 are both contributing to regulating B cell differentiation, single knockout mice lacking either *Utx* (**UTX sKO**) or *Jmjd3* (**JMJD3 sKO**) were created. Ctrl, dKO, and sKO mice were inoculated with LPS and sacrificed three days later to evaluate PC formation. Whereas PC formation in UTX sKO animals was comparable to that observed in dKO, PC formation in JMJD3 sKO mice mimicked that of Ctrl mice (**Fig. 3-3A and 3-3B**). Consistent with the increase in PC observed in dKO and UTX sKO, IgM antibody titers were also higher in those two genotypes relative to Ctrl or JMJD3 sKO mice (**Fig. 3-3C**). Thus, the data suggest that UTX is primarily responsible for the observed phenotype and increase in PC formed following *in vivo* stimulation. However, to ensure a complete loss of all active demethylation of H3K27me3, mice deficient in both UTX and JMJD3 were used for subsequent experiments.

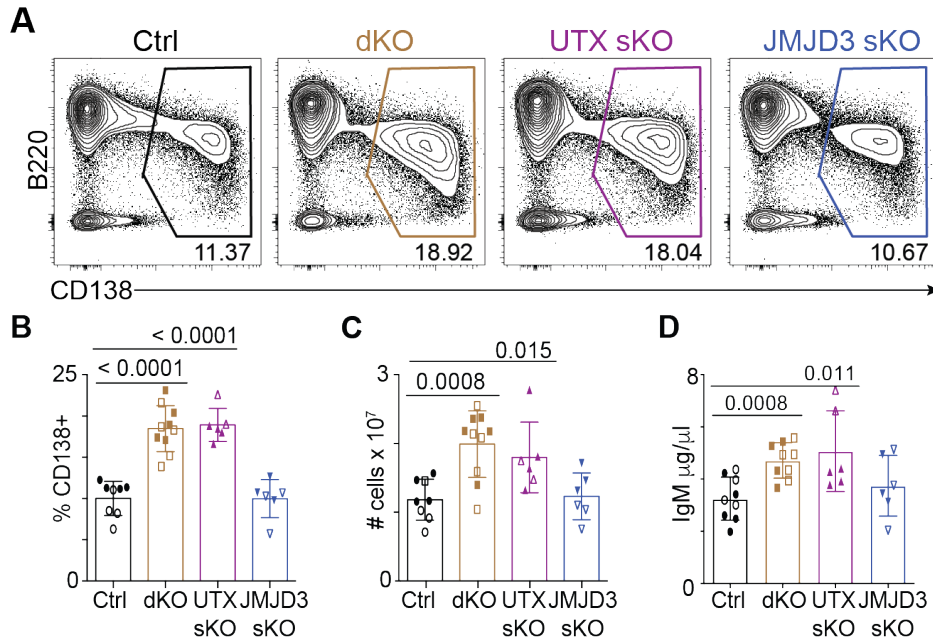


Figure 3-3. Loss of UTX alone leads to increases in PC formation.

(A) Representative plots of B220 and CD138 expression in Ctrl, dKO, UTX sKO, JMJD3 sKO mice three days after stimulation with 50 μ g LPS. Quantification of splenic CD138⁺ PC frequency (B) and absolute cell numbers (C) from (A). (D) Serum IgM antibody titers of Ctrl, dKO, UTX sKO, JMJD3 sKO mice from (A). Females are designated with open symbols and males with closed symbols. The data represent combined results of two independent experiments with a minimum of 3 mice per group. Significance was determined by two-tailed Student's *t* test with *p*-values ≤ 0.05 considered significant.

Deletion of *Utx* and *Jmjd3* leads to changes in the B cell transcriptome

To begin to understand the molecular mechanism by which UTX and JMJD3 regulate B cell differentiation, RNA-seq was performed on FACS-isolated splenic MZB (B220⁺CD93⁻CD21⁺CD23⁻) and FOB (B220⁺CD93⁻CD21^{mid}CD23⁺) cells from naïve Ctrl and dKO animals, as well as PC that were generated after three days of ex vivo culture of both MZB and FOB (Sup. Fig. 3-3B and 3-3C). The gene expression profiles of the sorted populations corresponded with previously published gene sets and a subset of differentially expressed genes (DEG) was validated by RT-qPCR (Sup. Fig. 3-3E, 3-3F, 3-4A) (46, 148). Differential expression analysis revealed that in each comparison, were skewed toward genes downregulated following deletion of *Utx* and

Jmjd3, which is consistent with the role of these enzymes in promoting gene expression (**Fig. 3-4A**). Furthermore, consistent with the phenotypic analysis, the highest numbers of DEG were observed in the naïve MZB comparison and the MZB-PC (**Fig. 3-4A**). To identify pathways regulated by UTX and JMJD3 during B cell differentiation, gene set enrichment analysis (GSEA) (262) was performed. This analysis revealed that naïve dKO MZB upregulated *Myc* expression and downstream MYC target genes, which has been shown to function as a division timer regulating lymphocyte proliferation (284, 285)(**Fig. 3-4B, 3-4C**). Furthermore, UTX- and JMJD3-deficient MZB also upregulated other pathways associated with cell growth and metabolism, such as ribosome biogenesis, peptide metabolic process, and translation (**Fig. 3-4B, 3-4C**). Examples of genes upregulated in dKO MZB include the eukaryotic translation initiation factor 5B (*Eif5b*), and the metabolic enzyme Glutathione S-Transferase Omega (*Gsto1*). Both genes normally become upregulated upon PC differentiation and exhibited heightened expression in naïve dKO MZB (**Fig. 3-4D**). Taken together, the data suggest that dKO MZB have an enhanced transcriptional program that supports proliferation and morphological changes associated with differentiating into PC.

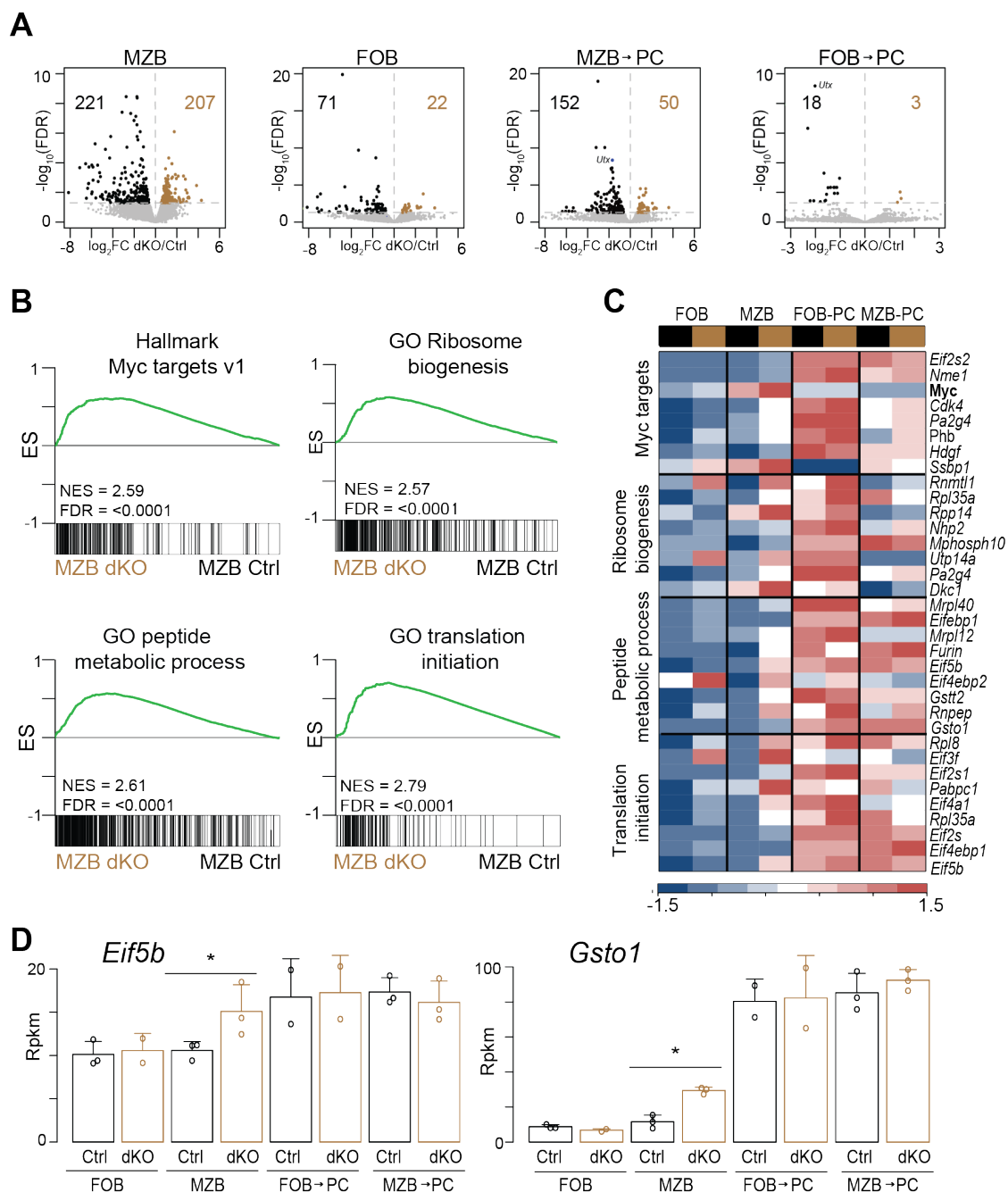


Figure 3-4. Deletion of *Utx* and *Jmjd3* results in upregulation of genes associated with cell growth and proliferation.

Splenic B220⁺CD93⁻CD21⁺ MZB and B220⁺CD93⁻CD21^{mid/low}CD23⁺ FOB from Ctrl and dKO mice were FACS isolated and saved for RNA-seq or cultured ex vivo with LPS, IL-2, and IL-5 as described in the methods section. Three days later, CD138⁺ PC generated from these cultures were isolated via FACS for RNA-seq. (A) Volcano plots representing DEG (FDR≤0.05) between Ctrl and dKO samples in each comparison. (B) GSEA plots for top pathways upregulated in dKO MZB. (C) Heatmap of z-score normalized Rpkms average expression top genes in gene datasets from (B) in each group. (D) Bar plots representing the expression of the indicated genes in all sample groups.

Asterisk represent DEG between the indicated pair. The data are the summary of results obtained from three biological replicates of Ctrl MZB, dKO MZB, Ctrl FOB, Ctrl MZB-PC, dKO MZB-PC and two biological replicates of dKO FOB, Ctrl FOB-PC, dKO FOB-PC.

dKO MZB exhibit a proliferative advantage

The upregulation of genes associated with cell growth and proliferation in dKO MZB raised the possibility that these transcriptional changes might lead to increased proliferation. To test this hypothesis and to assess the cell intrinsic nature of the PC phenotype, magnetically enriched Ctrl (CD45.1/2) and dKO (CD45.2) MZB or FOB were mixed at a 1:1 ratio, stained with CTV, and adoptively transferred into μ MT (CD45.1) mice, which lack B cells (91). The hosts were stimulated with LPS and bromodeoxyuridine (**BrdU**) was administered i.v. 60 h after LPS injection and 1 h before euthanasia to identify actively proliferating cells (**Fig. 3-5A, 3-5B, 3-5C**). In the MZB comparison, a significant increase in the frequency of CD138⁺ PC was observed in the dKO compartment compared to Ctrl mice (**Fig. 3-5D**). Importantly, dKO FOB also generated more PC than their Ctrl counterparts, suggesting that this phenotype was common to all differentiating B cells (**Fig. 3-5E**). Furthermore, PC formation was evaluated after a transfer into new hosts, suggesting that the increase in the frequency of PC occurred in a cell-intrinsic manner.

Cell division by CTV dilution revealed that more dKO MZB made it to the last detectable cell division compared with Ctrl MZB (**Fig. 3-5F**). Furthermore, the frequency of actively proliferating cells was significantly higher in dKO MZB (**Fig. 3-5H**). RNA-seq data analysis revealed no significant difference in *Tlr4* expression between Ctrl and dKO MZB (**Sup. Fig. 3-3G**), suggesting that the levels of the LPS receptor do not explain the increased proliferation observed in dKO MZB. No difference in cell proliferation between Ctrl and dKO was observed in the FOB comparison, consistent with the higher expression of cell proliferation genes in the dKO MZB (**Fig. 3-5G, 3-5I**). Thus, although both MZB and FOB dKO cells showed increases in

PC frequencies, MZB dKO cells also displayed a proliferative advantage over the Ctrl counterparts, a property likely due to an increased expression of *Myc* and its target genes.

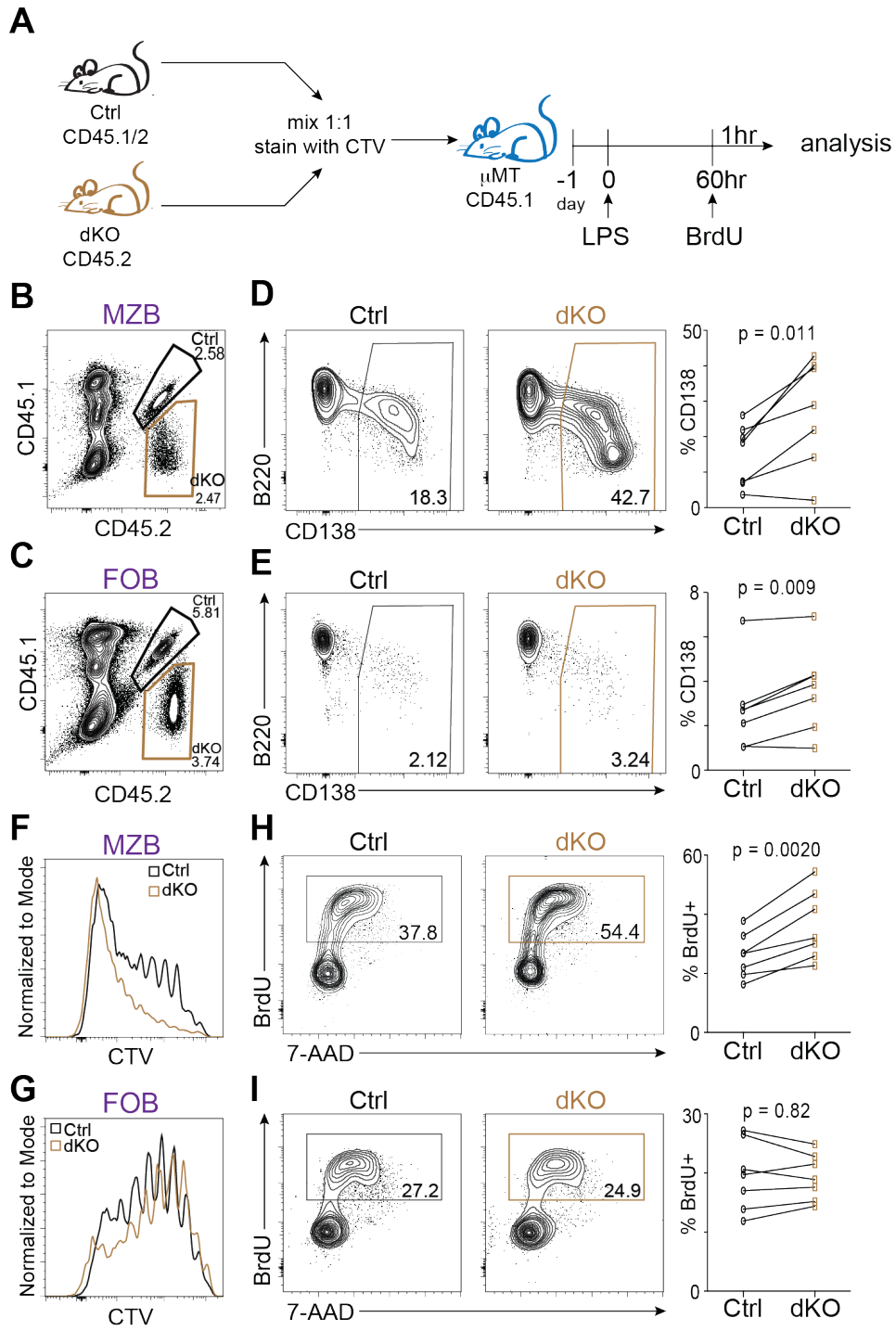


Figure 3-5. UTX- and JMJD3-deficient MZB have a proliferative advantage.

(A) Schematic of experimental design. Splenic B220⁺CD93⁻CD21⁺ MZB and B220⁺CD93⁻CD21^{mid/low}CD23⁺ FOB were magnetically enriched from Ctrl (CD45.1/2) and dKO (CD45.2) mice, mixed at a 1:1 ratio, stained with CTV, and adoptively transferred into CD45.1 μ MT hosts. Host mice were inoculated with 50 μ g of LPS the next day, injected with BrdU 60 hours later, and sacrificed one hour later. Representative plots of transferred MZB (B) and FOB (C) populations sixty-one hours post LPS stimulation. Representative plots of B220 and CD138 expression and quantification of splenic CD138⁺ PC derived from the transferred Ctrl and dKO MZB (D) OR FOB (E). Representative CTV histograms of adoptively transferred Ctrl and dKO MZB (F) or FOB (G). Representative plots of BrdU and 7-AAD incorporation (left) and quantification of BrdU⁺ cells (right) in transferred Ctrl and dKO MZB (H) or FOB (I). These results were derived from two independent experiments with 3-4 adoptive transfers per group (MZB or FOB). Females are designated with open symbols and males with closed symbols. Statistical analysis was performed using paired two-tailed Student's *t* test with *p*-value ≤ 0.05 considered significant.

UTX and JMJD3 regulate PC metabolism

The above adoptive transfer experiment revealed that dKO MZB and dKO FOB generated more PC than their CreCtrl counterparts irrespective of increased proliferation observed for dKO MZB. This suggested the enhanced proliferation of dKO MZB does not fully explain the observed increase in PC. In fact, hierarchical clustering of genes differentially expressed between CreCtrl and dKO in either PC comparison revealed that the samples clustered by genotype rather than the cell type they were derived from, suggesting common mechanisms by which UTX and JMJD3 regulate B cell differentiation (**Fig. 3-6A**). GSEA revealed that dKO PC upregulated genes associated with oxidative phosphorylation (OXPHOS) (**Fig. 3-6B**), which is highly upregulated in PC (52, 60). This is exemplified by the downregulation of *Pdk1* in dKO PC. *Pdk1* encodes pyruvate dehydrogenase kinase-1, which phosphorylates and inhibits the activity of pyruvate dehydrogenase (PDH), with the latter converting pyruvate into acetyl-CoA for use in the tricarboxylic acid cycle and oxidative phosphorylation (**Fig. 3-6C**) (286, 287). Thus, downregulation of *Pdk1* promotes OXPHOS at the expense of glycolysis. To evaluate whether the changes in gene expression resulted in functional differences, CreCtrl and dKO B cells were

cultured *ex vivo* with LPS, IL-2, and IL-5. After three days of culture, CD138⁺ PC were magnetically enriched and examined in a seahorse extracellular flux assay. In this assay, the cellular oxygen consumption rate (**OCR**) was measured as a readout of mitochondria respiration and OXPHOS. Consistent with the gene expression data, UTX- and JMJD3-deficient PC exhibited higher spare respiratory capacity (**Fig. 3-6D**). These data suggest that H3K27me3 demethylases modulate mitochondrial PC metabolism, with dKO PC displaying higher energy reserves.

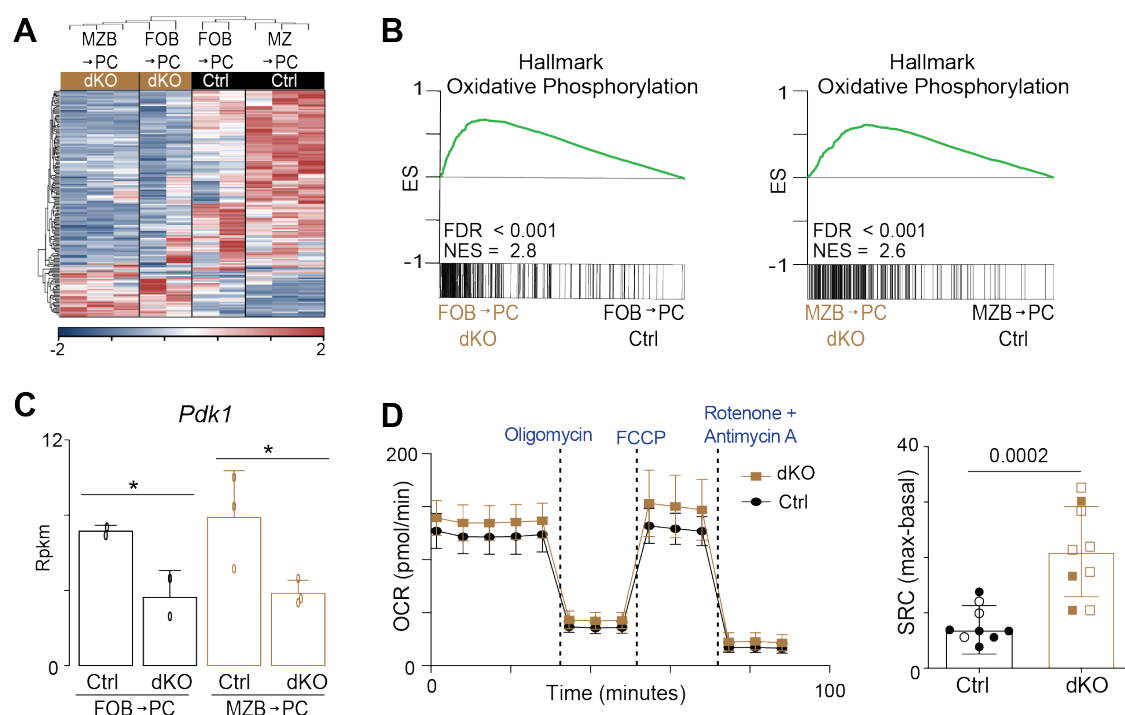


Figure 3-6. UTX- and JMJD3-deficient PC upregulate OXPHOS.

A) Heatmap of hierarchical-clustering, Z-score normalized DEG between Ctrl and dKO PC derived from either MZB (MZB → PC) or FOB (FOB → PC). **(B)** GSEA for Hallmark Oxidative Phosphorylation gene set for Ctrl and dKO PC from (A). **(C)** Bar plot representing the expression of the *Pdk1* gene in each experimental group. Asterisk indicates FDR ≤ 0.05. **(D)** Splenic naïve B cells from Ctrl and dKO mice were cultured *ex vivo* with LPS, IL-2, IL-5. Three days later, CD138⁺ PC were magnetically enriched and assessed for their oxygen consumption rates (OCR) using the Seahorse extracellular flux assay. OCR was measured before and after administration of the indicated metabolic inhibitors (left). Spare respiratory capacity (SRC) was calculated as the difference between maximal and basal OCR. The data is a summary of two independent experiments with at least four biological replicates per group. Females are designated with open symbols and males with closed symbols. Significance was determined by two-tailed Student's *t* test with *p*-values ≤ 0.05 considered significant.

UTX and JMJD3 modulate H3K27me3 enrichment and chromatin accessibility in PC

To identify genes directly regulated by UTX and JMJD3, ChIP-seq and CUT&Tag (C&T) (288) for H3K27me3 were performed on FACS-isolated PC from CreCtrl and dKO mice at day 3 post LPS stimulation *in vivo*. Differential analysis of ChIP-seq H3K27me3 enrichment revealed regions with both increased and decreased levels of this histone modification in dKO PC (**Fig. 3-7A**). Surprisingly, 66% of the differentially enriched regions had lower H3K27me3 enrichment in dKO PC, suggesting that those regions might undergo passive, rather than active loss of this histone modification during B cell differentiation. As expected, genes with statistically significant increased levels of H3K27me3 in dKO PC were also downregulated in these cells (**Fig. 7B, brown dots**). This is consistent with the repressive function of this histone modification.

To assess whether changes in H3K27me3 enrichment at a given locus resulted in changes in chromatin accessibility, ATAC-seq was performed on FACS-isolated PC from CreCtrl and dKO mice at day 3 post LPS stimulation *in vivo*. Consistent with the role of UTX and JMJD3 in promoting gene expression, 92% of differentially accessible regions (DAR) corresponded to regions with lower accessibility in dKO (downDAR) (**Fig. 3-7C**). Furthermore, the regions surrounding downDAR exhibited higher levels of H3K27me3 in dKO PC (**Fig. 3-7D**), suggesting an interplay between gains in H3K27me3 and reduced chromatin accessibility. To gain insight into the transcription factor motifs associated with the changes in accessibility in dKO PC, transcription factor (TF) motif analysis was performed. The top motifs enriched in downDAR were in families for ETS, ETS:IRF, POU, and RUNT factors (**Fig. 3-7E**). These families represent TF such SPIB, PU.1, PU.1:IRF8, OCT2, which are all important in PC formation (107, 108, 289). Integrative analysis of the CreCtrl/dKO PC RNA-seq and ATAC-seq data was performed using the PageRank algorithm, which ranks TF based on their impact on predicted target gene expression (290). The

change in PageRank score between CreCtrl and dKO PC was plotted against the change in gene expression of each TF examined (**Fig. 3-7F**). TF most likely to be contributing to the increased differentiation of dKO B cells were reasoned to be repressors of PC fate that are 1) downregulated in dKO PC and/or 2) fail to regulate their target gene expression upon deletion of *Utx* and *Jmjd3*. Such factors would have lower PageRank score (bottom quadrants) and lower expression in dKO (left quadrants). SPIB, KLF9, IKAROS (encoded by *Ikzf1*) fall into this category, having lower expression and rank in dKO PC (bottom left quadrant); and thus, are more likely to be critical PC repressors contributing to the increased B cell differentiation following deletion of *Utx* and *Jmjd3*. In fact, the ETS factors SPIB and PU.1 have been previously shown to function as negative regulators of PC formation by regulating gene expression directly or by heterodimerizing with IRF factors (107, 108). Similarly, low basal levels of *Klf9* in human memory B cells were attributed to their rapid proliferation of these cells following stimulation *in vitro* (291), and deletion of *Ikzf1* resulted in increased proliferation following stimulation via TLR ligands and spontaneous autoimmunity (292). TF with higher importance and increased expression in the dKO included FOXO1 and STAT6. These data therefore imply that UTX and JMJD3 are critical regulators of chromatin accessibility at regions important for PC-dependent TF binding.

Intriguingly, genes encoding several proteins known to regulate cell survival and apoptosis exhibited significantly higher H3K27me3 enrichment, as well as lower chromatin accessibility (downDAR) and gene expression in dKO PC, suggesting that they were directly regulated by UTX and JMJD3. Examples include, *Bcl2l11*, which encodes BIM, a well-established proapoptotic factor (293), as well as *Trp73*, which encodes the p53 homolog P73 (294) (**Fig. 3-7G, Sup. Fig. 3-4C**). Reduced levels of apoptosis in dKO PC were also observed in PC generated following stimulation with one-tenth of the standard dose of LPS *in vivo*, suggesting that the strength of

stimulation does not impact the differences in apoptosis. To examine whether these transcriptional and epigenetic changes led phenotypic differences, apoptosis was evaluated in CreCtrl and dKO PC three days after LPS stimulation *in vivo*. As CD138 can be downregulated in apoptotic PC (295), TACI and CD98 double positive cells were considered PC. Consistent with the reduced expression of the above proapoptotic factors, dKO PC exhibited lower levels of apoptosis as determined by Annexin V and active caspase 3 staining (**Fig. 3-7H and 3-7I**). Taken together, the data suggest that UTX and JMJD3 regulate PC apoptosis by modulating gene expression and H3K27me3 levels, which likely contribute to the observed phenotype.

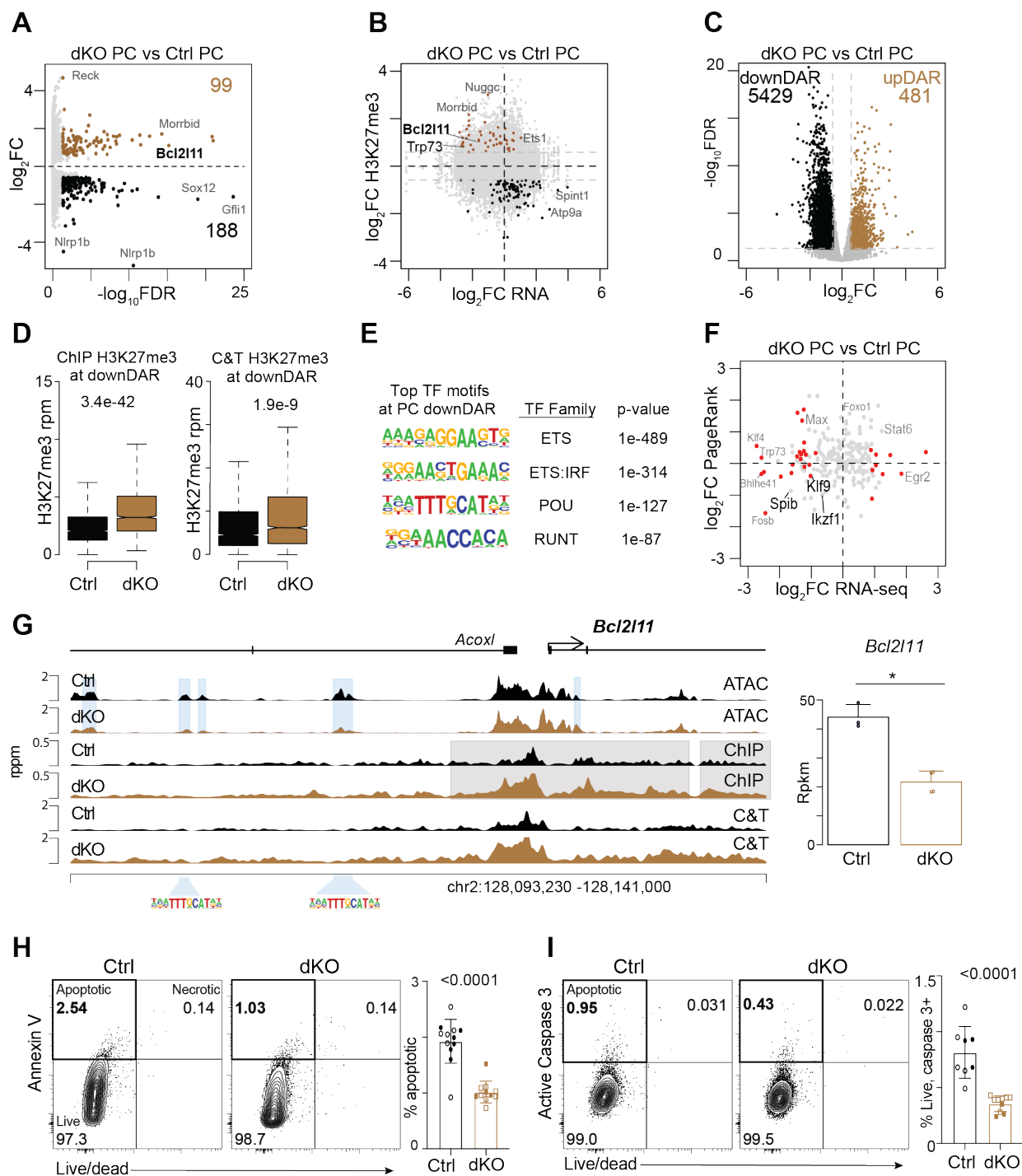


Figure 3-7. UTX and JMJD3 regulate H3K27me3 enrichment and chromatin accessibility. ATAC-seq, ChIP-seq, and C&T were performed on FACS-isolated Ctrl and dKO PC three days after LPS inoculation *in vivo*. (A) ChIP-seq data scatterplot representing regions with 1.5-fold change in enrichment (FDR \leq 0.05) in H3K27me3 levels between Ctrl and dKO PC. Genes with large changes are highlighted. (B) Scatterplot of changes in H3K27me3 (ChIP-seq) enrichment versus gene expression (RNA-seq) between Ctrl and dKO PC. (C) Volcano plot representing DAR (1.5-fold change, FDR \leq 0.05) between Ctrl and dKO PC. (D) H3K27me3 enrichment within 1kb

of downDAR from (C) in Ctrl and dKO PC based on results from ChIP-seq (left) or C&T (right). (E) Top TF motif, family, and p -value enriched at downDAR. (F) Scatterplot of Page Rank score versus gene expression between Ctrl and dKO PC. Red dots indicate DEG ($FDR \leq 0.05$). (G) Genome plot for *Bcl2l11* depicting chromatin accessibility (ATAC-seq) and H3K27me3 enrichment from ChIP-seq and C&T in Ctrl and dKO PC (left). The blue and gray shaded regions indicate DAR and g regions with differential levels of H3K27me3 enrichment in ChIP-seq, respectively. Bar plot of *Bcl2l11* gene expression (right). Representative plots of Annexin V versus viability (H) and active caspase 3 versus viability (I) in splenic TACI+CD98+ Ctrl and dKO PC three days after stimulation with 50 μ g LPS *in vivo* (left) with quantification (right). The ATAC-seq and ChIP-seq were performed on three Ctrl and four dKO PC. C&T was performed on four Ctrl and four dKO PC. Data in (H) and (I) are the summary of two independent experiments with at least three biological replicates. Females are designated with open symbols and males with closed symbols. Statistical analysis was performed using two-tailed Student's t test with p -value ≤ 0.05 considered significant.

IV. Discussion

This study demonstrated that H3K27me3 demethylases play a critical role in fine tuning B cell differentiation to PC. Deletion of these demethylases resulted in an increase in PC following stimulation with TI antigens, establishing them as negative regulators of B cell differentiation. Although the bulk of experiments assessed immune responses and transcriptional and epigenetic changes in mice lacking both *Utx* and *Jmjd3*, analysis of single deletion mice ultimately showed that UTX and not JMJD3 was responsible for the observed increases in PC formation in response to antigenic challenge. This is consistent with RNA-seq data showing that *Jmjd3* mRNA levels are very low in naïve cells and do not increase during differentiation to PC; whereas *Utx* mRNA expression increases during the differentiation process (133). Thus, we conclude that the effects observed were due to UTX. Major transcriptional programs that were affected by UTX included those controlling metabolism and cell proliferation. Moreover, H3K27me3 demethylase deficiency resulted in modulation of H3K27me3 enrichment and chromatin accessibility at genes involved in cell survival, resulting in reduced apoptosis of dKO PC. Together, this study demonstrated a critical role for UTX in restraining B cell formation.

MZB and FOB play unique but equally important roles during the immune response (27). MZB are known for their rapid responses to TI blood-borne antigens. A recent study demonstrated that MZB can differentiate into PC without undergoing cell division (96). Notch2 is essential for MZB development (30, 296) and was shown to drive the rapid MZB differentiation by promoting the expression of MYC and mTORC1 target genes (96). Deletion of *Myc* significantly impaired the ability of MZB to differentiate into PC; whereas deletion of *Tsc1* (a negative regulator of mTORC1) resulted in division-independent differentiation of FOB (96). Here, the expression of *Myc* and its target genes was higher in dKO MZB, which correlated with increased proliferative

capacity. However, PC formation was not detected until the last detectable cell division, regardless of cell type or genotype. This discrepancy between systems is not unusual as differences in B cell differentiation have been reported depending on the antigen used and stimulation conditions (70, 93, 297). Interestingly, no differences in the expression of genes associated with mTORC1 or UPR pathways were observed between dKO and CreCtrl MZB, suggesting that UTX fine tunes the ability of mature MZB to proliferate through the regulation of *Myc* and its target genes.

B cell development is marked by many examples in which epigenetic and chromatin alterations occur. For example, commitment to the B cell lineage is associated with an acquisition of a distinct pattern of chromatin accessibility and histone modifications mediated by the pioneering TF EBF1 (298). Additionally, deletion of the H3K79 methyltransferase, DOT1L, in pro-B cells significantly impaired B cell development in the bone marrow (151). Furthermore, H3K4me1/2 demethylase, LSD1, has also been shown to promote MZB formation by cooperating to the non-canonical NF- κ B TF p52 to control gene expression (148). This study adds to our understanding of the epigenetic regulation of B cell development by demonstrating that deletion of *Utx* and *Jmjd3* resulted in an increase in T2 transitional B cells and MZB.

ChIP-seq for H3K27me3 in dKO PC revealed regions with increased and decreased levels of this histone modification compared to their control counterparts undergoing differentiation. Loss of H3K27me3 can occur via active demethylation mediated by UTX and JMJD3 or by passive loss during cell division (299). Our data suggest that both processes are responsible for H3K27me3 loss during B cell differentiation. Regions with higher H3K27me3 in dKO PC are most likely normally regulated via direct demethylation by UTX; whereas regions with decreased H3K27me3 in dKO PC likely undergo a passive loss of H3K27me3 during cell division. *In vivo*, differentiation to PC requires eight cell divisions (93, 95); thus, providing the cells with multiple opportunities to

alter their epigenome by either process. We speculate that the increased proliferation and number of cell divisions of dKO B cells may lead to an increase in passive loss of H3K27me3 during the differentiation process.

UTX and JMJD3 have been shown to regulate gene expression in a demethylase-independent manner by partnering with other proteins or protein complexes including the chromatin modifiers BRG1 (181), CHD4 (251), P300 (182) and members of MLL complex (186). Notably, the demethylase dependent and independent functions are not mutually exclusive within a cell type or differentiation stage. This context and gene dependent method of regulation is observed in EL4 T cells where the demethylase activity of JMJD3 was required to promote the expression of *Ccl3*, but not *Cxcr3* (184). In our study, dKO PC exhibited reduced gene expression and increased levels of H3K27me3 at regions that mapped to genes involved in cell survival and apoptosis, suggesting direct regulation of these genes.

UTX is encoded on the X chromosome, whereas its homolog UTY is encoded on the Y chromosome. Due to point mutations in the catalytic domain, UTY does not possess significant H3K27 demethylase activity (169, 171, 175); however, because of the high structural homology, UTY can potentially regulate gene expression in a demethylase-independent manner (169, 175, 200). As a result, comparing male and female dKO mice allows us to discriminate between demethylase-dependent and independent functions of UTX in B cell differentiation. Interestingly, while the increase in PC following stimulation with TI antigens occurred in dKO mice of both sexes, the increase in PC frequency following influenza infection was only observed in females. This suggests that only the former requires the demethylase activity of UTX. Moreover, these results suggest that the mechanism by which UTX regulates B cell differentiation likely depends on the antigen, the signaling, and/or cytokines microenvironment.

Epigenetic modifiers such as UTX and JMJD3 lack DNA-binding domains and are recruited to their target genes by TF (300). In other cell types, such as those in invariant NK T cells, UTX interacted with JunB and PLZF (203). Here, regions with reduced chromatin accessibility in dKO PC were enriched for ETS family TF motifs and ETS:IRF composite motifs, including PU1, SPIB, and PU1:IRF8 single or composite motifs, which have been shown to negatively regulate PC formation (107, 108). Additionally, KLF9 and IKAROS, were identified via PageRank analysis, suggesting that UTX might be regulating gene expression through interactions with multiple transcription factor families.

Long-term survival of PC is the cornerstone of humoral immunity (33). PC survival depends on both cell extrinsic factors, such as access to APRIL and BAFF (301), but also cell-intrinsic factors, including transcription factors such as IRF4 (114). Furthermore, whereas the role of the anti-apoptotic factor MCL-1 in PC survival has been well established (301, 302), a recent study demonstrated that in addition to upregulating anti-apoptotic factors, human bone marrow LLPC also downregulated the expression of proapoptotic factors (303). Deletion of *Utx* and *Jmjd3* further reduced expression of proapoptotic genes, such as *Bcl2l11* and *Trp73*, in PC. These transcriptional changes corresponded to significant reduction in apoptosis of dKO PC *in vivo*, suggesting that regulation of these genes might be critical to PC survival.

B cell differentiation requires substantial metabolic reprogramming to support the high rate of antibody secretion of PC (52, 304). However, not all PC are created equal. Spare respiratory capacity, which is thought to function as an energy reserve in case of bioenergetic crisis (305), has been shown to be much higher in LLPC than SLPC (60). These differences correlated with the longer survival of LLPC and occurred in a pyruvate-dependent manner (60). Deletion of *Utx* and *Jmjd3* resulted in upregulation of OXPHOS genes and higher spare respiratory capacity of dKO

PC, which together with the reduced levels of apoptosis, suggests the UTX might be regulating PC survival via multiple mechanisms.

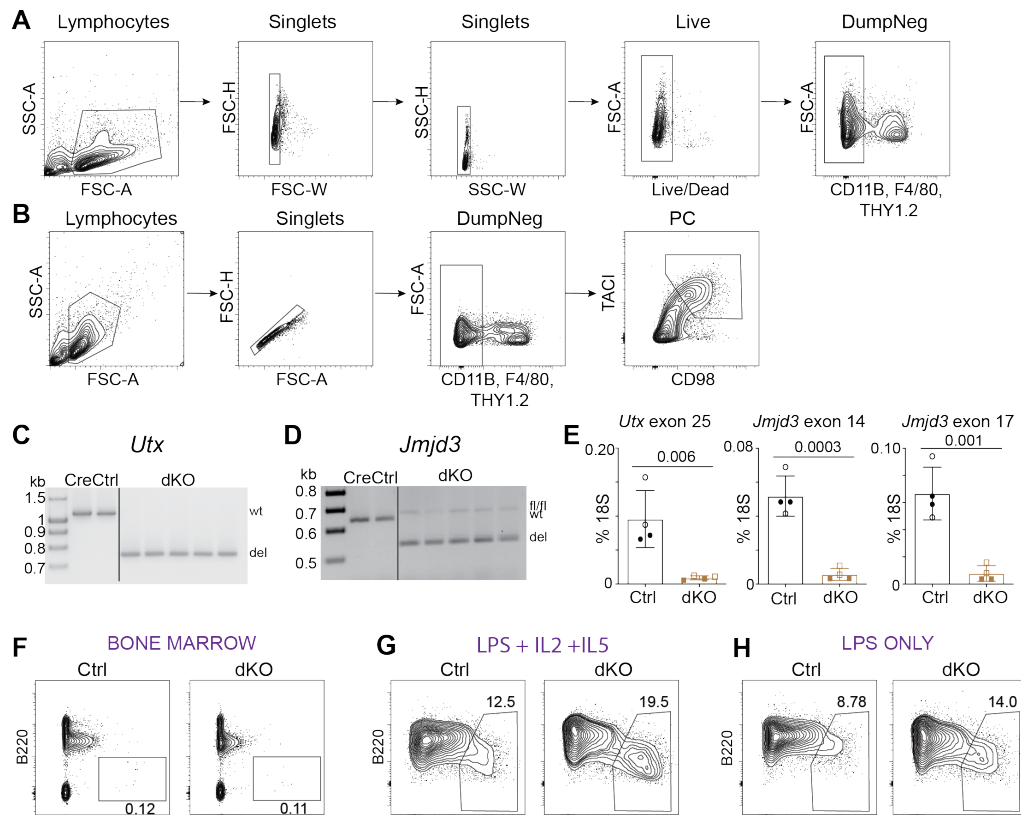
B cell differentiation is accompanied by substantial transcriptional and epigenetic reprogramming, including progressive DNA hypomethylation and redistribution of histone modifications (34, 92, 117, 146). This can be exemplified by the studies on EZH2, the H3K27me3 methyltransferase, which was shown to promote PC formation through repression of the B cell transcriptional program (141). Intriguingly, whereas loss of EZH2 impaired B cell proliferation and differentiation (141), deletion of *Utx* and *Jmjd3* resulted in increased proliferation and PC formation. Thus, modulation of H3K27me3 enrichment during B cell differentiation is likely necessary to fine tune the gene expression to ensure proper reprogramming during B cell differentiation

The maintenance of appropriate H3K27me3 levels also have important clinical implications as mutations in *EZH2* and *UTX* have been reported in various human malignances. However, whereas *EZH2* mutations are typically gain-of-function resulting in increased levels of H3K27me3, mutations in *UTX* are typically loss-of-function (306-308). The crosstalk between these enzymes is further exemplified by the fact that loss of *UTX* in multiple myeloma or lung cancer sensitized the tumors to EZH2 inhibitors (231, 309). These findings would be of great clinical relevance since development of a UTX specific inhibitor has been hindered by the high homology of the Jumonji C (JmjC) domain of all demethylases (310).

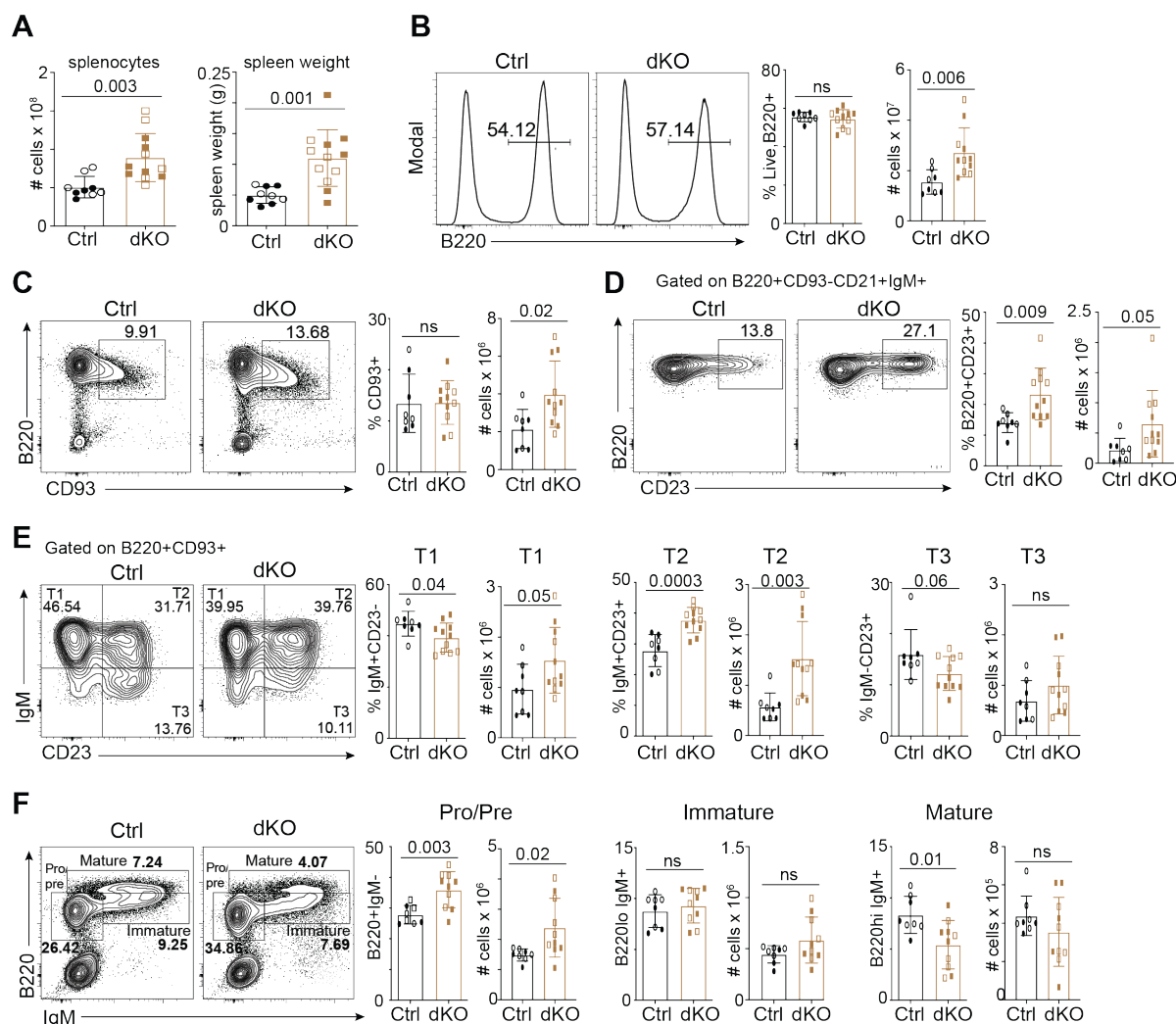
Taken together, this study demonstrated a novel role of UTX in B cell differentiation into PC; thus, adding to our growing understanding of the epigenetic changes that occur during B cell differentiation. These enzymes regulated many of the same pathways as EZH2 suggesting that the

levels of H3K27me3 must be tightly controlled for optimal B cell differentiation. Thus, whereas EZH2 promotes cell proliferation and PC formation, UTX restrains these activities.

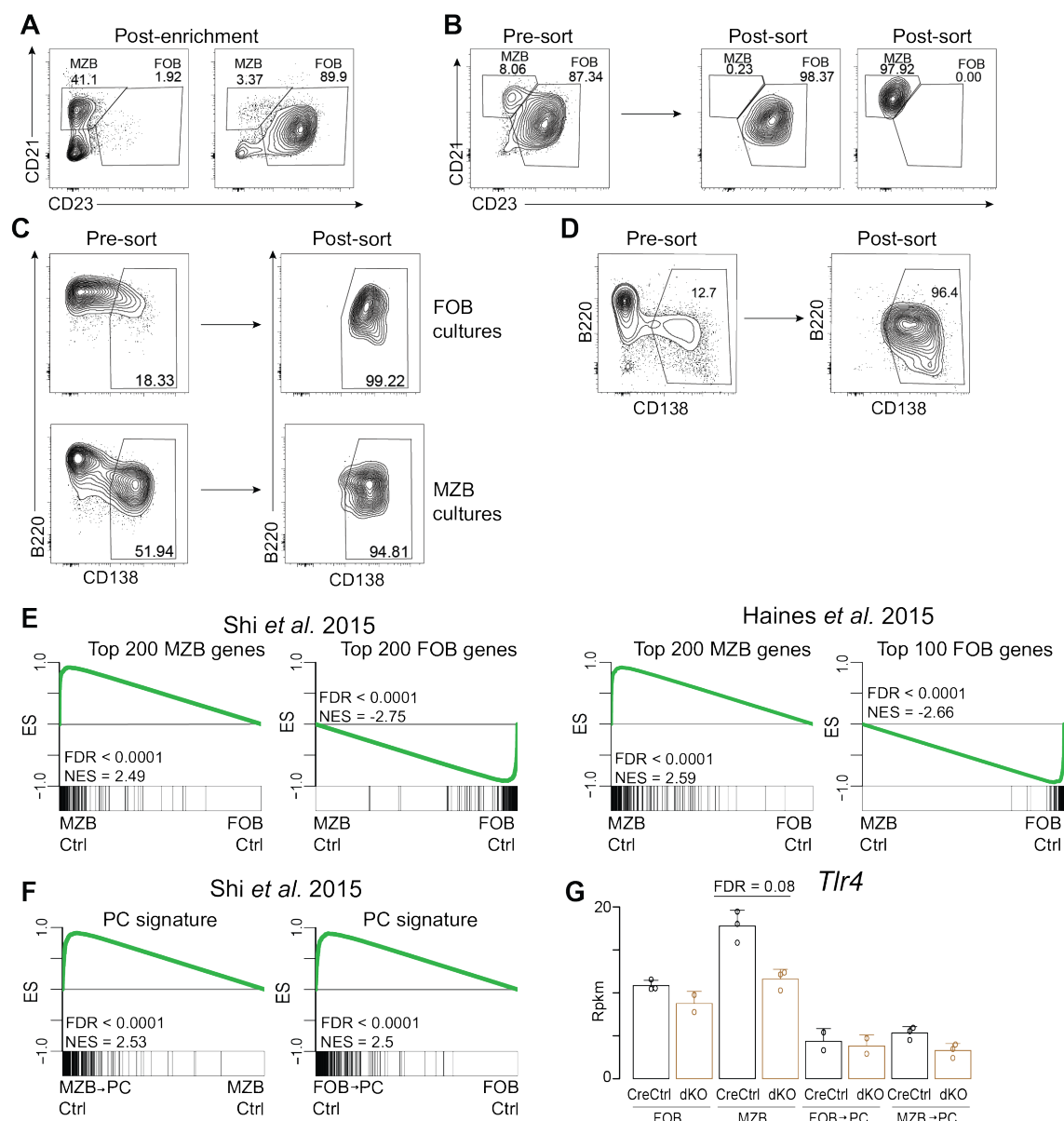
V. SUPPORTING DATA



Supplemental Figure 3-1. Efficient deletion of *Utx* and *Jmjd3* by *CD19^{cre}*. (A) General gating strategy used for analysis and FACS sorting. After excluding dead cells and non-B cells, other parameters such as PC formation (Fig. 1, Fig. 2) or congenic markers were analyzed (Fig. 4). (B) Gating strategy used to evaluate apoptosis of Ctrl and dKO PC in Fig. 6H and Fig. 6I. Following exclusion of non-B cells, TACI and CD98 expression was used to identify PC because CD138 can be downregulated in apoptotic PC (295). (C and D) PCR genotyping of genomic DNA isolated from Ctrl and dKO naïve B cells using primers designed to amplify the floxed (top band), wild-type (middle band), and deleted (lower band) regions. (E) mRNA expression of *Utx* and *Jmjd3* in Ctrl and dKO naïve B cells was determined by RT-qPCR using primers specific for the floxed exons and quantified as %18S. (F) Representative plots of B220 and CD138 expression (left) and quantification of CD138⁺ PC from the highlighted gates (right) in bone marrow of naïve Ctrl and dKO mice. Representative plots of B220 and CD138 expression and quantification of CD138⁺ PC three days after ex vivo stimulation with LPS, IL2, and IL-5 (G) or LPS alone (H).

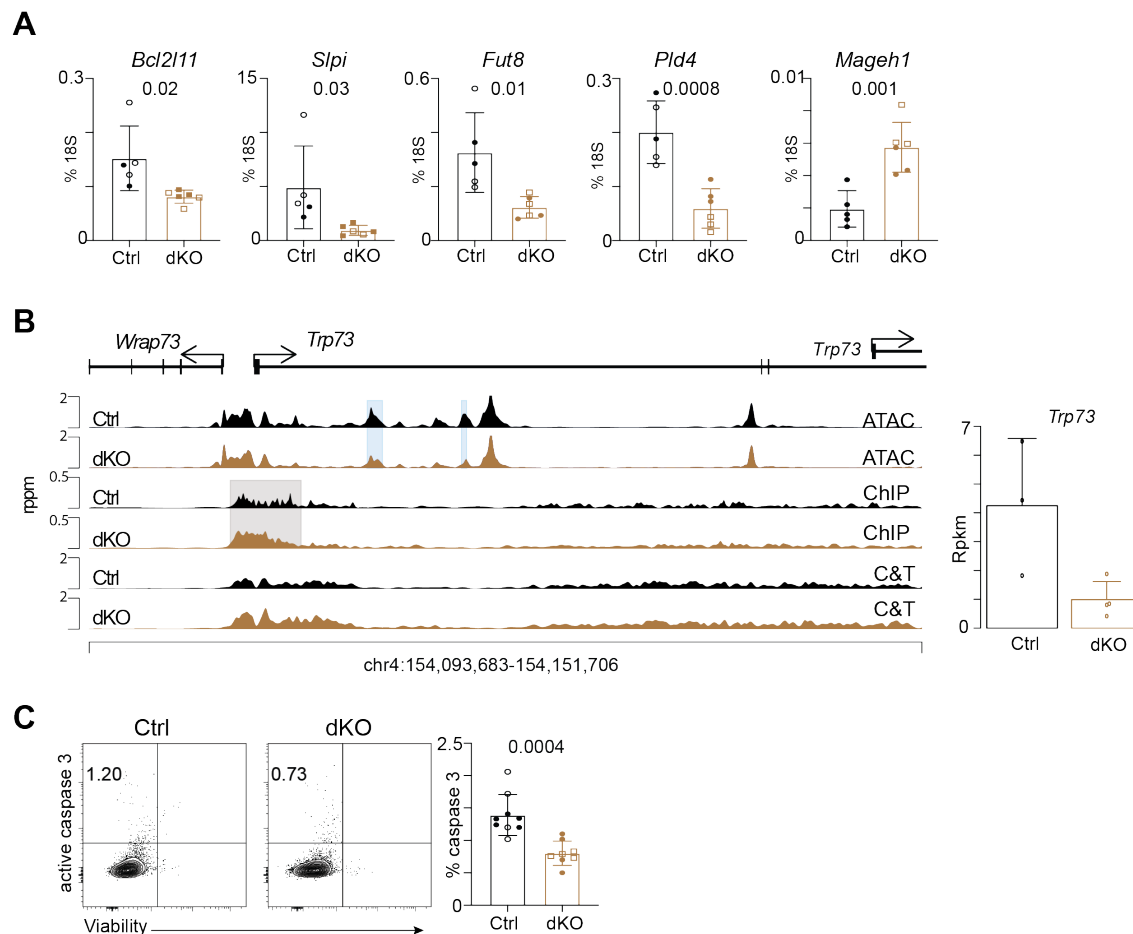


Supplemental Figure 3-2. Phenotypic analysis of B cell development in dKO mice. (A-D) Flow cytometry analysis of B cell development in spleen of naïve Ctrl and dKO mice. Representative plots and quantification of the following population are shown: B220⁺ B cells (A), B220⁺CD93⁺ immature B cells (B), B220⁺CD93⁻IgM⁺CD21⁺CD23⁺ marginal zone precursors (C), B220⁺CD93⁺IgM⁺CD23⁻ T1, B220⁺CD93⁺IgM⁺CD23⁺ T2, and B220⁺CD93⁺IgM⁻CD23⁺ T3 transitional B cells (D). (E) Flow cytometry analysis and quantification of B220^{mid}IgM⁻ pro/pre-, B220^{mid}IgM⁺ immature, and B220^{mid}IgM^{high} mature B cells in the bone marrow from naïve Ctrl and dKO mice. (A-E) Results are a summary of two independent experiments with at least three biological replicates per group. Statistical analysis was performed using two-tailed Student's *t* test with *p*-value ≤ 0.05 considered significant.



Supplemental Figure 3-3. Magnetic enrichment and FACS sorting of B cells and PC.

(A) Representative plots of the frequencies of MZB and FOB after magnetic enrichment. (B) Representative plots of the frequencies of $CD21^+CD23^-$ MZB and $CD21^{low/mid}CD23^+$ FOB before and after FACS isolation for RNA-seq. (C) MZB and FOB cells were cultured *ex vivo* with LPS, IL-2, IL5. Representative plots of the frequencies of $CD138^+$ PC at day 3 of *ex vivo* cultures before and after FACS isolation for RNA-seq. (D) Representative plots of the frequencies of $CD138^+$ PC at day 3 post LPS inculcation *in vivo* before and after FACS sorting for ATAC-seq. (E) GSEA plots representing the enrichment of top genes upregulated in MZB or FOB from Shi et al. 2015 (46) and Haines et al. 2019 (148) in the Ctrl MZB vs Ctrl FOB comparison. (F) GSEA plots displaying the enrichment of the PC signature genes from Shi et al. 2015 (46) in MZB \rightarrow PC and FOB \rightarrow PC compared to their naïve counterparts.



Supplemental Figure 3-4. Validation of DEG and genome plots for *Trp73*.

(A) mRNA expression of selected DEG from Fig. 4A between Ctrl and dKO PC was determined by RT-qPCR and quantified as %18S. (B) Genome plot for *Trp73* depicting chromatin accessibility (ATAC-seq) and H3K27me3 enrichment from ChIP-seq and C&T in Ctrl and dKO PC. The blue shade indicates DAR and gray shade marks regions with differential levels of H3K27me3 enrichment in ChIP-seq. Bar plot representing gene expression is shown to the right. (C) Representative plots of active caspase 3 versus viability in TACI+CD98+ Ctrl and dKO PC (left) three days after stimulation with 5 μ g LPS *in vivo* with quantification (right).

VI. METHODS

Mice

Mice with floxed *Utx* and *Jmjd3* alleles were previously described (205) and were obtained from Dr. R. Bosselut (National Cancer Institute). $Utx^{fl/fl}Jmjd3^{fl/fl}$ were bred to $Cd19^{Cre/+}$ (006785; The Jackson Laboratory) to obtain $Utx^{fl/fl}Jmjd3^{fl/fl}Cd19^{Cre/+}$. $CD45.2$ μ MT mice (008100; The Jackson Laboratory) (91) were bred onto the $CD45.1$ background to obtain $CD45.1$ μ MT mice. All experiments were performed with 7-12 weeks old mice of both sexes. For LPS experiments, mice were injected i.v. with 50 μ g of LPS (ALX-581-008; Enzo Life Sciences) and sacrificed three days later for analysis. In some experiments, mice were injected with 50 μ g NP-Ficoll (F-114 1420-10, Biosearch Technologies) i.v. and sacrificed seven days later for analysis. For influenza infections, mice were infected intranasally with 15,000 virus forming units (vfu) of A/PR8/34 (PR8) and sacrificed ten days later for analysis. For adoptive transfer experiments, magnetically enriched MZB or FOB from $CD45.1/2$ CreCtrl ($Cd19^{Cre/+}$) and $CD45.2$ dKO ($Utx^{fl/fl}Jmjd3^{fl/fl}Cd19^{Cre/+}$) mice were mixed at a 1:1 ratio, stained with 5 μ M Cell Trace Violet (CTV, C34557; Invitrogen), and adoptively transferred into $CD45.1$ μ MT mice together with 10 million $CD45.1$ B-cell depleted splenocytes. The next day, host mice were stimulated with 50 μ g LPS. In some experiments, one hour before analysis, the $CD45.1$ μ MT host mice were injected with 0.8 mg bromodeoxyuridine (BrdU; 423401; Biolegend). All animals were housed by the Emory Division of Animal Resources, and all protocols were approved by the Emory Institutional Animal Care and Use Committee (IACUC).

Ex vivo differentiation

Naïve splenic B cells were magnetically enriched by negative selection using CD43 (Ly-48) MicroBeads (130-097-148, Miltenyi Biotec) with >95% purity following the manufacturer's instructions. These cells were either cultured directly or further enriched or purified by magnetic bead separation or FACS, respectively. For magnetic enrichment of MZB, CD43⁻ B cells were stained with a CD23-PE antibody (B3B4; BioLegend), followed by magnetic separation using anti-PE MicroBeads (130-105-639; Miltenyi Biotec) leaving MZB in the flow-through and FoB in the enriched bound fractions. In some experiments, MZB (B220+CD93⁻ CD21+CD23⁻) and FoB (B220+CD93⁻ CD21⁻/loCD23⁺) were isolated by FACS. Purified B cells were cultured at 0.5×10^6 cells/ml of B cell media (RPMI 1640, 10% heat-inactivated FBS, 0.05 mM 2-Mercaptoethanol, 1X nonessential amino acids, 1X penicillin/streptomycin, 10 mM HEPES, and 1 mM sodium pyruvate) with 20 µg/ml LPS (L2630; Sigma), 20 ng/ml IL-2 (575406; Biolegend), and 5 ng/ml IL-5 (581504; Biolegend). LPS and cytokines were supplemented at a half dose at 24h and 48h of ex vivo culture as described before (259).

Flow Cytometry

Cells were resuspended at $10^6/100$ µl in FACS buffer (1X PBS, 1% BSA, and 2 mM EDTA) and blocked with anti-Fc (anti-CD16/CD32; BD Bioscience). The following antibodies were used for staining and are from Biolegend: B220 PE-Cy7 (RA3-6B2) B220 Alexa 700 (RA3-6B2), CD138 APC (281-2), CD138 PE (281-2), CD98 PE-Cy7 (RL388B), CD11b APC-Cy7 (M1/70F4/80 APC-Cy7 (BM8), Thy1.2 APC-Cy7 (30H12), CD93 PE (AA4.1), CD45.1 APC (A20), CD45.2 FITC (104); BD Bioscience: CD138 BV711 (281-2), IgD BV711(11-26c.2a), IgD BV605 (IA6-2), CD21 APC (7G6), CD93 BV711 (AA4.1); and ThermoFisher Scientific: TACI PE (ebio8F10-3), GL7 eFluor660 (GL-7), IgM FITC (II/41), GL7 eFlour450 (GL-7), CD23 eFlour450 (B3B4).

Zombie Yellow Viability Dye (423104; Biolegend) and Zombie NIR Viability Dye (423106; Biolegend) were used to assess cell viability. Cells were stained for 40 min and fixed using 1% paraformaldehyde. For some experiments, apoptosis was assessed using an Annexin V FITC kit (BMS500FI-100; eBioscience) and CaspGLOW Fluorescein Active Caspase-3 Staining Kit (K183-25; BioVision) according to the manufactures' protocols. BrdU analysis was performed using the Phase-Flow™ FITC BrdU Kit (370704; Biolegend). Flow cytometry was performed on a BD Fortessa X20 or BD Symphony A3 using FACSDiva and analyzed using FlowJo v10 software. The following gating strategy preceded all flow cytometry analyses presented. Cells were gated on 1) lymphocytes (forward light scatter [FSC]–area by side scatter [SSC]–area), 2) singlets by FSC-height/FSC- width or FSC-height/ FSC- area. CD11B, F4/80, and THY1.2 markers were used to exclude non-B cells (Sup. Fig. 1A and Sup. Fig. 1B).

Enzyme-Linked Immunosorbent Assay (ELISA)

ELISA plates (M9410; Sigma) were coated with goat anti-mouse Ig (5300-05B; Southern Biotechnology) overnight at 4°C and blocked with 3% nonfat dry milk for 2 h. A Standard curve of IgM antibody (5300-01B; Southern Biotechnology) and serum samples were incubated at 4°C overnight. The next day, the plates were washed and incubated with HRP-conjugated goat anti-mouse secondary antibody (1021-05; Southern Biotechnology) for 2 h at room temperature. The plates were developed using TMB ELISA peroxidase substrate (800-666-7625; Rockland) and the reaction was stopped using 0.2M sulfuric acid. Plates were read using ELx808 Absorbance plate reader (BioTek).

Seahorse

A FluxPak cartridge was hydrated for at least 12 h prior to the experiment with 200 μ l dH₂O in a 37°C non-CO₂ incubator. The water was replaced with 200 μ l Seahorse Calibrant solution (103059-000; Agilent) one hour before the assay. The Seahorse XFe96 cell culture plate was coated with 22.4 mg/ml CellTak (354420; Corning) for 20 min followed by a wash with dH₂O. Cells were resuspended in Seahorse XF Assay Media, pH 7.4 \pm 0.1, supplemented with 1 mM sodium pyruvate, 2 mM L-glutamine (G7513; Sigma), and 5.5 mM glucose and incubated in the Seahorse XFe96 cell culture plate at 37°C in a non-CO₂ incubator for 45 min prior to beginning the assay. The indicated drugs were diluted in assay-specific media prior to injection into each port. For the mitochondrial stress test, the ports were as follows: port A, oligomycin (75351; Sigma) was used at a final concentration of 1 mM; port B, carbonyl cyanide-4-(trifluoromethoxy) phenylhydrazone (C2920; Sigma) was used at a final concentration of 2.5 mM; and port C injected a combination of Rotenone (R8875; Sigma) and Antimycin A (A8674; Sigma), each at a final concentration of 1 mM. All drugs were diluted in assay media prior to injection into the ports. At least six technical replicates per sample were performed.

RT-qPCR

Cells were lysed in RLT buffer (79216; Qiagen) containing 1% 2-Mercaptoethanol and RNA was isolated using Zymo Quick-RNA MicroPrep Kit (11-328M; Zymo Research). Reverse transcription was performed with SuperScriptII (18064022; ThermoFisher Scientific) using random hexamers and oligo dT primers. RT-qPCR was performed using SYBR Green on a Bio-Rad iCycler and gene expression was quantified as a percentage of 18S rRNA as previously described (61).

RNA-seq

One thousand cells were sorted directly into RLT buffer (79216; Qiagen) containing 1% 2-Mercaptoethanol. RNA was isolated using Zymo Quick-RNA MicroPrep Kit (11-328M; Zymo Research). Synthesis of cDNA was performed using SMART-Seq v4 Ultra Low Input RNA Kit (634894; Takara Bio) kit. Final libraries were generated using 200 pg of cDNA as input for the NexteraXT kit (Illumina, FC-131-1024). RNA-seq libraries for naïve B cells and ex vivo generated PC were sequenced at University of Alabama Birmingham Helfin Center for Genomic Sciences on a NextSeq500/550 using 75 bp paired-end chemistry. RNA-seq libraries for PC generated in vivo were sequenced on NovaSeq6000 at Novogene. Raw sequencing reads were mapped to the mm10 genome using STAR v2.5.3a (311). Raw reads per kilobase per million (Rpkm) normalized gene expression counts were determined by annotating the coverage across all exons for all unique ENTREZ genes using the GenomicAlignments (312) package. Differential expression analysis was performed using edgeR (313) with $FDR \leq 0.05$ being considered significant. Gene Set Enrichment Analysis (GSEA) (262) was performed using a pre-ranked gene list generated by multiplying the sign of the fold change (negative or positive) by the $-\log_{10}$ of the edgeR derived p value.

ATAC-seq

Five thousand cells were sorted into FACS buffer and ATAC-seq libraries were prepared as previously described (141). ATAC-seq libraries were sequenced on a NovaSeq6000 at Novogene using 75 bp paired-end chemistry. Sequencing reads were mapped to the mm10 genome using Bowtie v1.1.1 (314). Enriched peaks were called using MACS2 v2.1.0 (315) and annotated to the nearest gene using HOMER (316). Differentiation analysis of accessible peaks was performed

using DESeq2 (317) with $FDR \leq 0.05$ and >1.5 -fold change considered significant. Transcription factor motif analysis was performed using HOMER function findMotifsGenome.pl script using randomly generated genomic sequences as background. PageRank (290) analysis was performed using all the ATAC-seq peaks and RNA-seq expression matrix.

ChIP-seq

ChIP was performed based on previously published protocols (167, 259, 318) Specifically, for this study, FACS-sorted PC were crosslinked with formaldehyde for 10 min followed by quenching with glycine. Cells were lysed in nuclei lysis buffer (50 mM Tris pH 8.0, 10mM EDTA, 1% SDS). Chromatin was sonicated and quantified by Qubit 3 Fluorometer (Q33216; Invitrogen). One μg of chromatin was used for each immunoprecipitation following. Chromatin was incubated with anti-H3K27me3 (C15410069; Diagenode) or anti-IgG (12-370; Milipore) antibody overnight at 4°C . Chromatin-antibody complexes were then bound to Dynal Protein G magnetic beads (10004D; Invitrogen) for 2 h at 4°C , washed, heated to reverse crosslinks, and DNA was isolated using a QIAquick PCR Purification kit (28106; Qiagen). Enrichment for H3K27me3 was validated at the Hox9a (positive) and Actin (negative) loci by qPCR using a 1:10 dilution. Remaining DNA was used to prepare ChIP-seq libraries using KAPA Hyper Prep (Roche; KK8500) . Libraries were sequenced at Emory Integrated Genomics Core on NextSeq500/550 using 75 bp paired-end chemistry. Raw sequencing reads were mapped to the mm10 version of the mouse genome using Bowtie v2.2.4 (314). Peak calling was performed using MACS v.2.1.1 (315) using the following parameters "--nomodel --nolambda --broad". Differential analysis was performed using DESeq2 with $FDR \leq 0.05$ and >1.5 -fold change ($\log_2\text{FC} > 0.58$) being considered significant.

Purification of pA-Tn5 Transposase

The 3XFlag-pA-Tn5-F1 expression vector (Addgene plasmid # 124601) was transformed into C3013 *E.coli* strain (NEB C3013I) following the manufacturer's protocol. Purification of adapter-loaded Protein A-Tn5 transposase (pA-Tn5) chimeric protein was performed using previously described methods with the following modifications (33, 73). Bacteria containing the expression vector were grown until A600 of ~0.6 was reached and pA-Tn5 protein expression was induced with 0.25mM fresh isopropyl β -d-1-thiogalactopyranoside at 25°C for 4hrs. Cells were lysed in lysis buffer containing 0.1mg/ml lysozyme, incubated on ice for 10 min, sonicated on ice 15 times at 30 s intervals separated by 30 s breaks at 60% duty cycle for further purification by affinity chromatography and oligonucleotide loading as described previously (33). The activity of the protein was tested for its ability to digest plasmid DNA and tagment genomic DNA from Raji cells (73).

CUT&Tag

CUT&Tag was performed as described in detail previously with some modifications (74). Nuclei were isolated by resuspension in chilled nuclear extraction (NE) buffer (20 mM HEPES-KOH [pH7.9], 10mM KCl, 0.5mM spermidine, 0.1% Triton X-100, 20% glycerol) with EDTA free protease inhibitor tablet (Sigma 11873580001), incubated on ice for 10 min, washed with ice-cold NE buffer, bound to pre-washed magnetic bead slurry for 1h at room temperature on a rotator for further antibody incubation, tagmentation and library preparation (74). Previously described barcoded i5 and i7 Illumina Inc primers were utilized for library amplification (75). Final libraries were purified using double SPRI-bead size selection (1.3x positive followed by 1.0x positive selection) and library size distribution was assessed using an Agilent Bioanalyzer 2100.

CUT&Tag libraries were sequenced at the Emory Integrated Genomics Core on a NextSeq500/550 using 75 bp paired-end chemistry.

Data and Code Availability

All sequencing data have been deposited in NCBI Gene Expression Omnibus (GEO) under the following accession numbers GSE185095 for RNA-seq, GSE185096 for ATAC-seq, GSE185097 for ChIP-seq, and GSE185098 for CUT&Tag. Code and data processing scripts are available from the corresponding author upon request and at <https://github.com/cdschar/>.

Chapter 4. Work in progress: The role of UTX and JMJD3 in B cell responses to TD antigens

Anna K. Kania, Madeline J. Price, Christopher D. Scharer, and Jeremy M. Boss

Department of Microbiology and Immunology, Emory University School of Medicine, Atlanta,
GA 30322, USA

Author Contributions

A.K.K. designed and performed experiments, analyzed, and interpreted the data. M.J.P. performed experiments. C.D.S. and J.M.B designed experiments and interpreted the data.

Introduction and Results

Chapters 2 and 3 have focused on the role of UTX and JMJD3 in B cell differentiation into PC and have demonstrated that loss of these enzymes resulted in an increase in PC. As mentioned in chapter 1, B cells responding to TD antigens such as the influenza virus either differentiate into SLPC or early memory B cells, or migrate to the GC. After undergoing several rounds of somatic hypermutation, GC B cells differentiate into LLPC or memory B cells (39, 40). In this chapter, the role of H3K27me3 demethylase in GC response and LLPC formation was examined.

To evaluate whether UTX and JMJD3 regulate GC response, CreCtrl and dKO mice were infected with PR8 influenza virus and sacrificed 14 days later for analysis. Flow cytometry analysis revealed an increase in GL7+FAS+ GC B cells in the draining lymph node (LN) (**Figure 4-1A**). However, these differences occurred in a sex-specific manner as the changes were not statistically significant in males. GC can be divided into the dark zone, where B cells undergo rapid proliferation and somatic hypermutation, and the light zone, which is the site of affinity selection (8, 321). Cells in the different compartments can be distinguished based on the surface expression of CXCR4 and CD86 with the former expressed by B cells in the dark zone B cells and the latter in the light zone (8, 42). Staining for these surface markers revealed that dKO GC B cells of both sexes were skewed towards the dark zone in LN (**Figure 4-1B**), thus placing UTX and JMJD3 as important regulators of GC responses.

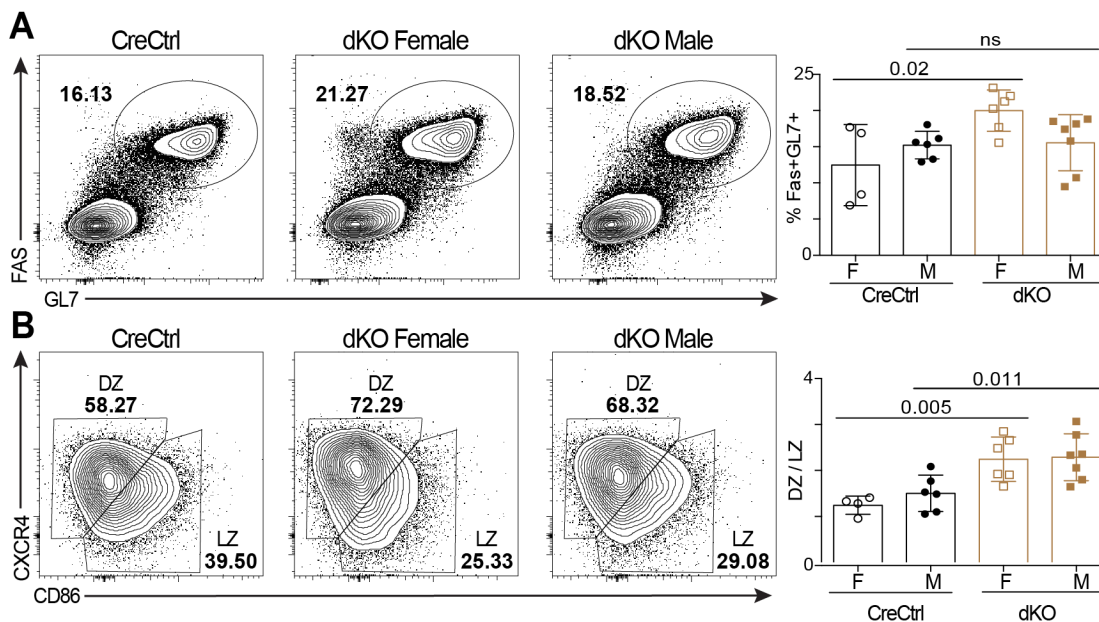


Figure 4-1. Loss of *Utx* and *Jmjd3* leads to an increase in GC B cells.

(A) Representative flow plots of GL7 and FAS expression in B220+ B cells and quantification of GL7+FAS+ GC B cells in LN 14 days after PR8 influenza infection. (B) Representative flow plots of CXCR4 and CD86 expression in GC B cells from (A) and quantification of the ratio of dark zone to light zone GC B cells.

To assess whether the UTX and JMJD3 regulated GC responses in a cell-intrinsic manner, a mixed bone marrow chimera experiment was performed. Bone marrow cells from CD45.1/2 CreCtrl and CD45.2 dKO mice were adoptively transferred into lethally irradiated CD45.1 hosts. After six weeks, the host mice were infected with PR8 influenza virus and sacrificed two weeks later for analysis. CreCtrl and dKO cells could be readily identified using congenic markers to assess GC formation in each compartment (Figure 5-2A). The analysis revealed that loss of *Utx* and *Jmjd3* in the transferred cells of both sexes resulted in a significant increase in GC B cells in LN (Figure 5-2B). Furthermore, the analysis of CXCR4 and CD86 expression on GC B cells showed a significant skewing towards the DZ (Figure 5-2C). Taken together, the results indicated that UTX and JMJD3 regulate GC B cell responses in a cell-intrinsic manner.

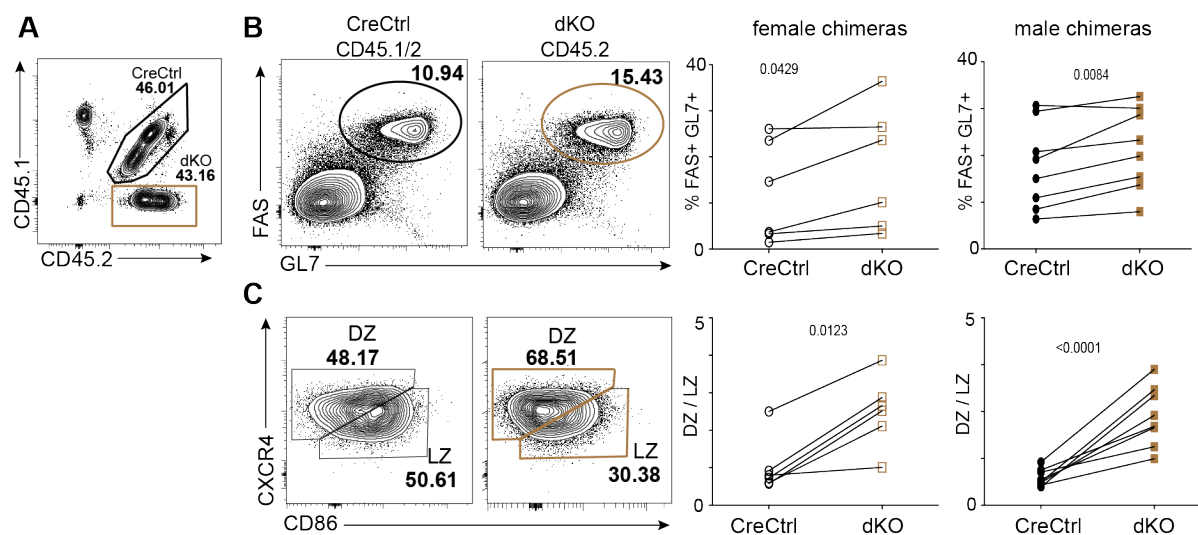


Figure 4-2. UTX and JMJD3 regulate GC B cell response in a cell-intrinsic manner.

Bone marrow cells from CD45.1/2 CreCtrl and CD45.2 dKO mice were adoptively transferred into lethally irradiated CD45.1 hosts. Six weeks later, host mice were infected with PR8 and analyzed two weeks post infection. (A) Frequencies of the chimeric populations after PR8 infection. (B) Representative plots of FAS and GL7 expression in B220⁺ B cells in CreCtrl and dKO compartments with quantification to the right. (C) Representative plots of CXCR4 and CD86 expression in GC B cells from (B) with quantification to the right.

To begin to understand the molecular mechanism by which UTX and JMJD3 regulate GC responses, RNA-seq was performed on FACS-isolated FAS⁺GL7⁺ B cells from LN from female CreCtrl and dKO mice at day 14 post infection. Differential expression analysis revealed 323 DEG ($\log_2FC > 1$ and $FDR \leq 0.05$). Consistent with the role of H3K27me3 demethylases in promoting gene expression, the majority of the DEG were downregulated in dKO GC B cells (221/323 or 68%) (Figure 4-3A and 4-3B). Loss of *Utx* and *Jmjd3* resulted in downregulation of genes associated with actin polymerization, signaling, and chemotaxis (Figure 4-3C). Examples of genes downregulated in dKO GC B cells include *Cxcr3*, which promotes homing to the lungs (322, 323), and *Evl*, which is involved in actin remodeling and cell movement (324) (Figure 4-3D). Additionally, dKO GC B cells upregulated genes associated with oxidative phosphorylation and fatty acid metabolism, both of which were shown to be the energy sources of GC B cells (53, 325)

(Figure 4-3C). Furthermore, genes that have previously been shown have high H3K27me3 enrichment in GC B cells were downregulated in dKO B cells, suggesting that demethylase activity of UTX and JMJD3 might be required to regulate the expression of those genes (Figure 4-3E)

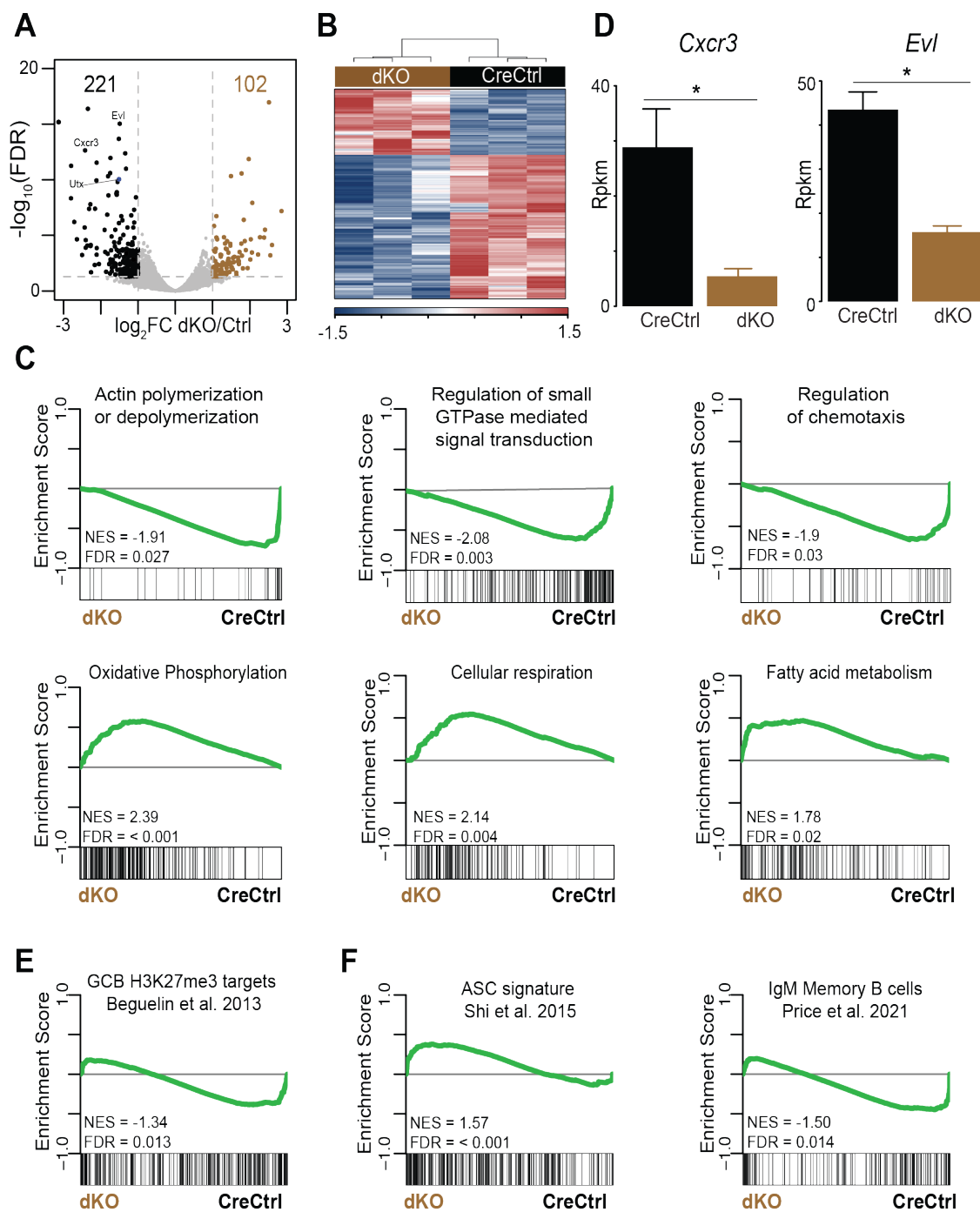


Figure 4-3. UTX and JMJD3 regulate GC B cells transcriptome.

(A) Volcano plot summarizing the results of differential expression analysis. (B) Heatmap of hierarchical clustering of z-score normalized Rpkm of DEG between CreCtrl and dKO GC B cells. (C) GSEA plots for top up- and downregulated pathways in dKO GC B cells. (D) Bar plots representing the Rkpm values for the indicated genes in both samples groups. GSEA plots displaying the enrichment of genes with H3K27me3 in GC B cells (Beguelin et al. 2013) (E) PC signature genes (Shi et. al 2015), IgM+ memory genes (Price et al. 2021) (F).

After several rounds of somatic mutation and affinity selection, GC B cells exit either as LLPC or memory B cells. Gene set enrichment analysis using previously published genes signatures revealed that dKO GC B cells had higher expression of genes associated with PC fate and downregulated genes associated with memory B cells (46, 118) (**Figure 4-3F**). The results suggest that UTX and JMJD3 might regulate the formation of GC-derived LLPC.

To assess whether loss of *Utx* and *Jmjd3* impacted LLPC formation, CreCtrl and dKO mice were infected with PR8 and sacrificed 35 days post infection for analysis. Assessment of hemagglutinin (HA) specific antibody titers in the serum of infected mice, revealed no significant differences between CreCtrl and dKO mice (**Figure4-4A**). Furthermore, preliminary analysis of HA-specific bone marrow LLPC expressing the kappa light chain, which is expressed by the majority of B cells, also showed no significant differences (**Figure 4-4B, 4-4C**). Thus, the preliminary data suggest that UTX and JMJD3 might not be involved in the formation of LLPC. However, further analysis is required to assess the formation of LLPC specific for the other flu antigens for each of the antibody isotypes.

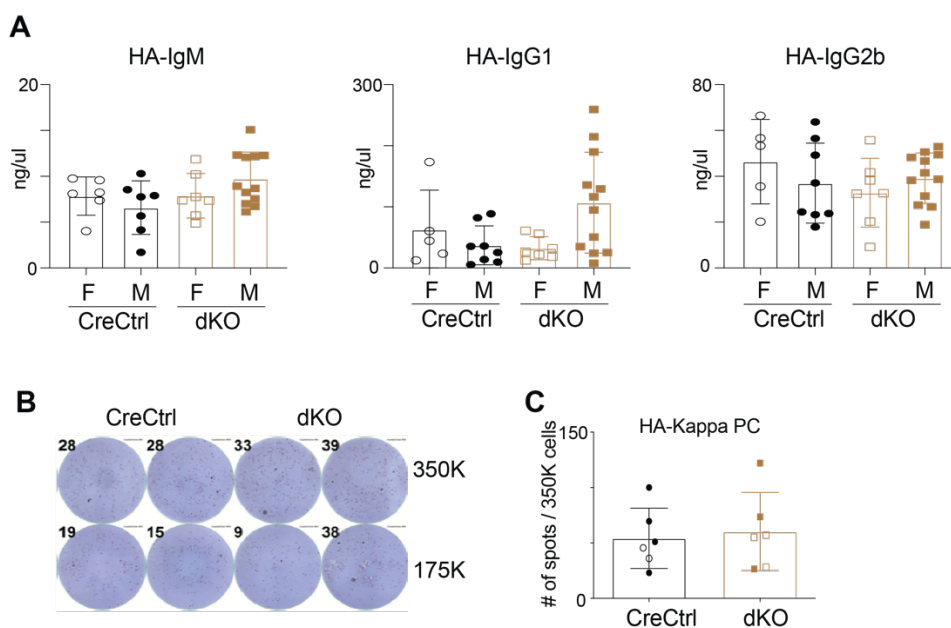


Figure 4-4. LLPC formation in UTX and JMJD3-deficient mice.

(A) HA-specific serum antibody titers in CreCtrl and dKO mice 35+ days after PR8 infection. (B) ELISPOT analysis of HA+ LLPC in the bone marrow expressing the kappa light chain. Two technical replicates per genotype are shown. (C) Quantification of ELISPOTS from (B).

As discussed in chapter 3, the use of mice with single deletion of either *Utx* or *Jmjd3* revealed that the increase in PC observed in dKO mice was mediated by UTX alone. To investigate whether this enzyme is also the primary H3K27me3 demethylase in GC B cells, CreCtrl, dKO, UTX-sKO, and JMJD3-sKO mice were infected with PR8 influenza virus. After 14 days, a significant increase in GC was observed in dKO females consistent with previous results. Interestingly, while UTX-sKO phenocopied dKO mice, JMJD3-sKO exhibited a slight reduction in GC B cells, suggesting that the two H3K27me3 might have opposite functions in controlling the GC response (Figure 4-5A). Furthermore, evaluation of CXCR4 and CD86 expression in GC B cells revealed modest, but not statistically significant, skewing towards the dark zone in UTX-deficient GC B cells. However, in JMJD3-deficient mice a significant increase in LZ GC B cells was observed, once again suggesting that the two H3K27me3 demethylases likely have distinct functions in the GC response (Figure 4-5B).

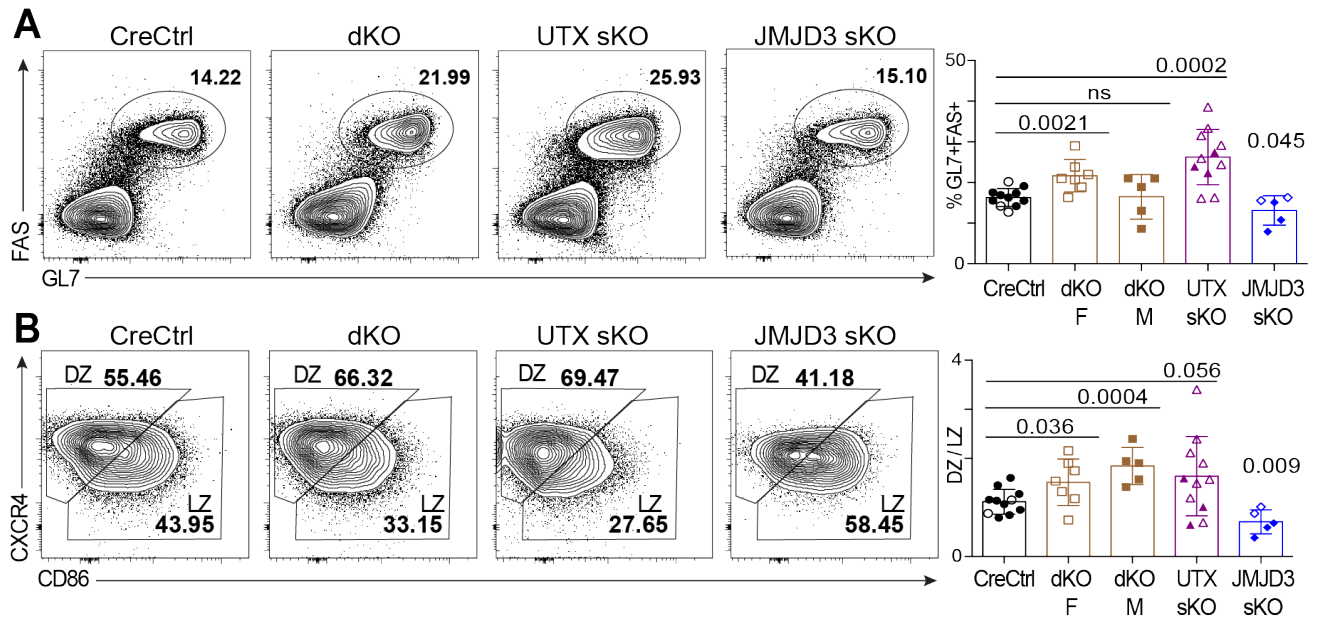


Figure 4-5. UTX and JMJD3 single knockout mice exhibit distinct GC phenotypes.

(A) Representative flow plots of GL7 and FAS expression in B220+ B cells and quantification of GL7+FAS+ GC B cells in LN 14 days after PR8 influenza infection. (B) Representative flow plots of CXCR4 and CD86 expression in GC B cells from (A) and quantification of the ratio of the dark zone to light zone B cells.

Discussion

The data presented in this chapter demonstrated that in addition to regulating the initial wave of PC formation, UTX and JMJD3 also regulate the GC response. Loss of these enzymes resulted in a significant increase in GC in the female mice with a modest but not statistically significant difference in the males. Interestingly, mixed bone marrow chimera experiments revealed significant differences in GC B cells in UTX and JMJD3-deficient B cells of both sexes, suggesting that dKO B cells can outcompete their CreCtrl counterparts when in competition. Furthermore, dKO B cells of both sexes were skewed towards the DZ of the GC, which could be caused by enhanced proliferation and expansion of dKO DZ B cells and/or failure to transition to the light zone. Given that loss of *Utx* and *Jmjd3* led to downregulation of genes involved in the trafficking of cells between the light and dark zone, including chemotaxis and actin

polymerization, it is plausible that dKO B cells exhibit a defect in trafficking between the light and dark zone.

Epigenetic modifiers have been shown to be critical regulators of B cell fate decisions, including GC formation. In fact, gain of function mutations in *EZH2*, the H3K27me3 methyltransferase, occur in ~20% of cases of diffuse large B cell lymphoma, which led to a great interest in understanding the role of this enzyme in GC B cells (326). Mouse studies revealed that loss of *Ezh2* impaired GC formation, while a gain of function mutation in *Ezh2* accelerated lymphoma formation (137). Loss of *Utx* and *Jmjd3* mimicked the phenotype of mice with gain-of-function EZH2, which is consistent with the fact that both scenarios are predicted to increase levels of H3K27me3. These findings also suggest that UTX and EZH2 likely regulate the same group of genes. Thus, the data presented in this chapter highlight the importance of maintaining optimal levels of H3K27me3 in GC B cells.

While dKO GC B cells upregulated genes associated with the PC fate compared to their CreCtrl counterparts, no differences in HA-specific LLPC or HA-specific antibody titers were observed. One possible explanation is that UTX and JMJD3 regulate the initial B cells responses following stimulation such as the formation of SLPC described in Chapter 3 and GC B cells in this chapter. Alternatively, UTX and JMJD3 might be necessary to control the formation of a specific subset of LLPC specific to one of the other influenza antigens or the quality of the antibody generated, both of which would require further studies.

The experiments conducted using single knockout mice revealed that while loss of *Utx* alone led to an increase in GC B cells and skewing towards the DZ, the opposite phenotype was observed in JMJD3 sKO. The differences in the activity of the enzymes likely stem from their structural differences, which ultimately dictate their binding partners. Unlike JMJD3, UTX harbors

six tetratricopeptide domains, which play a critical role in protein-protein interactions (180). In fact, loss of these domains was shown to impair the ability of UTX to partner with members of the MLL complex (179). Furthermore, while paradoxical at first, the obtained results are consistent with the clinical studies of GC-derived lymphomas, such as diffuse large B cell lymphoma. Mutations in *UTX* are predominately loss of function, suggesting that UTX is a tumor suppressor in lymphoma (232). Other studies, however, revealed an increased expression of *JMJD3*, suggesting it promotes the disease phenotype (234, 235). A full understanding of the differences in the regulation of GC B cells by UTX and JMJD3 requires further studies using single knockout mice and would be of great clinical relevance.

METHODS

Mice

Mice with floxed *Utx* and *Jmjd3* alleles were previously described (59) and were obtained from Dr. R. Bosselut (National Cancer Institute). *Utx^{fl/fl}*; *Jmjd3^{fl/fl}* were bred to *Cd19^{Cre/+}* (006785; The Jackson Laboratory) to obtain *Utx^{fl/fl}*; *Jmjd^{fl/fl}*; *Cd19^{Cre/+}*. All experiments were performed with 9-11 weeks old mice of both sexes. Mice were infected with influenza A/PR8/34 (PR8) at 15,000 virus forming units per dose and monitored for two weeks for weight loss. Mice that lost more than 25% of their initial body weight were euthanized in accordance with IACUC protocols.

For bone marrow chimera experiments, 15×10^6 million bone marrow cells from CD45.1/2 CreCtrl and CD45.2 dKO were mixed at 1:1 ratio and transferred into lethally irradiated CD45.1 B6 hosts (002014; The Jackson Laboratory). Six weeks later, host mice were infected with PR8 influenza virus.

Flow cytometry

Cells were resuspended at $10^6/100 \mu\text{l}$ in FACS buffer (1X PBS, 1% BSA, and 2 mM EDTA) and blocked with anti-Fc (anti-CD16/CD32; BD Bioscience). The following antibodies were used for staining and are from Biolegend: B220 PE-Cy7 (RA3-6B2), B220 Alexa 700 (RA3-6B2), FAS (Jo2), CD11b APC-Cy7 (M1/70F4/80), F4/80 APC-Cy7 (BM8), Thy1.2 APC-Cy7 (30H12), CD45.1 APC (A20), CD45.2 BV785 (104); BD Bioscience: CD138 BV711 (281-2), CXCR4 (2B11), CD86 (GL-1) ; and ThermoFisher Scientific: GL7 eFluor660 (GL-7), IgM FITC (II/41), GL7 eFluor450 (GL-7). Zombie Yellow Viability Dye (423104; Biolegend) and Zombie NIR Viability Dye (423106; Biolegend) were used to assess cell viability. Cells were stained for 40 min and fixed using 1% paraformaldehyde. Flow cytometry was performed on a BD Fortessa X20 using FACSDiva and analyzed using FlowJo v10 software. The following gating strategy preceded all flow cytometry analyses presented. Cells were gated on 1) lymphocytes (forward light scatter [FSC]–area by side scatter [SSC]–area), 2) singlets by FSC-height/FSC- width or FSC-height/FSC- area. CD11B, F4/80, and THY1.2 markers were used to exclude non-B cells

Enzyme-Linked Immunosorbent Assay (ELISA)

ELISA plates (M9410; Sigma) were coated with HA at $1 \mu\text{g/ml}$ overnight at 4°C and blocked with 3% nonfat dry milk for 2 h. A Standard curve for each antibody isotype (5300-01B; Southern Biotechnology) and serum samples were incubated at 4°C overnight. The next day, the plates were washed and incubated with HRP-conjugated goat anti-mouse secondary antibody (1021-05; Southern Biotechnology) for 2 h at room temperature. The plates were developed using TMB ELISA peroxidase substrate (800-666-7625; Rockland) and the reaction was stopped using 0.2M sulfuric acid. Plates were read using ELx808 Absorbance plate reader (BioTek).

ELISPOTS

Multiscreen HA plates (Millipore, MAHAS4510) were coated with purified HA at 10 µg/ml in PBS overnight at 4°C. Plates were washed with PBS and blocked in B cell media for at least 1h at room temperature. Bone marrow cells were isolated from both femurs and tibias. Following lysis of red blood cells, single cell suspensions were layered on top of Ficoll (GE 17-1440-02; Sigma) and centrifuge for 15min at 2,000 rpm with no accelerate and no deceleration. Cells in the mononuclear layers were harvested, washed, diluted in B cells media, and cultured in the coated plates overnight in a 37°C incubator with 5% CO₂. The next day, plates were washed with PBS containing 0.2% Tween-20 and incubated with alkaline phosphatase–conjugated goat anti–mouse kappa (Southern Biotech, 1050-04) in PBS containing 0.2% Tween-20 and 0.5% BSA for 1 hr at 37°C. Plates were washed and developed with BCIP/NBT (Moss Substrates). The plates were visualized on ImmunoSpot S6 ULTIMATE Analyzer (Cellular Technology Limited) and quantified using ImmunoSpot software v5.0.9.21.

RNA-seq

One thousand cells were sorted directly into RLT buffer (79216; Qiagen) containing 1% 2-Mercaptoethanol. RNA was isolated using Zymo Quick-RNA MicroPrep Kit (11-328M; Zymo Research). Synthesis of cDNA was performed using SMART-Seq v4 Ultra Low Input RNA Kit (634894; Takara Bio) kit. The generated cDNA was used as an input for the NexteraXT kit (Illumina, FC-131-1024). Raw sequencing reads were mapped to the mm10 genome using STAR v2.5.3a (311). Raw and reads per kilobase per million (RpkM) normalized gene expression counts were determined by annotating the coverage across all exons for all unique ENTREZ genes using the GenomicAlignments (312) package. Differential expression analysis was performed using

edgeR (313) with $\log_2FC > 1$ and $FDR \leq 0.05$ being considered significant. Gene Set Enrichment Analysis (GSEA) (262) was performed using a pre-ranked gene list generated by multiplying the sign of the fold change (negative or positive) by the $-\log_{10}$ of the edgeR derived p value.

Chapter 5. Discussion

Anna K. Kania

Department of Microbiology and Immunology, Emory University School of Medicine, Atlanta,
GA 30322, USA

The ability of naïve B cells to differentiate into PC is the corner of humoral immunity, which provides us with long-lasting protection against pathogens and has been the basis behind vaccine development (3, 33). The transition from a quiescent B cell to an antibody-secreting PC requires substantial physiological, metabolic, transcriptional, and epigenetic reprogramming (34, 246, 304). However, when dysregulated, B cell differentiation can lead to the development of B-cell malignancies and autoimmune diseases (9, 13). A complete understanding of the programming events that occur during B cell development is necessary to fully understand the etiology of B cell-mediated diseases and develop novel therapeutics for their treatment. While the physiological and transcriptional changes that occur during B cell differentiation have been well-established, a full understanding of the epigenetic changes that occur during PC formation is still developing. This dissertation contributes to this gap in knowledge and establishes the H3K27me3 demethylases as novel epigenetic regulators of B development, differentiation, and GC response. The primary focus of this work has been on the role of UTX and JMJD3 in PC formation, which was investigated by chemical inhibition and genetic deletion of *Utx* and *Jmjd3*. Collectively, the data establishes UTX as a novel factor restraining B cell differentiation.

B cells can respond to a wide range of antigens in either TI or TD manner and differentiate into PC to facilitate clearance of pathogens (7, 34). Depending on the nature of the antigen, B cells can undergo different fate decisions. Following stimulation with TI antigens, activated B cells differentiate into PC or die. However, B cells responding to TD antigen, such as the influenza virus, can follow one of three cell fates: SLPC, early memory B cells, or GC B cells (39, 40). Chemical inhibitor or genetic deletion of *Utx* and *Jmjd3* resulted in an increase in PC following stimulation with TI antigens; whereas, following influenza infection loss of these demethylases led to a significant increase in GC B cells. Furthermore, in both cases, the changes were driven by

loss of *Utx* as UTX-sKO mimicked the phenotype observed in dKO mice. Thus, taken together, the data suggest that UTX is a negative regulator of the early B cell fate decisions following stimulation. Moreover, the results are consistent with the tumor suppressor functions of UTX reported in B cell lymphoma and multiple myeloma (231, 232, 306).

A robust response upon secondary infection with previously encountered antigen is mediated by both LLPC and memory B cells, both of which are predominately GC-derived (3, 45). Whereas LLPC constitutively secrete antibodies to promote clearance of previously encountered antigens upon reinfection, memory B cells rapidly regenerated a new wave of PC to prevent infection (3, 7, 45). Loss of *Utx* and *Jmjd3* led to an increase in the early wave of PC, but no difference in the GC-derived LLPC despite an increase in GC B cells, which could be interpreted in one of three ways. First, UTX only regulates the early wave of B cell differentiation following antigen engagement. Second, UTX and JMJD3-deficient B cells fail to exit the GC leading to the observed increase in GC B cells. Third, loss of H3K27me3 demethylases leads to a preferential differentiation of the dKO GC B cells into memory B cells rather than LLPC. The third hypothesis is supported by the fact that similar observations have been reported in CD8 T cells. Loss of *Utx* led to an increase in memory CD8 T cells and a more robust response upon secondary re-challenge (216, 217). Furthermore, a recent study demonstrated that primed chromatin landscape contributes to the rapid secondary responses of memory B cells, thus strongly suggesting epigenetic reprogramming plays a critical role in these cells (118). As such, it would be of great value for future studies to examine the role of UTX and JMJD3 in the formation and reactivation of memory B cells.

It is becoming increasingly appreciated that males and females differ in their immune response to antigens. Generally, females mount more robust immune responses and have a lower

mortality rate following viral infections, but they are also more prone to autoimmune diseases. These sex-specific differences are mediated by the sex hormones and dosage of genes encoded on the X chromosome (327, 328). While the majority of genes encoded on the sex chromosomes are dosage compensated, a fraction of these genes (15% in humans and 3% in mice) escapes X-inactivation, thus contributing to the sex differences. Examples of such genes include *CD40LG*, *CXCR3*, *TLR7*, which are known to regulate immune responses (329, 330). This list also includes *UTX*, which was shown in this dissertation to fine-tune B cell responses to a variety of antigens. Thus, the differential expression of *UTX* between sexes might also contribute to the sex-specific immune responses. In fact, the lower *UTX* expression was associated with poor survival in B cell lymphoma patients and the majority of male patients were in the high-risk group (232).

In addition to the single copy of *UTX*, males also carry a single copy of *UTY* on the Y chromosome. Due to point mutations in the catalytic domain, *UTY* does not possess any catalytic activity; however, because of the high structural homology, it can still regulate gene expression in a demethylase-independent manner (169, 175, 200). As a result, comparing male and female dKO mice allows us to discriminate between demethylase-dependent and independent functions of *UTX* in B cell differentiation. Interestingly, while the increase in PC following stimulation with TI antigens occurred in dKO mice of both sexes, the increase in GC B cells following flu infection was only observed in females, suggesting that only the former requires the catalytic activity of *UTX*. Interestingly, when in competition, loss of *Utx* and *Jmjd3* led to an increase in more GC B cells in both sexes, thus suggesting that under certain circumstances the demethylase activity of *UTX* is nevertheless required. The alternative explanation is that the loss of H3K27me3 demethylases puts the cells in a hyperactivated state that allows them to more rapidly respond to antigen stimulation; however, because the differences are rather small in magnitude, they are only

significant when directly compared in competition. Furthermore, it is possible that the increase in basal surface IgM BCR observed in naïve dKO B cells (data not shown) persist in GC B cells thus providing the cells with a competitive advantage for binding the antigen in the LZ resulting in increased proliferation in the DZ and the overall increase in GC B cells.

Loss of *Utx* and *Jmjd3* led to an expansion of the GC and skewing towards the DZ, which is the site of rapid proliferation and somatic hypermutation. However, it is unclear whether this phenotype results from increased proliferation of dKO DZ B cells or a failure to reenter the LZ. The former would suggest that dKO GC B cells are receiving a higher amount of proliferative signals in the LZ as the number of cell divisions the cells undergo in the DZ is directly proportional to the amount of T cell help received in the LZ, which in turn is proportional to the amount of antigen presented by B cells (285). A failure to exit DZ, the second hypothesis, is equally possible and supported by RNA-seq data. Loss of *Utx* and *Jmjd3* led to downregulation of genes associated with chemotaxis, cell signaling, and actin polymerization, all of which play a critical role in the irritative cycling of the cells between the DZ and LZ of GC (7, 321, 331). Such results could also lead to fewer cycles of affinity selection resulting in a failure to generate high-affinity antibodies, which might result in failure to clear the virus upon reinfection.

It is becoming increasingly appreciated that changes in chromatin accessibility and the distribution of histone modifications and DNA methylation play a critical role in fine-tuning B cell responses (34, 120). Loss of the H3K4 methyltransferase *Kmt2d* resulted in an increase in GC B cells (147), while loss of the H3K4me1/2 demethylase *Lsd1* had the opposite effect (278). Furthermore, while KMT2D-deficient B cells showed enhanced proliferation (147), LSD1-deficient cells exhibited impaired proliferation and differentiation in PC (146). Similar parallels can be made in regards to the regulation of H3K27me3 levels (**Figure 5-1**). Loss of *Ezh2*, the

methyltransferase, impaired B cell proliferation and PC formation in response to TI antigens (141), while loss of the *Utx* and *Jmjd3* enhanced B cell differentiation. Furthermore, EZH2 deficiency compromised the formation of GC (137, 138), while loss of the two H3K27me3 demethylases resulted in an increase in GC B cells. Moreover, these findings are also consistent with the fact that gain of function mutations in *EZH2* are frequently found in B cell lymphomas (307, 326), while mutations in *UTX* are typically loss of function (232, 306). Enhanced activity of EZH2 activity or loss of *UTX* both lead to an increase in H3K27me3 levels, suggesting that maintaining the homeostatic levels of this histone modification is crucial for normal B cell function and preventing malignancies.

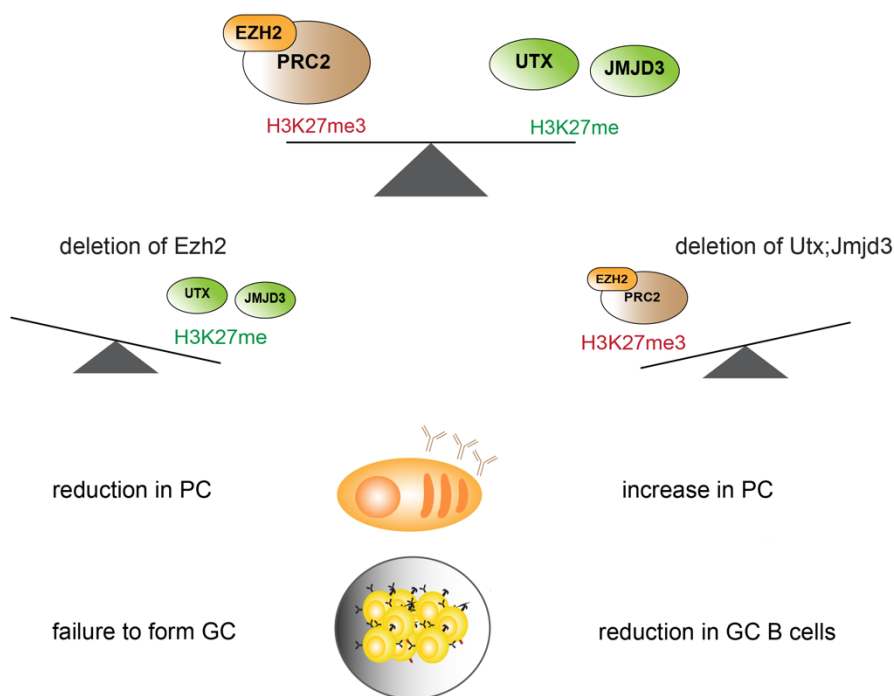


Figure 5-1. Balanced levels of H3K27me3 are required for proper B cell responses.

Loss of *Ezh2*, the methyltransferase, impaired B cell differentiation into PC and GC formation (137, 138, 141). Loss *Utx* and *Jmjd3* had the opposite effect.

While mutation in *EZH2* occurs in ~20% of cases of DLBCL (332), the incidence of *UTX* mutations is much lower in lymphoma raising the question as to why. One possible explanation is that the gain of function mutations in *EZH2* are typically heterozygous. While the mutant *EZH2* allele is very efficient at adding the third methyl group to H3K27, it relies on the wild-type copy of *EZH2* to promote H3K27me₂ (333, 334). A complete loss of *UTX* on the other hand would require the deletion of both copies of the gene, which is mechanistically more difficult to produce than single amino acid substitutions. Furthermore, while the *EZH2* is the only H3K27me₃ methyltransferase, there are two H3K27me₃ demethylases.

Epigenetic regulation of biological processes includes changes in DNA methylation and histone modifications, which together modulate gene expression (116). The presence of histone modifications can also be used as a proxy for the identification of important genomic regions. Active promoters are typically associated with H3K4me₃ and H3K27ac, while active enhancers are enriched for H3K27ac but not H3K4me₁ (335). Additionally, transcriptionally inactive regions are associated with H3K27me₃ and H3K9me₃ (116). However, despite the fact that various histone modifications tend to co-occur, less is known about the cooperative activity of the various epigenetic modifiers. Several studies have demonstrated that *UTX* and *JMJD3* physically interact with members of the *MLL* complex, which promotes H3K4 methylation (200, 228, 252). Additionally, these enzymes were also shown to interact with *P300*, which promotes histone acetylation (182), as well as chromatin remodelers *BRG1* (184, 190, 205) and *CHD4* (251). Together, these data suggest that the coordinated action of various epigenetic modifiers is required to modulate gene expression. In fact, in ESC, *UTX* was required to promote the activity of *P300* and *MLL* complex and to modulate gene expression (182). While the protein complex of *UTX*-*P300*-*MLL* is just one example, it is likely that other epigenetic modifiers also interact with each

other to rapidly alter the epigenetic landscape. In fact, LSD1 is known to interact with histone deacetylases to promote gene silencing (336). Moreover, one study reported that the DNA methyltransferases DNMT3a physically interacts with the H3K36me2 methyltransferase to regulate the chromatin landscape (337). However, the majority of studies, including this dissertation, focus on investigating the role of a single epigenetic enzyme or a single histone modification at a time. As a result, our understanding of the cooperative activity of various chromatin modifiers is still in its infancy and requires further investigation.

Loss of H3K27me3 can occur via two mechanisms: an active removal of methyl groups by UTX and JMJD3 or a passive loss of the histone modification during cell division (299). As discussed in chapter 3, loss of *Utx* and *Jmjd3* resulted in 99 regions with significantly higher enrichment of H3K27me3 in UTX and JMJD3-deficient PC, suggesting that only a small subset of genes undergo an active loss of H3K27me3 during B cell differentiation and require the demethylase activity of UTX. However, these regions corresponded to several pro-apoptotic genes, such as *Bcl2l11* and *Trp73*, and resulted in the reduced apoptosis of dKO PC, thus illustrating the critical role of H3K27me3 in PC biology. Additionally, the changes in histone enrichment correlated with vast changes in chromatin accessibility with ~90% of DAR corresponding to regions with lower chromatin accessibility in dKO PC, thus highlighting the interplay between H3K27me3 and chromatin accessibility. Given that UTX has been previously demonstrated to regulate enhancer activity in a demethylase-independent manner, it is plausible that a subset of the downDAR were regulated via such mechanism. It is important to note that the demethylase-dependent and independent functions of UTX are not mutually exclusive. During differentiation of ESC into cardiac cells, the catalytic activity of UTX was required to remove methyl groups from H3K27me3 at cardiac-specific genes, while the non-catalytic activity was

required to recruit the chromatin remodeler BRG1 (190). Thus, it is possible that both activities of UTX are also required for its role in B cell differentiation.

Epigenetic enzymes, including UTX and JMJD3, do not possess DNA binding domains and are recruited to their target genes by TF (320). Regions with lower chromatin accessibility in dKO PC were enriched for ETS and ETS:IRF8 family TF such as SPIB, PU.1, PU1:IRF8. Furthermore, SPIB was also identified by PageRank as an important transcriptional regulator and, as shown in chapter 2, is one of the key TF that gain H3K27me3 during B cell differentiation. Combined with the fact that SPIB and its closely related homolog PU.1 are known repressors of PC fate (107, 108), the results suggest that SPIB could be one of the TF that recruits UTX to its target genes to modulate gene expression and ultimately PC formation. Further experiments such as co-immunoprecipitation would be necessary to directly assess whether SPIB and UTX physically interact.

In summary, the data presented in this dissertation provide a novel insight into our understanding of the epigenetic reprogramming that occurs during B cell differentiation (**Figure 5-2**). We demonstrated that inhibition or genetic deletion of both H3K27me3 demethylases led to an increase in PC establishing these enzymes are negative regulators of B cell differentiation. Moreover, we demonstrated that UTX is the primary H3K27me3 demethylase during B cell differentiation. UTX regulated the expression of genes associated with OXPHOS, proliferation, and apoptosis, and modulated chromatin accessibility and H3K27me3 enrichment in PC. Additionally, we also showed that loss of H3K27me3 demethylases led to an increase in GC B cells and skewing to the dark zone, both of which were driven by loss of *Utx*. In this setting, UTX regulated the expression of genes associated with chemotaxis, signaling, and metabolism. Taken

together, this dissertation has established UTX as a critical epigenetic factor restraining PC and GC B cell formation.

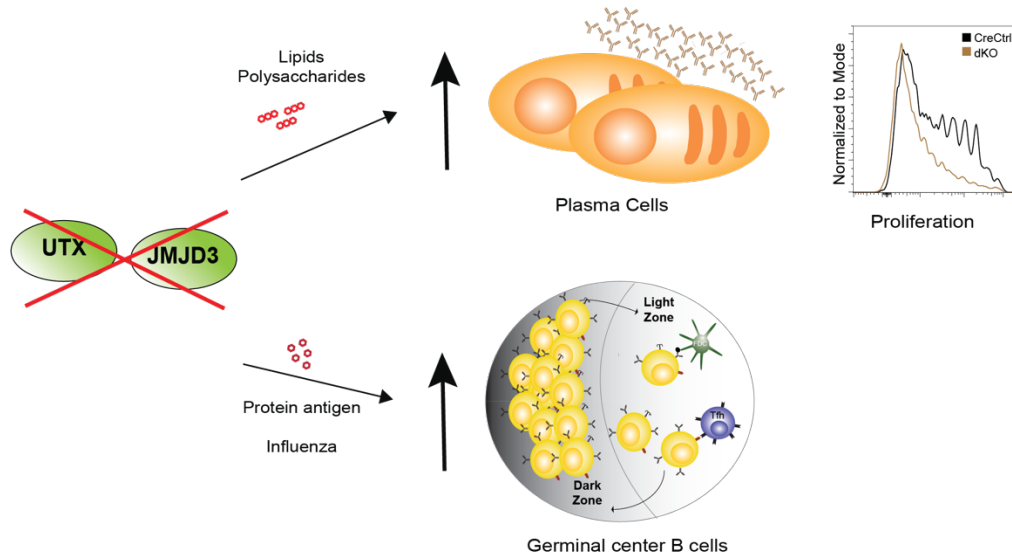


Figure 5-2. H3K27me3 demethylases are negative regulators of B cell responses.

Graphical representation of key findings presented in this dissertation. In response to T-cell independent antigens, loss of Utx and Jmjd3 led to an increase in cell proliferation and plasma cells formation. Stimulation with the influenza virus led to an increase in GC B cells in dKO mice.

REFERENCES

1. Forthal, D. N. 2014. Functions of Antibodies. *Microbiol Spectr* 2: AID-0019-2014.
2. Lu, L. L., T. J. Suscovich, S. M. Fortune, and G. Alter. 2018. Beyond binding: antibody effector functions in infectious diseases. *Nat Rev Immunol* 18: 46-61.
3. Akkaya, M., K. Kwak, and S. K. Pierce. 2020. B cell memory: building two walls of protection against pathogens. *Nat Rev Immunol* 20: 229-238.
4. Palm, A. E., and C. Henry. 2019. Remembrance of Things Past: Long-Term B Cell Memory After Infection and Vaccination. *Front Immunol* 10: 1787.
5. Amanna, I. J., N. E. Carlson, and M. K. Slifka. 2007. Duration of humoral immunity to common viral and vaccine antigens. *N Engl J Med* 357: 1903-1915.
6. Pollard, A. J., and E. M. Bijker. 2021. A guide to vaccinology: from basic principles to new developments. *Nat Rev Immunol* 21: 83-100.
7. Cyster, J. G., and C. D. C. Allen. 2019. B Cell Responses: Cell Interaction Dynamics and Decisions. *Cell* 177: 524-540.
8. Victora, G. D., and M. C. Nussenzweig. 2012. Germinal centers. *Annu Rev Immunol* 30: 429-457.
9. Klein, U., and R. Dalla-Favera. 2008. Germinal centres: role in B-cell physiology and malignancy. *Nat Rev Immunol* 8: 22-33.
10. Barwick, B. G., V. A. Gupta, P. M. Vertino, and L. H. Boise. 2019. Cell of Origin and Genetic Alterations in the Pathogenesis of Multiple Myeloma. *Front Immunol* 10: 1121.
11. Hoehn, K. B., A. Fowler, G. Lunter, and O. G. Pybus. 2016. The Diversity and Molecular Evolution of B-Cell Receptors during Infection. *Mol Biol Evol* 33: 1147-1157.
12. Musette, P., and J. D. Bouaziz. 2018. B Cell Modulation Strategies in Autoimmune Diseases: New Concepts. *Front Immunol* 9: 622.
13. Davidson, A., and B. Diamond. 2001. Autoimmune diseases. *N Engl J Med* 345: 340-350.
14. Jenks, S. A., K. S. Cashman, M. C. Woodruff, F. E. Lee, and I. Sanz. 2019. Extrafollicular responses in humans and SLE. *Immunol Rev* 288: 136-148.
15. Busslinger, M. 2004. Transcriptional control of early B cell development. *Annu Rev Immunol* 22: 55-79.
16. Urbanek, P., Z. Q. Wang, I. Fetka, E. F. Wagner, and M. Busslinger. 1994. Complete block of early B cell differentiation and altered patterning of the posterior midbrain in mice lacking Pax5/BSAP. *Cell* 79: 901-912.
17. Nutt, S. L., B. Heavey, A. G. Rolink, and M. Busslinger. 1999. Commitment to the B-lymphoid lineage depends on the transcription factor Pax5. *Nature* 401: 556-562.
18. Jung, D., C. Giallourakis, R. Mostoslavsky, and F. W. Alt. 2006. Mechanism and control of V(D)J recombination at the immunoglobulin heavy chain locus. *Annu Rev Immunol* 24: 541-570.
19. Melchers, F. 2015. Checkpoints that control B cell development. *J Clin Invest* 125: 2203-2210.
20. Vettermann, C., K. Herrmann, and H. M. Jack. 2006. Powered by pairing: the surrogate light chain amplifies immunoglobulin heavy chain signaling and pre-selects the antibody repertoire. *Semin Immunol* 18: 44-55.
21. Shimizu, T., C. Mundt, S. Licence, F. Melchers, and I. L. Martensson. 2002. VpreB1/VpreB2/lambda 5 triple-deficient mice show impaired B cell development but functional allelic exclusion of the IgH locus. *J Immunol* 168: 6286-6293.

22. Schuh, W., S. Meister, E. Roth, and H. M. Jack. 2003. Cutting edge: signaling and cell surface expression of a mu H chain in the absence of lambda 5: a paradigm revisited. *J Immunol* 171: 3343-3347.
23. Melchers, F., T. Yamagami, A. Rolink, and J. Andersson. 2007. Rules for the rearrangement events at the L chain gene loci of the mouse. *Adv Exp Med Biol* 596: 63-70.
24. Simmons, S., and M. Ishii. 2014. Sphingosine-1-phosphate: a master regulator of lymphocyte egress and immunity. *Arch Immunol Ther Exp (Warsz)* 62: 103-115.
25. Allende, M. L., G. Tuymetova, B. G. Lee, E. Bonifacino, Y. P. Wu, and R. L. Proia. 2010. S1P1 receptor directs the release of immature B cells from bone marrow into blood. *J Exp Med* 207: 1113-1124.
26. Pillai, S., and A. Cariappa. 2009. The follicular versus marginal zone B lymphocyte cell fate decision. *Nat Rev Immunol* 9: 767-777.
27. Allman, D., and S. Pillai. 2008. Peripheral B cell subsets. *Curr Opin Immunol* 20: 149-157.
28. Allman, D., R. C. Lindsley, W. DeMuth, K. Rudd, S. A. Shinton, and R. R. Hardy. 2001. Resolution of three nonproliferative immature splenic B cell subsets reveals multiple selection points during peripheral B cell maturation. *J Immunol* 167: 6834-6840.
29. Teague, B. N., Y. Pan, P. A. Mudd, B. Nakken, Q. Zhang, P. Szodoray, X. Kim-Howard, P. C. Wilson, and A. D. Farris. 2007. Cutting edge: Transitional T3 B cells do not give rise to mature B cells, have undergone selection, and are reduced in murine lupus. *J Immunol* 178: 7511-7515.
30. Saito, T., S. Chiba, M. Ichikawa, A. Kunisato, T. Asai, K. Shimizu, T. Yamaguchi, G. Yamamoto, S. Seo, K. Kumano, E. Nakagami-Yamaguchi, Y. Hamada, S. Aizawa, and H. Hirai. 2003. Notch2 is preferentially expressed in mature B cells and indispensable for marginal zone B lineage development. *Immunity* 18: 675-685.
31. Hozumi, K., N. Negishi, D. Suzuki, N. Abe, Y. Sotomaru, N. Tamaoki, C. Mailhos, D. Ish-Horowicz, S. Habu, and M. J. Owen. 2004. Delta-like 1 is necessary for the generation of marginal zone B cells but not T cells in vivo. *Nat Immunol* 5: 638-644.
32. Cinamon, G., M. Matloubian, M. J. Lesneski, Y. Xu, C. Low, T. Lu, R. L. Proia, and J. G. Cyster. 2004. Sphingosine 1-phosphate receptor 1 promotes B cell localization in the splenic marginal zone. *Nat Immunol* 5: 713-720.
33. Fairfax, K. A., A. Kallies, S. L. Nutt, and D. M. Tarlinton. 2008. Plasma cell development: from B-cell subsets to long-term survival niches. *Semin Immunol* 20: 49-58.
34. Patterson, D. G., A. K. Kania, Z. Zuo, C. D. Scharer, and J. M. Boss. 2021. Epigenetic gene regulation in plasma cells. *Immunol Rev*.
35. Martin, F., and J. F. Kearney. 2002. Marginal-zone B cells. *Nat Rev Immunol* 2: 323-335.
36. Martin, F., A. M. Oliver, and J. F. Kearney. 2001. Marginal zone and B1 B cells unite in the early response against T-independent blood-borne particulate antigens. *Immunity* 14: 617-629.
37. Mond, J. J., A. Lees, and C. M. Snapper. 1995. T cell-independent antigens type 2. *Annu Rev Immunol* 13: 655-692.
38. Goodnow, C. C., C. G. Vinuesa, K. L. Randall, F. Mackay, and R. Brink. 2010. Control systems and decision making for antibody production. *Nat Immunol* 11: 681-688.

39. Chan, T. D., D. Gatto, K. Wood, T. Camidge, A. Basten, and R. Brink. 2009. Antigen affinity controls rapid T-dependent antibody production by driving the expansion rather than the differentiation or extrafollicular migration of early plasmablasts. *J Immunol* 183: 3139-3149.
40. Coffey, F., B. Alabyev, and T. Manser. 2009. Initial clonal expansion of germinal center B cells takes place at the perimeter of follicles. *Immunity* 30: 599-609.
41. Mintz, M. A., and J. G. Cyster. 2020. T follicular helper cells in germinal center B cell selection and lymphomagenesis. *Immunol Rev* 296: 48-61.
42. Victora, G. D., T. A. Schwickert, D. R. Fooksman, A. O. Kamphorst, M. Meyer-Hermann, M. L. Dustin, and M. C. Nussenzweig. 2010. Germinal center dynamics revealed by multiphoton microscopy with a photoactivatable fluorescent reporter. *Cell* 143: 592-605.
43. Gitlin, A. D., Z. Shulman, and M. C. Nussenzweig. 2014. Clonal selection in the germinal centre by regulated proliferation and hypermutation. *Nature* 509: 637-640.
44. Roco, J. A., L. Mesin, S. C. Binder, C. Nefzger, P. Gonzalez-Figueroa, P. F. Canete, J. Ellyard, Q. Shen, P. A. Robert, J. Cappello, H. Vohra, Y. Zhang, C. R. Nowosad, A. Schiepers, L. M. Corcoran, K. M. Toellner, J. M. Polo, M. Meyer-Hermann, G. D. Victora, and C. G. Vinuesa. 2019. Class-Switch Recombination Occurs Infrequently in Germinal Centers. *Immunity* 51: 337-350 e337.
45. Suan, D., C. Sundling, and R. Brink. 2017. Plasma cell and memory B cell differentiation from the germinal center. *Curr Opin Immunol* 45: 97-102.
46. Shi, W., Y. Liao, S. N. Willis, N. Taubenheim, M. Inouye, D. M. Tarlinton, G. K. Smyth, P. D. Hodgkin, S. L. Nutt, and L. M. Corcoran. 2015. Transcriptional profiling of mouse B cell terminal differentiation defines a signature for antibody-secreting plasma cells. *Nat Immunol* 16: 663-673.
47. Bortnick, A., and D. Allman. 2013. What is and what should always have been: long-lived plasma cells induced by T cell-independent antigens. *J Immunol* 190: 5913-5918.
48. Vose, B. M., and G. D. Bonnard. 1983. Limiting dilution analysis of the frequency of human T cells and large granular lymphocytes proliferating in response to interleukin 2. I. The effect of lectin on the proliferative frequency and cytotoxic activity of cultured lymphoid cells. *J Immunol* 130: 687-693.
49. Boothby, M., and R. C. Rickert. 2017. Metabolic Regulation of the Immune Humoral Response. *Immunity* 46: 743-755.
50. Aronov, M., and B. Tirosh. 2016. Metabolic Control of Plasma Cell Differentiation-What We Know and What We Don't Know. *J Clin Immunol* 36 Suppl 1: 12-17.
51. Dufort, F. J., B. F. Bleiman, M. R. Gumina, D. Blair, D. J. Wagner, M. F. Roberts, Y. Abu-Amer, and T. C. Chiles. 2007. Cutting edge: IL-4-mediated protection of primary B lymphocytes from apoptosis via Stat6-dependent regulation of glycolytic metabolism. *J Immunol* 179: 4953-4957.
52. Price, M. J., D. G. Patterson, C. D. Scharer, and J. M. Boss. 2018. Progressive Upregulation of Oxidative Metabolism Facilitates Plasmablast Differentiation to a T-Independent Antigen. *Cell Rep* 23: 3152-3159.
53. Weisel, F. J., S. J. Mullett, R. A. Elsner, A. V. Menk, N. Trivedi, W. Luo, D. Wikenheiser, W. F. Hawse, M. Chikina, S. Smita, L. J. Conter, S. M. Joachim, S. G. Wendell, M. J. Jurczak, T. H. Winkler, G. M. Delgoffe, and M. J. Shlomchik. 2020.

- Germinal center B cells selectively oxidize fatty acids for energy while conducting minimal glycolysis. *Nat Immunol* 21: 331-342.
54. Saijo, K., I. Mecklenbrauker, A. Santana, M. Leitger, C. Schmedt, and A. Tarakhovsky. 2002. Protein kinase C beta controls nuclear factor kappaB activation in B cells through selective regulation of the IkappaB kinase alpha. *J Exp Med* 195: 1647-1652.
 55. Su, T. T., B. Guo, Y. Kawakami, K. Sommer, K. Chae, L. A. Humphries, R. M. Kato, S. Kang, L. Patrone, R. Wall, M. Teitell, M. Leitges, T. Kawakami, and D. J. Rawlings. 2002. PKC-beta controls I kappa B kinase lipid raft recruitment and activation in response to BCR signaling. *Nat Immunol* 3: 780-786.
 56. Tsui, C., N. Martinez-Martin, M. Gaya, P. Maldonado, M. Llorian, N. M. Legrave, M. Rossi, J. I. MacRae, A. J. Cameron, P. J. Parker, M. Leitges, A. Bruckbauer, and F. D. Batista. 2018. Protein Kinase C-beta Dictates B Cell Fate by Regulating Mitochondrial Remodeling, Metabolic Reprogramming, and Heme Biosynthesis. *Immunity* 48: 1144-1159 e1145.
 57. Sanchez, W. Y., S. L. McGee, T. Connor, B. Mottram, A. Wilkinson, J. P. Whitehead, S. Vuckovic, and L. Catley. 2013. Dichloroacetate inhibits aerobic glycolysis in multiple myeloma cells and increases sensitivity to bortezomib. *Br J Cancer* 108: 1624-1633.
 58. Shen, Y. C., D. L. Ou, C. Hsu, K. L. Lin, C. Y. Chang, C. Y. Lin, S. H. Liu, and A. L. Cheng. 2013. Activating oxidative phosphorylation by a pyruvate dehydrogenase kinase inhibitor overcomes sorafenib resistance of hepatocellular carcinoma. *Br J Cancer* 108: 72-81.
 59. Stockwin, L. H., S. X. Yu, S. Borgel, C. Hancock, T. L. Wolfe, L. R. Phillips, M. G. Hollingshead, and D. L. Newton. 2010. Sodium dichloroacetate selectively targets cells with defects in the mitochondrial ETC. *Int J Cancer* 127: 2510-2519.
 60. Lam, W. Y., A. M. Becker, K. M. Kennerly, R. Wong, J. D. Curtis, E. M. Llufrío, K. S. McCommis, J. Fahrman, H. A. Pizzato, R. M. Nunley, J. Lee, M. J. Wolfgang, G. J. Patti, B. N. Finck, E. L. Pearce, and D. Bhattacharya. 2016. Mitochondrial Pyruvate Import Promotes Long-Term Survival of Antibody-Secreting Plasma Cells. *Immunity* 45: 60-73.
 61. Caro-Maldonado, A., R. Wang, A. G. Nichols, M. Kuraoka, S. Milasta, L. D. Sun, A. L. Gavin, E. D. Abel, G. Kelsoe, D. R. Green, and J. C. Rathmell. 2014. Metabolic reprogramming is required for antibody production that is suppressed in anergic but exaggerated in chronically BAFF-exposed B cells. *J Immunol* 192: 3626-3636.
 62. McBrayer, S. K., J. C. Cheng, S. Singhal, N. L. Krett, S. T. Rosen, and M. Shanmugam. 2012. Multiple myeloma exhibits novel dependence on GLUT4, GLUT8, and GLUT11: implications for glucose transporter-directed therapy. *Blood* 119: 4686-4697.
 63. Spencer, J. A., F. Ferraro, E. Roussakis, A. Klein, J. Wu, J. M. Runnels, W. Zaher, L. J. Mortensen, C. Alt, R. Turcotte, R. Yusuf, D. Cote, S. A. Vinogradov, D. T. Scadden, and C. P. Lin. 2014. Direct measurement of local oxygen concentration in the bone marrow of live animals. *Nature* 508: 269-273.
 64. Hetz, C., K. Zhang, and R. J. Kaufman. 2020. Mechanisms, regulation and functions of the unfolded protein response. *Nat Rev Mol Cell Biol* 21: 421-438.
 65. Yoshida, H., T. Matsui, A. Yamamoto, T. Okada, and K. Mori. 2001. XBP1 mRNA is induced by ATF6 and spliced by IRE1 in response to ER stress to produce a highly active transcription factor. *Cell* 107: 881-891.

66. Sriburi, R., S. Jackowski, K. Mori, and J. W. Brewer. 2004. XBP1: a link between the unfolded protein response, lipid biosynthesis, and biogenesis of the endoplasmic reticulum. *J Cell Biol* 167: 35-41.
67. Shaffer, A. L., M. Shapiro-Shelef, N. N. Iwakoshi, A. H. Lee, S. B. Qian, H. Zhao, X. Yu, L. Yang, B. K. Tan, A. Rosenwald, E. M. Hurt, E. Petroulakis, N. Sonenberg, J. W. Yewdell, K. Calame, L. H. Glimcher, and L. M. Staudt. 2004. XBP1, downstream of Blimp-1, expands the secretory apparatus and other organelles, and increases protein synthesis in plasma cell differentiation. *Immunity* 21: 81-93.
68. McGehee, A. M., S. K. Dougan, E. J. Klemm, G. Shui, B. Park, Y. M. Kim, N. Watson, M. R. Wenk, H. L. Ploegh, and C. C. Hu. 2009. XBP-1-deficient plasmablasts show normal protein folding but altered glycosylation and lipid synthesis. *J Immunol* 183: 3690-3699.
69. Taubenheim, N., D. M. Tarlinton, S. Crawford, L. M. Corcoran, P. D. Hodgkin, and S. L. Nutt. 2012. High rate of antibody secretion is not integral to plasma cell differentiation as revealed by XBP-1 deficiency. *J Immunol* 189: 3328-3338.
70. Gaudette, B. T., D. D. Jones, A. Bortnick, Y. Argon, and D. Allman. 2020. mTORC1 coordinates an immediate unfolded protein response-related transcriptome in activated B cells preceding antibody secretion. *Nat Commun* 11: 723.
71. Benner, R., W. Hijmans, and J. J. Haaijman. 1981. The bone marrow: the major source of serum immunoglobulins, but still a neglected site of antibody formation. *Clin Exp Immunol* 46: 1-8.
72. Ellyard, J. I., D. T. Avery, T. G. Phan, N. J. Hare, P. D. Hodgkin, and S. G. Tangye. 2004. Antigen-selected, immunoglobulin-secreting cells persist in human spleen and bone marrow. *Blood* 103: 3805-3812.
73. Chernova, I., D. D. Jones, J. R. Wilmore, A. Bortnick, M. Yucel, U. Hershberg, and D. Allman. 2014. Lasting antibody responses are mediated by a combination of newly formed and established bone marrow plasma cells drawn from clonally distinct precursors. *J Immunol* 193: 4971-4979.
74. Ho, F., J. E. Lortan, I. C. MacLennan, and M. Khan. 1986. Distinct short-lived and long-lived antibody-producing cell populations. *Eur J Immunol* 16: 1297-1301.
75. Hargreaves, D. C., P. L. Hyman, T. T. Lu, V. N. Ngo, A. Bidgol, G. Suzuki, Y. R. Zou, D. R. Littman, and J. G. Cyster. 2001. A coordinated change in chemokine responsiveness guides plasma cell movements. *J Exp Med* 194: 45-56.
76. Cheng, Q., L. Khodadadi, A. Taddeo, J. Klotsche, F. H. B, A. Radbruch, and F. Hiepe. 2018. CXCR4-CXCL12 interaction is important for plasma cell homing and survival in NZB/W mice. *Eur J Immunol* 48: 1020-1029.
77. Erickson, L. D., L. L. Lin, B. Duan, L. Morel, and R. J. Noelle. 2003. A genetic lesion that arrests plasma cell homing to the bone marrow. *Proc Natl Acad Sci U S A* 100: 12905-12910.
78. Hauser, A. E., G. F. Debes, S. Arce, G. Cassese, A. Hamann, A. Radbruch, and R. A. Manz. 2002. Chemotactic responsiveness toward ligands for CXCR3 and CXCR4 is regulated on plasma blasts during the time course of a memory immune response. *J Immunol* 169: 1277-1282.
79. Kunkel, E. J., C. H. Kim, N. H. Lazarus, M. A. Vierra, D. Soler, E. P. Bowman, and E. C. Butcher. 2003. CCR10 expression is a common feature of circulating and mucosal epithelial tissue IgA Ab-secreting cells. *J Clin Invest* 111: 1001-1010.

80. Nutt, S. L., P. D. Hodgkin, D. M. Tarlinton, and L. M. Corcoran. 2015. The generation of antibody-secreting plasma cells. *Nat Rev Immunol* 15: 160-171.
81. Belnoue, E., M. Pihlgren, T. L. McGaha, C. Tougne, A. F. Rochat, C. Bossen, P. Schneider, B. Huard, P. H. Lambert, and C. A. Siegrist. 2008. APRIL is critical for plasmablast survival in the bone marrow and poorly expressed by early-life bone marrow stromal cells. *Blood* 111: 2755-2764.
82. Benson, M. J., S. R. Dillon, E. Castigli, R. S. Geha, S. Xu, K. P. Lam, and R. J. Noelle. 2008. Cutting edge: the dependence of plasma cells and independence of memory B cells on BAFF and APRIL. *J Immunol* 180: 3655-3659.
83. Nguyen, D. C., S. Garimalla, H. Xiao, S. Kyu, I. Albizua, J. Galipeau, K. Y. Chiang, E. K. Waller, R. Wu, G. Gibson, J. Roberson, F. E. Lund, T. D. Randall, I. Sanz, and F. E. Lee. 2018. Factors of the bone marrow microniche that support human plasma cell survival and immunoglobulin secretion. *Nat Commun* 9: 3698.
84. Jelinek, D. F., and P. E. Lipsky. 1983. The role of B cell proliferation in the generation of immunoglobulin-secreting cells in man. *J Immunol* 130: 2597-2604.
85. Weston, S. A., and C. R. Parish. 1990. New fluorescent dyes for lymphocyte migration studies. Analysis by flow cytometry and fluorescence microscopy. *J Immunol Methods* 133: 87-97.
86. Quah, B. J., and C. R. Parish. 2012. New and improved methods for measuring lymphocyte proliferation in vitro and in vivo using CFSE-like fluorescent dyes. *J Immunol Methods* 379: 1-14.
87. Tangye, S. G., and P. D. Hodgkin. 2004. Divide and conquer: the importance of cell division in regulating B-cell responses. *Immunology* 112: 509-520.
88. Hawkins, E. D., M. L. Turner, C. J. Wellard, J. H. Zhou, M. R. Dowling, and P. D. Hodgkin. 2013. Quantal and graded stimulation of B lymphocytes as alternative strategies for regulating adaptive immune responses. *Nat Commun* 4: 2406.
89. Heinzl, S., J. M. Marchingo, M. B. Horton, and P. D. Hodgkin. 2018. The regulation of lymphocyte activation and proliferation. *Curr Opin Immunol* 51: 32-38.
90. Turner, M. L., E. D. Hawkins, and P. D. Hodgkin. 2008. Quantitative regulation of B cell division destiny by signal strength. *J Immunol* 181: 374-382.
91. Kitamura, D., J. Roes, R. Kuhn, and K. Rajewsky. 1991. A B cell-deficient mouse by targeted disruption of the membrane exon of the immunoglobulin mu chain gene. *Nature* 350: 423-426.
92. Barwick, B. G., C. D. Scharer, A. P. R. Bally, and J. M. Boss. 2016. Plasma cell differentiation is coupled to division-dependent DNA hypomethylation and gene regulation. *Nat Immunol* 17: 1216-1225.
93. Scharer, C. D., D. G. Patterson, T. Mi, M. J. Price, S. L. Hicks, and J. M. Boss. 2020. Antibody-secreting cell destiny emerges during the initial stages of B-cell activation. *Nat Commun* 11: 3989.
94. Hou, B., B. Reizis, and A. L. DeFranco. 2008. Toll-like receptors activate innate and adaptive immunity by using dendritic cell-intrinsic and -extrinsic mechanisms. *Immunity* 29: 272-282.
95. Patterson, D. G., A. K. Kania, M. J. Price, J. R. Rose, C. D. Scharer, and J. M. Boss. 2021. An IRF4-MYC-mTORC1 Integrated Pathway Controls Cell Growth and the Proliferative Capacity of Activated B Cells during B Cell Differentiation In Vivo. *J Immunol*.

96. Gaudette, B. T., C. J. Roman, T. A. Ochoa, D. Gomez Atria, D. D. Jones, C. W. Siebel, I. Maillard, and D. Allman. 2021. Resting innate-like B cells leverage sustained Notch2/mTORC1 signaling to achieve rapid and mitosis-independent plasma cell differentiation. *J Clin Invest*.
97. Revilla, I. D. R., I. Bilic, B. Vilagos, H. Tagoh, A. Ebert, I. M. Tamir, L. Smeenk, J. Trupke, A. Sommer, M. Jaritz, and M. Busslinger. 2012. The B-cell identity factor Pax5 regulates distinct transcriptional programmes in early and late B lymphopoiesis. *EMBO J* 31: 3130-3146.
98. Schebesta, A., S. McManus, G. Salvagiotto, A. Delogu, G. A. Busslinger, and M. Busslinger. 2007. Transcription factor Pax5 activates the chromatin of key genes involved in B cell signaling, adhesion, migration, and immune function. *Immunity* 27: 49-63.
99. Delogu, A., A. Schebesta, Q. Sun, K. Aschenbrenner, T. Perlot, and M. Busslinger. 2006. Gene repression by Pax5 in B cells is essential for blood cell homeostasis and is reversed in plasma cells. *Immunity* 24: 269-281.
100. Mora-Lopez, F., E. Reales, J. A. Brieva, and A. Campos-Caro. 2007. Human BSAP and BLIMP1 conform an autoregulatory feedback loop. *Blood* 110: 3150-3157.
101. Liu, G. J., M. Jaritz, M. Wohner, B. Agerer, A. Bergthaler, S. G. Malin, and M. Busslinger. 2020. Repression of the B cell identity factor Pax5 is not required for plasma cell development. *J Exp Med* 217.
102. Muto, A., S. Tashiro, O. Nakajima, H. Hoshino, S. Takahashi, E. Sakoda, D. Ikebe, M. Yamamoto, and K. Igarashi. 2004. The transcriptional programme of antibody class switching involves the repressor Bach2. *Nature* 429: 566-571.
103. Ochiai, K., Y. Katoh, T. Ikura, Y. Hoshikawa, T. Noda, H. Karasuyama, S. Tashiro, A. Muto, and K. Igarashi. 2006. Plasmacytic transcription factor Blimp-1 is repressed by Bach2 in B cells. *The Journal of biological chemistry* 281: 38226-38234.
104. Ochiai, K., A. Muto, H. Tanaka, S. Takahashi, and K. Igarashi. 2008. Regulation of the plasma cell transcription factor Blimp-1 gene by Bach2 and Bcl6. *Int Immunol* 20: 453-460.
105. Solomon, L. A., S. K. Li, J. Piskorz, L. S. Xu, and R. P. DeKoter. 2015. Genome-wide comparison of PU.1 and Spi-B binding sites in a mouse B lymphoma cell line. *BMC Genomics* 16: 76.
106. Garrett-Sinha, L. A., G. H. Su, S. Rao, S. Kabak, Z. Hao, M. R. Clark, and M. C. Simon. 1999. PU.1 and Spi-B are required for normal B cell receptor-mediated signal transduction. *Immunity* 10: 399-408.
107. Willis, S. N., J. Tellier, Y. Liao, S. Trezise, A. Light, K. O'Donnell, L. A. Garrett-Sinha, W. Shi, D. M. Tarlinton, and S. L. Nutt. 2017. Environmental sensing by mature B cells is controlled by the transcription factors PU.1 and SpiB. *Nat Commun* 8: 1426.
108. Carotta, S., S. N. Willis, J. Hasbold, M. Inouye, S. H. Pang, D. Emslie, A. Light, M. Chopin, W. Shi, H. Wang, H. C. Morse, 3rd, D. M. Tarlinton, L. M. Corcoran, P. D. Hodgkin, and S. L. Nutt. 2014. The transcription factors IRF8 and PU.1 negatively regulate plasma cell differentiation. *J Exp Med* 211: 2169-2181.
109. Tunyaplin, C., A. L. Shaffer, C. D. Angelin-Duclos, X. Yu, L. M. Staudt, and K. L. Calame. 2004. Direct repression of prdm1 by Bcl-6 inhibits plasmacytic differentiation. *J Immunol* 173: 1158-1165.

110. Shaffer, A. L., X. Yu, Y. He, J. Boldrick, E. P. Chan, and L. M. Staudt. 2000. BCL-6 represses genes that function in lymphocyte differentiation, inflammation, and cell cycle control. *Immunity* 13: 199-212.
111. Klein, U., S. Casola, G. Cattoretti, Q. Shen, M. Lia, T. Mo, T. Ludwig, K. Rajewsky, and R. Dalla-Favera. 2006. Transcription factor IRF4 controls plasma cell differentiation and class-switch recombination. *Nat Immunol* 7: 773-782.
112. Sciammas, R., A. L. Shaffer, J. H. Schatz, H. Zhao, L. M. Staudt, and H. Singh. 2006. Graded expression of interferon regulatory factor-4 coordinates isotype switching with plasma cell differentiation. *Immunity* 25: 225-236.
113. Lin, K. I., C. Angelin-Duclos, T. C. Kuo, and K. Calame. 2002. Blimp-1-dependent repression of Pax-5 is required for differentiation of B cells to immunoglobulin M-secreting plasma cells. *Mol Cell Biol* 22: 4771-4780.
114. Tellier, J., W. Shi, M. Minnich, Y. Liao, S. Crawford, G. K. Smyth, A. Kallies, M. Busslinger, and S. L. Nutt. 2016. Blimp-1 controls plasma cell function through the regulation of immunoglobulin secretion and the unfolded protein response. *Nat Immunol* 17: 323-330.
115. Minnich, M., H. Tagoh, P. Bonelt, E. Axelsson, M. Fischer, B. Cebolla, A. Tarakhovsky, S. L. Nutt, M. Jaritz, and M. Busslinger. 2016. Multifunctional role of the transcription factor Blimp-1 in coordinating plasma cell differentiation. *Nat Immunol* 17: 331-343.
116. Allis, C. D., and T. Jenuwein. 2016. The molecular hallmarks of epigenetic control. *Nat Rev Genet* 17: 487-500.
117. Scharer, C. D., B. G. Barwick, M. Guo, A. P. R. Bally, and J. M. Boss. 2018. Plasma cell differentiation is controlled by multiple cell division-coupled epigenetic programs. *Nat Commun* 9: 1698.
118. Price, M. J., C. D. Scharer, A. K. Kania, T. D. Randall, and J. M. Boss. 2021. Conserved Epigenetic Programming and Enhanced Heme Metabolism Drive Memory B Cell Reactivation. *J Immunol*.
119. Scharer, C. D., A. P. Bally, B. Gandham, and J. M. Boss. 2017. Cutting Edge: Chromatin Accessibility Programs CD8 T Cell Memory. *J Immunol* 198: 2238-2243.
120. Zhang, Y., and K. L. Good-Jacobson. 2019. Epigenetic regulation of B cell fate and function during an immune response. *Immunol Rev* 288: 75-84.
121. Willis, S. N., and S. L. Nutt. 2019. New players in the gene regulatory network controlling late B cell differentiation. *Curr Opin Immunol* 58: 68-74.
122. Cavalli, G., and E. Heard. 2019. Advances in epigenetics link genetics to the environment and disease. *Nature* 571: 489-499.
123. Lister, R., M. Pelizzola, R. H. Dowen, R. D. Hawkins, G. Hon, J. Tonti-Filippini, J. R. Nery, L. Lee, Z. Ye, Q. M. Ngo, L. Edsall, J. Antosiewicz-Bourget, R. Stewart, V. Ruotti, A. H. Millar, J. A. Thomson, B. Ren, and J. R. Ecker. 2009. Human DNA methylomes at base resolution show widespread epigenomic differences. *Nature* 462: 315-322.
124. Jjingo, D., A. B. Conley, S. V. Yi, V. V. Lunyak, and I. K. Jordan. 2012. On the presence and role of human gene-body DNA methylation. *Oncotarget* 3: 462-474.
125. Okano, M., D. W. Bell, D. A. Haber, and E. Li. 1999. DNA methyltransferases Dnmt3a and Dnmt3b are essential for de novo methylation and mammalian development. *Cell* 99: 247-257.

126. Hermann, A., R. Goyal, and A. Jeltsch. 2004. The Dnmt1 DNA-(cytosine-C5)-methyltransferase methylates DNA processively with high preference for hemimethylated target sites. *The Journal of biological chemistry* 279: 48350-48359.
127. Greenberg, M. V. C., and D. Bourc'his. 2019. The diverse roles of DNA methylation in mammalian development and disease. *Nat Rev Mol Cell Biol* 20: 590-607.
128. Caron, G., M. Hussein, M. Kulis, C. Delaloy, F. Chatonnet, A. Pignarre, S. Avner, M. Lemarie, E. A. Mahe, N. Verdaguer-Dot, A. C. Queiros, K. Tarte, J. I. Martin-Subero, G. Salbert, and T. Fest. 2015. Cell-Cycle-Dependent Reconfiguration of the DNA Methylome during Terminal Differentiation of Human B Cells into Plasma Cells. *Cell Rep* 13: 1059-1071.
129. Dominguez, P. M., H. Ghamlouch, W. Rosikiewicz, P. Kumar, W. Beguelin, L. Fontan, M. A. Rivas, P. Pawlikowska, M. Armand, E. Mouly, M. Torres-Martin, A. S. Doane, M. T. Calvo Fernandez, M. Durant, V. Della-Valle, M. Teater, L. Cimmino, N. Droin, S. Tadros, S. Motanagh, A. H. Shih, M. A. Rubin, W. Tam, I. Aifantis, R. L. Levine, O. Elemento, G. Inghirami, M. R. Green, M. E. Figueroa, O. A. Bernard, S. Aoufouchi, S. Li, R. Shaknovich, and A. M. Melnick. 2018. TET2 Deficiency Causes Germinal Center Hyperplasia, Impairs Plasma Cell Differentiation, and Promotes B-cell Lymphomagenesis. *Cancer Discov* 8: 1632-1653.
130. Schoeler, K., A. Aufschneider, S. Messner, E. Derudder, S. Herzog, A. Villunger, K. Rajewsky, and V. Labi. 2019. TET enzymes control antibody production and shape the mutational landscape in germinal centre B cells. *FEBS J* 286: 3566-3581.
131. Lio, C. J., V. Shukla, D. Samaniego-Castruita, E. Gonzalez-Avalos, A. Chakraborty, X. Yue, D. G. Schatz, F. Ay, and A. Rao. 2019. TET enzymes augment activation-induced deaminase (AID) expression via 5-hydroxymethylcytosine modifications at the Aicda superenhancer. *Sci Immunol* 4.
132. Qi, T., M. Sun, C. Zhang, P. Chen, C. Xiao, and X. Chang. 2020. Ascorbic Acid Promotes Plasma Cell Differentiation through Enhancing TET2/3-Mediated DNA Demethylation. *Cell Rep* 33: 108452.
133. Barwick, B. G., C. D. Scharer, R. J. Martinez, M. J. Price, A. N. Wein, R. R. Haines, A. P. R. Bally, J. E. Kohlmeier, and J. M. Boss. 2018. B cell activation and plasma cell differentiation are inhibited by de novo DNA methylation. *Nat Commun* 9: 1900.
134. Cao, R., L. Wang, H. Wang, L. Xia, H. Erdjument-Bromage, P. Tempst, R. S. Jones, and Y. Zhang. 2002. Role of histone H3 lysine 27 methylation in Polycomb-group silencing. *Science* 298: 1039-1043.
135. Czermin, B., R. Melfi, D. McCabe, V. Seitz, A. Imhof, and V. Pirrotta. 2002. Drosophila enhancer of Zeste/ESC complexes have a histone H3 methyltransferase activity that marks chromosomal Polycomb sites. *Cell* 111: 185-196.
136. Muller, J., C. M. Hart, N. J. Francis, M. L. Vargas, A. Sengupta, B. Wild, E. L. Miller, M. B. O'Connor, R. E. Kingston, and J. A. Simon. 2002. Histone methyltransferase activity of a Drosophila Polycomb group repressor complex. *Cell* 111: 197-208.
137. Beguelin, W., R. Popovic, M. Teater, Y. Jiang, K. L. Bunting, M. Rosen, H. Shen, S. N. Yang, L. Wang, T. Ezponda, E. Martinez-Garcia, H. Zhang, Y. Zheng, S. K. Verma, M. T. McCabe, H. M. Ott, G. S. Van Aller, R. G. Kruger, Y. Liu, C. F. McHugh, D. W. Scott, Y. R. Chung, N. Kelleher, R. Shaknovich, C. L. Creasy, R. D. Gascoyne, K. K. Wong, L. Cerchietti, R. L. Levine, O. Abdel-Wahab, J. D. Licht, O. Elemento, and A. M.

- Melnick. 2013. EZH2 is required for germinal center formation and somatic EZH2 mutations promote lymphoid transformation. *Cancer cell* 23: 677-692.
138. Caganova, M., C. Carrisi, G. Varano, F. Mainoldi, F. Zanardi, P. L. Germain, L. George, F. Alberghini, L. Ferrarini, A. K. Talukder, M. Ponzoni, G. Testa, T. Nojima, C. Doglioni, D. Kitamura, K. M. Toellner, I. H. Su, and S. Casola. 2013. Germinal center dysregulation by histone methyltransferase EZH2 promotes lymphomagenesis. *J Clin Invest* 123: 5009-5022.
 139. Su, I. H., A. Basavaraj, A. N. Krutchinsky, O. Hobert, A. Ullrich, B. T. Chait, and A. Tarakhovskiy. 2003. Ezh2 controls B cell development through histone H3 methylation and Igh rearrangement. *Nat Immunol* 4: 124-131.
 140. Beguelin, W., M. Teater, C. Meydan, K. B. Hoehn, J. M. Phillip, A. A. Soshnev, L. Venturutti, M. A. Rivas, M. T. Calvo-Fernandez, J. Gutierrez, J. M. Camarillo, K. Takata, K. Tarte, N. L. Kelleher, C. Steidl, C. E. Mason, O. Elemento, C. D. Allis, S. H. Kleinstein, and A. M. Melnick. 2020. Mutant EZH2 Induces a Pre-malignant Lymphoma Niche by Reprogramming the Immune Response. *Cancer cell* 37: 655-673 e611.
 141. Guo, M., M. J. Price, D. G. Patterson, B. G. Barwick, R. R. Haines, A. K. Kania, J. E. Bradley, T. D. Randall, J. M. Boss, and C. D. Scharer. 2018. EZH2 Represses the B Cell Transcriptional Program and Regulates Antibody-Secreting Cell Metabolism and Antibody Production. *J Immunol* 200: 1039-1052.
 142. Hyun, K., J. Jeon, K. Park, and J. Kim. 2017. Writing, erasing and reading histone lysine methylations. *Exp Mol Med* 49: e324.
 143. Metzger, E., M. Wissmann, N. Yin, J. M. Muller, R. Schneider, A. H. Peters, T. Gunther, R. Buettner, and R. Schule. 2005. LSD1 demethylates repressive histone marks to promote androgen-receptor-dependent transcription. *Nature* 437: 436-439.
 144. Shi, Y., F. Lan, C. Matson, P. Mulligan, J. R. Whetstine, P. A. Cole, R. A. Casero, and Y. Shi. 2004. Histone demethylation mediated by the nuclear amine oxidase homolog LSD1. *Cell* 119: 941-953.
 145. Su, S. T., H. Y. Ying, Y. K. Chiu, F. R. Lin, M. Y. Chen, and K. I. Lin. 2009. Involvement of histone demethylase LSD1 in Blimp-1-mediated gene repression during plasma cell differentiation. *Mol Cell Biol* 29: 1421-1431.
 146. Haines, R. R., B. G. Barwick, C. D. Scharer, P. Majumder, T. D. Randall, and J. M. Boss. 2018. The Histone Demethylase LSD1 Regulates B Cell Proliferation and Plasmablast Differentiation. *J Immunol* 201: 2799-2811.
 147. Zhang, J., D. Dominguez-Sola, S. Hussein, J. E. Lee, A. B. Holmes, M. Bansal, S. Vlasevska, T. Mo, H. Tang, K. Basso, K. Ge, R. Dalla-Favera, and L. Pasqualucci. 2015. Disruption of KMT2D perturbs germinal center B cell development and promotes lymphomagenesis. *Nat Med* 21: 1190-1198.
 148. Haines, R. R., C. D. Scharer, J. L. Lobby, and J. M. Boss. 2019. LSD1 Cooperates with Noncanonical NF-kappaB Signaling to Regulate Marginal Zone B Cell Development. *J Immunol* 203: 1867-1881.
 149. Barry, E. R., G. N. Corry, and T. P. Rasmussen. 2010. Targeting DOT1L action and interactions in leukemia: the role of DOT1L in transformation and development. *Expert Opin Ther Targets* 14: 405-418.
 150. Aslam, M. A., M. F. Alemdehy, E. M. Kwesi-Maliepaard, F. I. Muhaimin, M. Caganova, I. N. Pardieck, T. van den Brand, T. van Welsem, I. de Rink, J. Y. Song, E. de Wit, R.

- Arens, H. Jacobs, and F. van Leeuwen. 2021. Histone methyltransferase DOT1L controls state-specific identity during B cell differentiation. *EMBO Rep*: e51184.
151. Kealy, L., A. Di Pietro, L. Hailes, S. Scheer, L. Dalit, J. R. Groom, C. Zaph, and K. L. Good-Jacobson. 2020. The Histone Methyltransferase DOT1L Is Essential for Humoral Immune Responses. *Cell Rep* 33: 108504.
 152. Chan, W. F., T. M. Johanson, and R. S. Allan. 2020. Three-dimensional genome rewiring during the development of antibody-secreting cells. *Biochem Soc Trans* 48: 1109-1119.
 153. Schoenfelder, S., and P. Fraser. 2019. Long-range enhancer-promoter contacts in gene expression control. *Nat Rev Genet* 20: 437-455.
 154. Sati, S., and G. Cavalli. 2017. Chromosome conformation capture technologies and their impact in understanding genome function. *Chromosoma* 126: 33-44.
 155. Kieffer-Kwon, K. R., K. Nimura, S. S. P. Rao, J. Xu, S. Jung, A. Pekowska, M. Dose, E. Stevens, E. Mathe, P. Dong, S. C. Huang, M. A. Ricci, L. Baranello, Y. Zheng, F. Tomassoni Ardori, W. Resch, D. Stavreva, S. Nelson, M. McAndrew, A. Casellas, E. Finn, C. Gregory, B. G. St Hilaire, S. M. Johnson, W. Dubois, M. P. Cosma, E. Batchelor, D. Levens, R. D. Phair, T. Misteli, L. Tessarollo, G. Hager, M. Lakadamyali, Z. Liu, M. Floer, H. Shroff, E. L. Aiden, and R. Casellas. 2017. Myc Regulates Chromatin Decompaction and Nuclear Architecture during B Cell Activation. *Molecular cell* 67: 566-578 e510.
 156. Bortnick, A., Z. He, M. Aubrey, V. Chandra, M. Denholtz, K. Chen, Y. C. Lin, and C. Murre. 2020. Plasma Cell Fate Is Orchestrated by Elaborate Changes in Genome Compartmentalization and Inter-chromosomal Hubs. *Cell Rep* 31: 107876.
 157. Rivas, M. A., C. Meydan, C. R. Chin, M. F. Challman, D. Kim, B. Bhinder, A. Kloetgen, A. D. Viny, M. R. Teater, D. R. McNally, A. S. Doane, W. Beguelin, M. T. C. Fernandez, H. Shen, X. Wang, R. L. Levine, Z. Chen, A. Tsirigos, O. Elemento, C. E. Mason, and A. M. Melnick. 2021. Smc3 dosage regulates B cell transit through germinal centers and restricts their malignant transformation. *Nat Immunol* 22: 240-253.
 158. Chaudhri, V. K., K. Dienger-Stambaugh, Z. Wu, M. Shrestha, and H. Singh. 2020. Charting the cis-regulome of activated B cells by coupling structural and functional genomics. *Nat Immunol* 21: 210-220.
 159. Bunting, K. L., T. D. Soong, R. Singh, Y. Jiang, W. Beguelin, D. W. Poloway, B. L. Swed, K. Hatzi, W. Reisacher, M. Teater, O. Elemento, and A. M. Melnick. 2016. Multi-tiered Reorganization of the Genome during B Cell Affinity Maturation Anchored by a Germinal Center-Specific Locus Control Region. *Immunity* 45: 497-512.
 160. Choi, N. M., P. Majumder, and J. M. Boss. 2011. Regulation of major histocompatibility complex class II genes. *Curr Opin Immunol* 23: 81-87.
 161. Majumder, P., J. A. Gomez, B. P. Chadwick, and J. M. Boss. 2008. The insulator factor CTCF controls MHC class II gene expression and is required for the formation of long-distance chromatin interactions. *J Exp Med* 205: 785-798.
 162. Majumder, P., J. T. Lee, A. R. Rahmberg, G. Kumar, T. Mi, C. D. Scharer, and J. M. Boss. 2020. A super enhancer controls expression and chromatin architecture within the MHC class II locus. *J Exp Med* 217.
 163. Rowley, M. J., and V. G. Corces. 2018. Organizational principles of 3D genome architecture. *Nat Rev Genet* 19: 789-800.

164. Majumder, P., Gomez, J.A., Boss, J.M. 2006. The human major histocompatibility complex class II HLA-DRB1 and HLA-DQA1 genes are separated by a CTCF binding enhancer-blocking element. *Journal of Biological Chemistry* 281: 18435-18443.
165. Majumder, P., and J. M. Boss. 2010. CTCF controls expression and chromatin architecture of the human major histocompatibility complex class II locus. *Mol Cell Biol* 30: 4211-4223.
166. Majumder, P., and J. M. Boss. 2011. Cohesin regulates MHC class II genes through interactions with MHC class II insulators. *J Immunol* 187: 4236-4244.
167. Majumder, P., C. D. Scharer, N. M. Choi, and J. M. Boss. 2014. B cell differentiation is associated with reprogramming the CCCTC binding factor-dependent chromatin architecture of the murine MHC class II locus. *J Immunol* 192: 3925-3935.
168. Hnisz, D., B. J. Abraham, T. I. Lee, A. Lau, V. Saint-Andre, A. A. Sigova, H. A. Hoke, and R. A. Young. 2013. Super-enhancers in the control of cell identity and disease. *Cell* 155: 934-947.
169. Hong, S., Y. W. Cho, L. R. Yu, H. Yu, T. D. Veenstra, and K. Ge. 2007. Identification of JmjC domain-containing UTX and JMJD3 as histone H3 lysine 27 demethylases. *Proc Natl Acad Sci U S A* 104: 18439-18444.
170. Agger, K., P. A. Cloos, J. Christensen, D. Pasini, S. Rose, J. Rappsilber, I. Issaeva, E. Canaani, A. E. Salcini, and K. Helin. 2007. UTX and JMJD3 are histone H3K27 demethylases involved in HOX gene regulation and development. *Nature* 449: 731-734.
171. Lan, F., P. E. Bayliss, J. L. Rinn, J. R. Whetstine, J. K. Wang, S. Chen, S. Iwase, R. Alpatov, I. Issaeva, E. Canaani, T. M. Roberts, H. Y. Chang, and Y. Shi. 2007. A histone H3 lysine 27 demethylase regulates animal posterior development. *Nature* 449: 689-694.
172. Tsukada, Y., T. Ishitani, and K. I. Nakayama. 2010. KDM7 is a dual demethylase for histone H3 Lys 9 and Lys 27 and functions in brain development. *Genes Dev* 24: 432-437.
173. Yokoyama, A., Y. Okuno, T. Chikanishi, W. Hashiba, H. Sekine, R. Fujiki, and S. Kato. 2010. KIAA1718 is a histone demethylase that erases repressive histone methyl marks. *Genes Cells* 15: 867-873.
174. Greenfield, A., L. Carrel, D. Pennisi, C. Philippe, N. Quaderi, P. Siggers, K. Steiner, P. P. Tam, A. P. Monaco, H. F. Willard, and P. Koopman. 1998. The UTX gene escapes X inactivation in mice and humans. *Hum Mol Genet* 7: 737-742.
175. Walport, L. J., R. J. Hopkinson, M. Vollmar, S. K. Madden, C. Gileadi, U. Oppermann, C. J. Schofield, and C. Johansson. 2014. Human UTY(KDM6C) is a male-specific N-methyl lysyl demethylase. *The Journal of biological chemistry* 289: 18302-18313.
176. Sengoku, T., and S. Yokoyama. 2011. Structural basis for histone H3 Lys 27 demethylation by UTX/KDM6A. *Genes Dev* 25: 2266-2277.
177. Jones, S. E., L. Olsen, and M. Gajhede. 2018. Structural Basis of Histone Demethylase KDM6B Histone 3 Lysine 27 Specificity. *Biochemistry* 57: 585-592.
178. Klose, R. J., E. M. Kallin, and Y. Zhang. 2006. JmjC-domain-containing proteins and histone demethylation. *Nat Rev Genet* 7: 715-727.
179. Kato, H., K. Asamitsu, W. Sun, S. Kitajima, N. Yoshizawa-Sugata, T. Okamoto, H. Masai, and L. Poellinger. 2020. Cancer-derived UTX TPR mutations G137V and D336G impair interaction with MLL3/4 complexes and affect UTX subcellular localization. *Oncogene* 39: 3322-3335.

180. Zeytuni, N., and R. Zarivach. 2012. Structural and functional discussion of the tetra-trico-peptide repeat, a protein interaction module. *Structure* 20: 397-405.
181. Miller, S. A., A. C. Huang, M. M. Miazgowicz, M. M. Brassil, and A. S. Weinmann. 2008. Coordinated but physically separable interaction with H3K27-demethylase and H3K4-methyltransferase activities are required for T-box protein-mediated activation of developmental gene expression. *Genes Dev* 22: 2980-2993.
182. Wang, S. P., Z. Tang, C. W. Chen, M. Shimada, R. P. Koche, L. H. Wang, T. Nakadai, A. Chramiec, A. V. Krivtsov, S. A. Armstrong, and R. G. Roeder. 2017. A UTX-MLL4-p300 Transcriptional Regulatory Network Coordinately Shapes Active Enhancer Landscapes for Eliciting Transcription. *Mol Cell* 67: 308-321 e306.
183. Shi, B., W. Li, Y. Song, Z. Wang, R. Ju, A. Ulman, J. Hu, F. Palomba, Y. Zhao, J. P. Le, W. Jarrard, D. Dimoff, M. A. Digman, E. Gratton, C. Zang, and H. Jiang. 2021. UTX condensation underlies its tumour-suppressive activity. *Nature* 597: 726-731.
184. Miller, S. A., S. E. Mohn, and A. S. Weinmann. 2010. Jmjd3 and UTX play a demethylase-independent role in chromatin remodeling to regulate T-box family member-dependent gene expression. *Mol Cell* 40: 594-605.
185. Burgold, T., N. Voituron, M. Caganova, P. P. Tripathi, C. Menuet, B. K. Tusi, F. Spreafico, M. Bevengut, C. Gestreau, S. Buontempo, A. Simeone, L. Kruidenier, G. Natoli, S. Casola, G. Hilaire, and G. Testa. 2012. The H3K27 demethylase JMJD3 is required for maintenance of the embryonic respiratory neuronal network, neonatal breathing, and survival. *Cell Rep* 2: 1244-1258.
186. Wang, C., J. E. Lee, Y. W. Cho, Y. Xiao, Q. Jin, C. Liu, and K. Ge. 2012. UTX regulates mesoderm differentiation of embryonic stem cells independent of H3K27 demethylase activity. *Proc Natl Acad Sci U S A* 109: 15324-15329.
187. Welstead, G. G., M. P. Creighton, S. Bilodeau, A. W. Cheng, S. Markoulaki, R. A. Young, and R. Jaenisch. 2012. X-linked H3K27me3 demethylase Utx is required for embryonic development in a sex-specific manner. *Proc Natl Acad Sci U S A* 109: 13004-13009.
188. Morales Torres, C., A. Laugesen, and K. Helin. 2013. Utx is required for proper induction of ectoderm and mesoderm during differentiation of embryonic stem cells. *PLoS One* 8: e60020.
189. Shpargel, K. B., T. Sengoku, S. Yokoyama, and T. Magnuson. 2012. UTX and UTY demonstrate histone demethylase-independent function in mouse embryonic development. *PLoS Genet* 8: e1002964.
190. Lee, S., J. W. Lee, and S. K. Lee. 2012. UTX, a histone H3-lysine 27 demethylase, acts as a critical switch to activate the cardiac developmental program. *Dev Cell* 22: 25-37.
191. Lei, X., and J. Jiao. 2018. UTX Affects Neural Stem Cell Proliferation and Differentiation through PTEN Signaling. *Stem Cell Reports* 10: 1193-1207.
192. Tang, G. B., Y. Q. Zeng, P. P. Liu, T. W. Mi, S. F. Zhang, S. K. Dai, Q. Y. Tang, L. Yang, Y. J. Xu, H. L. Yan, H. Z. Du, Z. Q. Teng, F. Q. Zhou, and C. M. Liu. 2017. The Histone H3K27 Demethylase UTX Regulates Synaptic Plasticity and Cognitive Behaviors in Mice. *Front Mol Neurosci* 10: 267.
193. Wijayatunge, R., F. Liu, K. B. Shpargel, N. J. Wayne, U. Chan, J. V. Boua, T. Magnuson, and A. E. West. 2018. The histone demethylase Kdm6b regulates a mature gene expression program in differentiating cerebellar granule neurons. *Mol Cell Neurosci* 87: 4-17.

194. Umutoni, D., T. Iwagawa, Y. Baba, A. Tsuchiko, H. Honda, M. Aihara, and S. Watanabe. 2020. H3K27me3 demethylase UTX regulates the differentiation of a subset of bipolar cells in the mouse retina. *Genes Cells* 25: 402-412.
195. Naruse, C., S. Shibata, M. Tamura, T. Kawaguchi, K. Abe, K. Sugihara, T. Kato, T. Nishiuchi, S. Wakana, M. Ikawa, and M. Asano. 2017. New insights into the role of Jmjd3 and Utx in axial skeletal formation in mice. *FASEB J* 31: 2252-2266.
196. Agrawal Singh, S., M. Lerdrup, A. R. Gomes, H. J. van de Werken, J. Vilstrup Johansen, R. Andersson, A. Sandelin, K. Helin, and K. Hansen. 2019. PLZF targets developmental enhancers for activation during osteogenic differentiation of human mesenchymal stem cells. *Elife* 8.
197. Chakraborty, A. A., T. Laukka, M. Myllykoski, A. E. Ringel, M. A. Booker, M. Y. Tolstorukov, Y. J. Meng, S. R. Meier, R. B. Jennings, A. L. Creech, Z. T. Herbert, S. K. McBrayer, B. A. Olenchock, J. D. Jaffe, M. C. Haigis, R. Beroukhim, S. Signoretti, P. Koivunen, and W. G. Kaelin, Jr. 2019. Histone demethylase KDM6A directly senses oxygen to control chromatin and cell fate. *Science* 363: 1217-1222.
198. Thieme, S., T. Gyarfás, C. Richter, G. Ozhan, J. Fu, D. Alexopoulou, M. H. Muders, I. Michalk, C. Jakob, A. Dahl, B. Klink, J. Bandola, M. Bachmann, E. Schrock, F. Buchholz, A. F. Stewart, G. Weidinger, K. Anastasiadis, and S. Brenner. 2013. The histone demethylase UTX regulates stem cell migration and hematopoiesis. *Blood* 121: 2462-2473.
199. Ara, T., K. Tokoyoda, T. Sugiyama, T. Egawa, K. Kawabata, and T. Nagasawa. 2003. Long-term hematopoietic stem cells require stromal cell-derived factor-1 for colonizing bone marrow during ontogeny. *Immunity* 19: 257-267.
200. Gozdecka, M., E. Meduri, M. Mazan, K. Tzelepis, M. Dudek, A. J. Knights, M. Pardo, L. Yu, J. S. Choudhary, E. Metzakopian, V. Iyer, H. Yun, N. Park, I. Varela, R. Bautista, G. Collord, O. Dovey, D. A. Garyfallos, E. De Braekeleer, S. Kondo, J. Cooper, B. Gottgens, L. Bullinger, P. A. Northcott, D. Adams, G. S. Vassiliou, and B. J. P. Huntly. 2018. UTX-mediated enhancer and chromatin remodeling suppresses myeloid leukemogenesis through noncatalytic inverse regulation of ETS and GATA programs. *Nat Genet* 50: 883-894.
201. De Santa, F., V. Narang, Z. H. Yap, B. K. Tusi, T. Burgold, L. Austenaa, G. Bucci, M. Caganova, S. Notarbartolo, S. Casola, G. Testa, W. K. Sung, C. L. Wei, and G. Natoli. 2009. Jmjd3 contributes to the control of gene expression in LPS-activated macrophages. *EMBO J* 28: 3341-3352.
202. De Santa, F., M. G. Totaro, E. Prosperini, S. Notarbartolo, G. Testa, and G. Natoli. 2007. The histone H3 lysine-27 demethylase Jmjd3 links inflammation to inhibition of polycomb-mediated gene silencing. *Cell* 130: 1083-1094.
203. Beyaz, S., J. H. Kim, L. Pinello, M. E. Xifaras, Y. Hu, J. Huang, M. A. Kerényi, P. P. Das, R. A. Barnitz, A. Herault, R. Dogum, W. N. Haining, O. H. Yilmaz, E. Passegue, G. C. Yuan, S. H. Orkin, and F. Winau. 2017. The histone demethylase UTX regulates the lineage-specific epigenetic program of invariant natural killer T cells. *Nat Immunol* 18: 184-195.
204. Northrup, D., R. Yagi, K. Cui, W. R. Proctor, C. Wang, K. Placek, L. R. Pohl, R. Wang, K. Ge, J. Zhu, and K. Zhao. 2017. Histone demethylases UTX and JMJD3 are required for NKT cell development in mice. *Cell Biosci* 7: 25.

205. Manna, S., J. K. Kim, C. Bauge, M. Cam, Y. Zhao, J. Shetty, M. S. Vacchio, E. Castro, B. Tran, L. Tessarollo, and R. Bosselut. 2015. Histone H3 Lysine 27 demethylases Jmjd3 and Utx are required for T-cell differentiation. *Nat Commun* 6: 8152.
206. Fu, C., Q. Li, J. Zou, C. Xing, M. Luo, B. Yin, J. Chu, J. Yu, X. Liu, H. Y. Wang, and R. F. Wang. 2019. JMJD3 regulates CD4 T cell trafficking by targeting actin cytoskeleton regulatory gene Pdlim4. *J Clin Invest* 129: 4745-4757.
207. Vallenius, T., B. Scharm, A. Vesikansa, K. Luukko, R. Schafer, and T. P. Makela. 2004. The PDZ-LIM protein RIL modulates actin stress fiber turnover and enhances the association of alpha-actinin with F-actin. *Exp Cell Res* 293: 117-128.
208. Luckheeram, R. V., R. Zhou, A. D. Verma, and B. Xia. 2012. CD4(+)T cells: differentiation and functions. *Clin Dev Immunol* 2012: 925135.
209. Zhu, J., H. Yamane, and W. E. Paul. 2010. Differentiation of effector CD4 T cell populations (*). *Annu Rev Immunol* 28: 445-489.
210. Wilson, C. B., E. Rowell, and M. Sekimata. 2009. Epigenetic control of T-helper-cell differentiation. *Nat Rev Immunol* 9: 91-105.
211. Wei, G., L. Wei, J. Zhu, C. Zang, J. Hu-Li, Z. Yao, K. Cui, Y. Kanno, T. Y. Roh, W. T. Watford, D. E. Schones, W. Peng, H. W. Sun, W. E. Paul, J. J. O'Shea, and K. Zhao. 2009. Global mapping of H3K4me3 and H3K27me3 reveals specificity and plasticity in lineage fate determination of differentiating CD4+ T cells. *Immunity* 30: 155-167.
212. Cook, K. D., K. B. Shpargel, J. Starmer, F. Whitfield-Larry, B. Conley, D. E. Allard, J. E. Rager, R. C. Fry, M. L. Davenport, T. Magnuson, J. K. Whitmire, and M. A. Su. 2015. T Follicular Helper Cell-Dependent Clearance of a Persistent Virus Infection Requires T Cell Expression of the Histone Demethylase UTX. *Immunity* 43: 703-714.
213. Li, Q., J. Zou, M. Wang, X. Ding, I. Chepelev, X. Zhou, W. Zhao, G. Wei, J. Cui, K. Zhao, H. Y. Wang, and R. F. Wang. 2014. Critical role of histone demethylase Jmjd3 in the regulation of CD4+ T-cell differentiation. *Nat Commun* 5: 5780.
214. Liu, Z., W. Cao, L. Xu, X. Chen, Y. Zhan, Q. Yang, S. Liu, P. Chen, Y. Jiang, X. Sun, Y. Tao, Y. Hu, C. Li, Q. Wang, Y. Wang, C. D. Chen, Y. Shi, and X. Zhang. 2015. The histone H3 lysine-27 demethylase Jmjd3 plays a critical role in specific regulation of Th17 cell differentiation. *J Mol Cell Biol* 7: 505-516.
215. Xu, T., A. Schutte, L. Jimenez, A. N. A. Goncalves, A. Keller, M. E. Pipkin, H. I. Nakaya, R. M. Pereira, and G. J. Martinez. 2021. Kdm6b Regulates the Generation of Effector CD8(+) T Cells by Inducing Chromatin Accessibility in Effector-Associated Genes. *J Immunol* 206: 2170-2183.
216. Yamada, T., S. Nabe, K. Toriyama, J. Suzuki, K. Inoue, Y. Imai, A. Shiraishi, K. Takenaka, M. Yasukawa, and M. Yamashita. 2019. Histone H3K27 Demethylase Negatively Controls the Memory Formation of Antigen-Stimulated CD8(+) T Cells. *J Immunol* 202: 1088-1098.
217. Mitchell, J. E., M. M. Lund, J. Starmer, K. Ge, T. Magnuson, K. B. Shpargel, and J. K. Whitmire. 2021. UTX promotes CD8(+) T cell-mediated antiviral defenses but reduces T cell durability. *Cell Rep* 35: 108966.
218. Huppertz, S., K. Senger, A. Brown, H. Leins, K. Eiwen, M. A. Mulaw, H. Geiger, and M. Becker. 2021. KDM6A, a histone demethylase, regulates stress hematopoiesis and early B-cell differentiation. *Exp Hematol* 99: 32-43 e13.
219. Anderton, J. A., S. Bose, M. Vockerodt, K. Vrzalikova, W. Wei, M. Kuo, K. Helin, J. Christensen, M. Rowe, P. G. Murray, and C. B. Woodman. 2011. The H3K27me3

- demethylase, KDM6B, is induced by Epstein-Barr virus and over-expressed in Hodgkin's Lymphoma. *Oncogene* 30: 2037-2043.
220. Shangguan, H., C. Su, Q. Ouyang, B. Cao, J. Wang, C. Gong, and R. Chen. 2019. Kabuki syndrome: novel pathogenic variants, new phenotypes and review of literature. *Orphanet J Rare Dis* 14: 255.
221. Stagi, S., A. V. Gulino, E. Lapi, and D. Rigante. 2016. Epigenetic control of the immune system: a lesson from Kabuki syndrome. *Immunol Res* 64: 345-359.
222. Margot, H., G. Boursier, C. Duflos, E. Sanchez, J. Amiel, J. C. Andrau, S. Arpin, E. Brischoux-Boucher, O. Boute, L. Burglen, C. Caille, Y. Capri, P. Collignon, S. Conrad, V. Cormier-Daire, G. Delplancq, K. Dieterich, H. Dollfus, M. Fradin, L. Faivre, H. Fernandes, C. Francannet, V. Gatinois, M. Gerard, A. Goldenberg, J. Ghomid, S. Grotto, A. M. Guerrot, A. Guichet, B. Isidor, M. L. Jacquemont, S. Julia, P. Khau Van Kien, M. Legendre, K. H. Le Quan Sang, B. Leheup, S. Lyonnet, V. Magry, S. Manouvrier, D. Martin, G. Morel, A. Munnich, S. Naudion, S. Odent, L. Perrin, F. Petit, N. Philip, M. Rio, J. Robbe, M. Rossi, E. Sarrazin, A. Toutain, J. Van Gils, G. Vera, A. Verloes, S. Weber, S. Whalen, D. Sanlaville, D. Lacombe, N. Aladjidi, and D. Genevieve. 2020. Immunopathological manifestations in Kabuki syndrome: a registry study of 177 individuals. *Genet Med* 22: 181-188.
223. Hoffman, J. D., K. L. Ciprero, K. E. Sullivan, P. B. Kaplan, D. M. McDonald-McGinn, E. H. Zackai, and J. E. Ming. 2005. Immune abnormalities are a frequent manifestation of Kabuki syndrome. *Am J Med Genet A* 135: 278-281.
224. Bjornsson, H. T. 2015. The Mendelian disorders of the epigenetic machinery. *Genome Res* 25: 1473-1481.
225. Ng, S. B., A. W. Bigham, K. J. Buckingham, M. C. Hannibal, M. J. McMillin, H. I. Gildersleeve, A. E. Beck, H. K. Tabor, G. M. Cooper, H. C. Mefford, C. Lee, E. H. Turner, J. D. Smith, M. J. Rieder, K. Yoshiura, N. Matsumoto, T. Ohta, N. Niikawa, D. A. Nickerson, M. J. Bamshad, and J. Shendure. 2010. Exome sequencing identifies MLL2 mutations as a cause of Kabuki syndrome. *Nat Genet* 42: 790-793.
226. Lederer, D., B. Grisart, M. C. Digilio, V. Benoit, M. Crespian, S. C. Ghariani, I. Maystadt, B. Dallapiccola, and C. Verellen-Dumoulin. 2012. Deletion of KDM6A, a histone demethylase interacting with MLL2, in three patients with Kabuki syndrome. *Am J Hum Genet* 90: 119-124.
227. Faundes, V., S. Goh, R. Akilapa, H. Bezuidenhout, H. T. Bjornsson, L. Bradley, A. F. Brady, E. Brischoux-Boucher, H. Brunner, S. Bulk, N. Canham, D. Cody, M. L. Dentici, M. C. Digilio, F. Elmslie, A. E. Fry, H. Gill, J. Hurst, D. Johnson, S. Julia, K. Lachlan, R. R. Lebel, M. Byler, E. Gershon, E. Lemire, M. Gnazzo, F. R. Lepri, A. Marchese, M. McEntagart, J. McGaughran, S. Mizuno, N. Okamoto, C. Rieubland, J. Rodgers, E. Sasaki, E. Scalais, I. Scurr, M. Suri, I. van der Burgt, N. Matsumoto, N. Miyake, V. Benoit, D. Lederer, and S. Banka. 2021. Clinical delineation, sex differences, and genotype-phenotype correlation in pathogenic KDM6A variants causing X-linked Kabuki syndrome type 2. *Genet Med* 23: 1202-1210.
228. Issaeva, I., Y. Zonis, T. Rozovskaia, K. Orlovsky, C. M. Croce, T. Nakamura, A. Mazo, L. Eisenbach, and E. Canaani. 2007. Knockdown of ALR (MLL2) reveals ALR target genes and leads to alterations in cell adhesion and growth. *Mol Cell Biol* 27: 1889-1903.
229. Tran, N., A. Broun, and K. Ge. 2020. Lysine demethylase KDM6A in differentiation, development and cancer. *Mol Cell Biol*.

230. Lagunas-Rangel, F. A. 2021. KDM6B (JMJD3) and its dual role in cancer. *Biochimie* 184: 63-71.
231. Ezponda, T., D. Dupere-Richer, C. M. Will, E. C. Small, N. Varghese, T. Patel, B. Nabet, R. Popovic, J. Oyer, M. Bulic, Y. Zheng, X. Huang, M. Y. Shah, S. Maji, A. Riva, M. Occhionorelli, G. Tonon, N. Kelleher, J. Keats, and J. D. Licht. 2017. UTX/KDM6A Loss Enhances the Malignant Phenotype of Multiple Myeloma and Sensitizes Cells to EZH2 inhibition. *Cell Rep* 21: 628-640.
232. Li, X., Y. Zhang, L. Zheng, M. Liu, C. D. Chen, and H. Jiang. 2018. UTX is an escape from X-inactivation tumor-suppressor in B cell lymphoma. *Nat Commun* 9: 2720.
233. Pasquale, E. B. 2010. Eph receptors and ephrins in cancer: bidirectional signalling and beyond. *Nat Rev Cancer* 10: 165-180.
234. Mathur, R., L. Sehgal, O. Havranek, S. Kohrer, T. Khashab, N. Jain, J. A. Burger, S. S. Neelapu, R. E. Davis, and F. Samaniego. 2017. Inhibition of demethylase KDM6B sensitizes diffuse large B-cell lymphoma to chemotherapeutic drugs. *Haematologica* 102: 373-380.
235. Zhang, Y., L. Shen, D. G. Stupack, N. Bai, J. Xun, G. Ren, J. Han, L. Li, Y. Luo, R. Xiang, and X. Tan. 2016. JMJD3 promotes survival of diffuse large B-cell lymphoma subtypes via distinct mechanisms. *Oncotarget* 7: 29387-29399.
236. Cheng, Y., C. He, M. Wang, X. Ma, F. Mo, S. Yang, J. Han, and X. Wei. 2019. Targeting epigenetic regulators for cancer therapy: mechanisms and advances in clinical trials. *Signal Transduct Target Ther* 4: 62.
237. Duan, R., W. Du, and W. Guo. 2020. EZH2: a novel target for cancer treatment. *J Hematol Oncol* 13: 104.
238. Li, C., Y. Wang, Y. Gong, T. Zhang, J. Huang, Z. Tan, and L. Xue. 2021. Finding an easy way to harmonize: a review of advances in clinical research and combination strategies of EZH2 inhibitors. *Clin Epigenetics* 13: 62.
239. Lam, W. Y., and D. Bhattacharya. 2018. Metabolic Links between Plasma Cell Survival, Secretion, and Stress. *Trends Immunol* 39: 19-27.
240. Usui, T., Y. Wakatsuki, Y. Matsunaga, S. Kaneko, H. Koseki, and T. Kita. 1997. Overexpression of B cell-specific activator protein (BSAP/Pax-5) in a late B cell is sufficient to suppress differentiation to an Ig high producer cell with plasma cell phenotype. *J Immunol* 158: 3197-3204.
241. Nera, K. P., P. Kohonen, E. Narvi, A. Peippo, L. Mustonen, P. Terho, K. Koskela, J. M. Buerstedde, and O. Lassila. 2006. Loss of Pax5 promotes plasma cell differentiation. *Immunity* 24: 283-293.
242. Shapiro-Shelef, M., K. I. Lin, L. J. McHeyzer-Williams, J. Liao, M. G. McHeyzer-Williams, and K. Calame. 2003. Blimp-1 is required for the formation of immunoglobulin secreting plasma cells and pre-plasma memory B cells. *Immunity* 19: 607-620.
243. Kallies, A., J. Hasbold, D. M. Tarlinton, W. Dietrich, L. M. Corcoran, P. D. Hodgkin, and S. L. Nutt. 2004. Plasma cell ontogeny defined by quantitative changes in blimp-1 expression. *J Exp Med* 200: 967-977.
244. Soro, P. G., A. P. Morales, M. J. Martinez, A. S. Morales, S. G. Copin, M. A. Marcos, and M. L. Gaspar. 1999. Differential involvement of the transcription factor Blimp-1 in T cell-independent and -dependent B cell differentiation to plasma cells. *J Immunol* 163: 611-617.

245. Ochiai, K., M. Maienschein-Cline, G. Simonetti, J. Chen, R. Rosenthal, R. Brink, A. S. Chong, U. Klein, A. R. Dinner, H. Singh, and R. Sciammas. 2013. Transcriptional regulation of germinal center B and plasma cell fates by dynamical control of IRF4. *Immunity* 38: 918-929.
246. Li, G., H. Zan, Z. Xu, and P. Casali. 2013. Epigenetics of the antibody response. *Trends Immunol* 34: 460-470.
247. Zan, H., and P. Casali. 2015. Epigenetics of Peripheral B-Cell Differentiation and the Antibody Response. *Front Immunol* 6: 631.
248. Kuzmichev, A., K. Nishioka, H. Erdjument-Bromage, P. Tempst, and D. Reinberg. 2002. Histone methyltransferase activity associated with a human multiprotein complex containing the Enhancer of Zeste protein. *Genes Dev* 16: 2893-2905.
249. Mandal, M., S. E. Powers, M. Maienschein-Cline, E. T. Bartom, K. M. Hamel, B. L. Kee, A. R. Dinner, and M. R. Clark. 2011. Epigenetic repression of the Igk locus by STAT5-mediated recruitment of the histone methyltransferase Ezh2. *Nat Immunol* 12: 1212-1220.
250. Beguelin, W., M. Teater, M. D. Gearhart, M. T. Calvo Fernandez, R. L. Goldstein, M. G. Cardenas, K. Hatzi, M. Rosen, H. Shen, C. M. Corcoran, M. Y. Hamline, R. D. Gascoyne, R. L. Levine, O. Abdel-Wahab, J. D. Licht, R. Shaknovich, O. Elemento, V. J. Bardwell, and A. M. Melnick. 2016. EZH2 and BCL6 Cooperate to Assemble CBX8-BCOR Complex to Repress Bivalent Promoters, Mediate Germinal Center Formation and Lymphomagenesis. *Cancer Cell* 30: 197-213.
251. Biswas, M., S. S. Chatterjee, L. D. Boila, S. Chakraborty, D. Banerjee, and A. Sengupta. 2019. MBD3/NuRD loss participates with KDM6A program to promote DOCK5/8 expression and Rac GTPase activation in human acute myeloid leukemia. *FASEB J* 33: 5268-5286.
252. Cho, Y. W., T. Hong, S. Hong, H. Guo, H. Yu, D. Kim, T. Guszczynski, G. R. Dressler, T. D. Copeland, M. Kalkum, and K. Ge. 2007. PTIP associates with MLL3- and MLL4-containing histone H3 lysine 4 methyltransferase complex. *The Journal of biological chemistry* 282: 20395-20406.
253. Akdemir, K. C., A. K. Jain, K. Allton, B. Aronow, X. Xu, A. J. Cooney, W. Li, and M. C. Barton. 2014. Genome-wide profiling reveals stimulus-specific functions of p53 during differentiation and DNA damage of human embryonic stem cells. *Nucleic Acids Res* 42: 205-223.
254. Dhar, S. S., S. H. Lee, K. Chen, G. Zhu, W. Oh, K. Allton, O. Gafni, Y. Z. Kim, A. S. Tomoiga, M. C. Barton, J. H. Hanna, Z. Wang, W. Li, and M. G. Lee. 2016. An essential role for UTX in resolution and activation of bivalent promoters. *Nucleic Acids Res* 44: 3659-3674.
255. Satoh, T., O. Takeuchi, A. Vandenbon, K. Yasuda, Y. Tanaka, Y. Kumagai, T. Miyake, K. Matsushita, T. Okazaki, T. Saitoh, K. Honma, T. Matsuyama, K. Yui, T. Tsujimura, D. M. Standley, K. Nakanishi, K. Nakai, and S. Akira. 2010. The Jmjd3-Irf4 axis regulates M2 macrophage polarization and host responses against helminth infection. *Nat Immunol* 11: 936-944.
256. Pawlyn, C., M. F. Kaiser, C. Heuck, L. Melchor, C. P. Wardell, A. Murison, S. S. Chavan, D. C. Johnson, D. B. Begum, N. M. Dahir, P. Z. Proszek, D. A. Cairns, E. M. Boyle, J. R. Jones, G. Cook, M. T. Drayson, R. G. Owen, W. M. Gregory, G. H. Jackson, B. Barlogie, F. E. Davies, B. A. Walker, and G. J. Morgan. 2016. The Spectrum and

- Clinical Impact of Epigenetic Modifier Mutations in Myeloma. *Clin Cancer Res* 22: 5783-5794.
257. van Haafden, G., G. L. Dalglish, H. Davies, L. Chen, G. Bignell, C. Greenman, S. Ekins, C. Hardy, S. O'Meara, J. Teague, A. Butler, J. Hinton, C. Latimer, J. Andrews, S. Barthorpe, D. Beare, G. Buck, P. J. Campbell, J. Cole, S. Forbes, M. Jia, D. Jones, C. Y. Kok, C. Leroy, M. L. Lin, D. J. McBride, M. Maddison, S. Maquire, K. McLay, A. Menzies, T. Mironenko, L. Mulderrig, L. Mudie, E. Pleasance, R. Shepherd, R. Smith, L. Stebbings, P. Stephens, G. Tang, P. S. Tarpey, R. Turner, K. Turrell, J. Varian, S. West, S. Widaa, P. Wray, V. P. Collins, K. Ichimura, S. Law, J. Wong, S. T. Yuen, S. Y. Leung, G. Tonon, R. A. DePinho, Y. T. Tai, K. C. Anderson, R. J. Kohn, A. Massie, S. K. Khoo, B. T. Teh, M. R. Stratton, and P. A. Futreal. 2009. Somatic mutations of the histone H3K27 demethylase gene UTX in human cancer. *Nat Genet* 41: 521-523.
 258. Kruidenier, L., C. W. Chung, Z. Cheng, J. Liddle, K. Che, G. Joberty, M. Bantscheff, C. Bountra, A. Bridges, H. Diallo, D. Eberhard, S. Hutchinson, E. Jones, R. Katso, M. Leveridge, P. K. Mander, J. Mosley, C. Ramirez-Molina, P. Rowland, C. J. Schofield, R. J. Sheppard, J. E. Smith, C. Swales, R. Tanner, P. Thomas, A. Tumber, G. Drewes, U. Oppermann, D. J. Patel, K. Lee, and D. M. Wilson. 2012. A selective jumonji H3K27 demethylase inhibitor modulates the proinflammatory macrophage response. *Nature* 488: 404-408.
 259. Yoon, H. S., C. D. Scharer, P. Majumder, C. W. Davis, R. Butler, W. Zinzow-Kramer, I. Skountzou, D. G. Koutsonanos, R. Ahmed, and J. M. Boss. 2012. ZBTB32 is an early repressor of the CIITA and MHC class II gene expression during B cell differentiation to plasma cells. *J Immunol* 189: 2393-2403.
 260. Gloury, R., D. Zotos, M. Zuidschewoude, F. Masson, Y. Liao, J. Hasbold, L. M. Corcoran, P. D. Hodgkin, G. T. Belz, W. Shi, S. L. Nutt, D. M. Tarlinton, and A. Kallies. 2016. Dynamic changes in Id3 and E-protein activity orchestrate germinal center and plasma cell development. *J Exp Med* 213: 1095-1111.
 261. Heinemann, B., J. M. Nielsen, H. R. Hudlebusch, M. J. Lees, D. V. Larsen, T. Boesen, M. Labelle, L. O. Gerlach, P. Birk, and K. Helin. 2014. Inhibition of demethylases by GSK-J1/J4. *Nature* 514: E1-2.
 262. Subramanian, A., P. Tamayo, V. K. Mootha, S. Mukherjee, B. L. Ebert, M. A. Gillette, A. Paulovich, S. L. Pomeroy, T. R. Golub, E. S. Lander, and J. P. Mesirov. 2005. Gene set enrichment analysis: a knowledge-based approach for interpreting genome-wide expression profiles. *Proc Natl Acad Sci U S A* 102: 15545-15550.
 263. Serrano, M., G. J. Hannon, and D. Beach. 1993. A new regulatory motif in cell-cycle control causing specific inhibition of cyclin D/CDK4. *Nature* 366: 704-707.
 264. Kubbutat, M. H., S. N. Jones, and K. H. Vousden. 1997. Regulation of p53 stability by Mdm2. *Nature* 387: 299-303.
 265. Chinnadurai, G., S. Vijayalingam, and S. B. Gibson. 2008. BNIP3 subfamily BH3-only proteins: mitochondrial stress sensors in normal and pathological functions. *Oncogene* 27 Suppl 1: S114-127.
 266. Saunier, E., C. Benelli, and S. Bortoli. 2016. The pyruvate dehydrogenase complex in cancer: An old metabolic gatekeeper regulated by new pathways and pharmacological agents. *Int J Cancer* 138: 809-817.
 267. Holness, M. J., and M. C. Sugden. 2003. Regulation of pyruvate dehydrogenase complex activity by reversible phosphorylation. *Biochem Soc Trans* 31: 1143-1151.

268. Ito, K., and M. Groudine. 1997. A new member of the cationic amino acid transporter family is preferentially expressed in adult mouse brain. *The Journal of biological chemistry* 272: 26780-26786.
269. Vekony, N., S. Wolf, J. P. Boissel, K. Gnauert, and E. I. Closs. 2001. Human cationic amino acid transporter hCAT-3 is preferentially expressed in peripheral tissues. *Biochemistry* 40: 12387-12394.
270. Lu, Y., B. F. O'Dowd, H. Orrego, and Y. Israel. 1992. Cloning and nucleotide sequence of human liver cDNA encoding for cystathionine gamma-lyase. *Biochem Biophys Res Commun* 189: 749-758.
271. Sohm, B., M. Sissler, H. Park, M. P. King, and C. Florentz. 2004. Recognition of human mitochondrial tRNA^{Leu}(UUR) by its cognate leucyl-tRNA synthetase. *J Mol Biol* 339: 17-29.
272. Merk, M., R. A. Mitchell, S. Endres, and R. Bucala. 2012. D-dopachrome tautomerase (D-DT or MIF-2): doubling the MIF cytokine family. *Cytokine* 59: 10-17.
273. Wang, X., R. Yang, S. B. Jadhao, D. Yu, H. Hu, N. Glynn-Cunningham, C. Sztalryd, K. D. Silver, and D. W. Gong. 2012. Transmembrane emp24 protein transport domain 6 is selectively expressed in pancreatic islets and implicated in insulin secretion and diabetes. *Pancreas* 41: 10-14.
274. Stambolian, D., Y. Ai, D. Sidjanin, K. Nesburn, G. Sathe, M. Rosenberg, and D. J. Bergsma. 1995. Cloning of the galactokinase cDNA and identification of mutations in two families with cataracts. *Nat Genet* 10: 307-312.
275. Webb, G., V. Vaska, M. Coggan, and P. Board. 1996. Chromosomal localization of the gene for the human theta class glutathione transferase (GSTT1). *Genomics* 33: 121-123.
276. Allikmets, R., B. Gerrard, A. Hutchinson, and M. Dean. 1996. Characterization of the human ABC superfamily: isolation and mapping of 21 new genes using the expressed sequence tags database. *Hum Mol Genet* 5: 1649-1655.
277. Kee, B. L. 2009. E and ID proteins branch out. *Nat Rev Immunol* 9: 175-184.
278. Hatzi, K., H. Geng, A. S. Doane, C. Meydan, R. LaRiviere, M. Cardenas, C. Duy, H. Shen, M. N. C. Vidal, T. Baslan, H. P. Mohammad, R. G. Kruger, R. Shaknovich, A. M. Haberman, G. Inghirami, S. W. Lowe, and A. M. Melnick. 2019. Histone demethylase LSD1 is required for germinal center formation and BCL6-driven lymphomagenesis. *Nat Immunol* 20: 86-96.
279. Li, Y., M. Zhang, M. Sheng, P. Zhang, Z. Chen, W. Xing, J. Bai, T. Cheng, F. C. Yang, and Y. Zhou. 2018. Therapeutic potential of GSK-J4, a histone demethylase KDM6B/JMJD3 inhibitor, for acute myeloid leukemia. *J Cancer Res Clin Oncol* 144: 1065-1077.
280. Taube, J. H., N. Sphyris, K. S. Johnson, K. N. Reisenauer, T. A. Nesbit, R. Joseph, G. V. Vijay, T. R. Sarkar, N. A. Bhangre, J. J. Song, J. T. Chang, M. G. Lee, R. Soundararajan, and S. A. Mani. 2017. The H3K27me3-demethylase KDM6A is suppressed in breast cancer stem-like cells, and enables the resolution of bivalency during the mesenchymal-epithelial transition. *Oncotarget* 8: 65548-65565.
281. Tellier, J., and S. L. Nutt. 2019. Plasma cells: The programming of an antibody-secreting machine. *Eur J Immunol* 49: 30-37.
282. Arcipowski, K. M., C. A. Martinez, and P. Ntziachristos. 2016. Histone demethylases in physiology and cancer: a tale of two enzymes, JMJD3 and UTX. *Curr Opin Genet Dev* 36: 59-67.

283. Rickert, R. C., J. Roes, and K. Rajewsky. 1997. B lymphocyte-specific, Cre-mediated mutagenesis in mice. *Nucleic Acids Res* 25: 1317-1318.
284. Heinzl, S., T. Binh Giang, A. Kan, J. M. Marchingo, B. K. Lye, L. M. Corcoran, and P. D. Hodgkin. 2017. A Myc-dependent division timer complements a cell-death timer to regulate T cell and B cell responses. *Nat Immunol* 18: 96-103.
285. Finkin, S., H. Hartweger, T. Y. Oliveira, E. E. Kara, and M. C. Nussenzweig. 2019. Protein Amounts of the MYC Transcription Factor Determine Germinal Center B Cell Division Capacity. *Immunity* 51: 324-336 e325.
286. Stacpoole, P. W. 2017. Therapeutic Targeting of the Pyruvate Dehydrogenase Complex/Pyruvate Dehydrogenase Kinase (PDC/PDK) Axis in Cancer. *J Natl Cancer Inst* 109.
287. Woolbright, B. L., G. Rajendran, R. A. Harris, and J. A. Taylor, 3rd. 2019. Metabolic Flexibility in Cancer: Targeting the Pyruvate Dehydrogenase Kinase:Pyruvate Dehydrogenase Axis. *Mol Cancer Ther* 18: 1673-1681.
288. Kaya-Okur, H. S., S. J. Wu, C. A. Codomo, E. S. Pledger, T. D. Bryson, J. G. Henikoff, K. Ahmad, and S. Henikoff. 2019. CUT&Tag for efficient epigenomic profiling of small samples and single cells. *Nat Commun* 10: 1930.
289. Emslie, D., K. D'Costa, J. Hasbold, D. Metcalf, K. Takatsu, P. O. Hodgkin, and L. M. Corcoran. 2008. Oct2 enhances antibody-secreting cell differentiation through regulation of IL-5 receptor alpha chain expression on activated B cells. *J Exp Med* 205: 409-421.
290. Zhang, K., M. Wang, Y. Zhao, and W. Wang. 2019. Taiji: System-level identification of key transcription factors reveals transcriptional waves in mouse embryonic development. *Sci Adv* 5: eaav3262.
291. Good, K. L., and S. G. Tangye. 2007. Decreased expression of Kruppel-like factors in memory B cells induces the rapid response typical of secondary antibody responses. *Proc Natl Acad Sci U S A* 104: 13420-13425.
292. Schwickert, T. A., H. Tagoh, K. Schindler, M. Fischer, M. Jaritz, and M. Busslinger. 2019. Ikaros prevents autoimmunity by controlling anergy and Toll-like receptor signaling in B cells. *Nat Immunol* 20: 1517-1529.
293. O'Connor, L., A. Strasser, L. A. O'Reilly, G. Hausmann, J. M. Adams, S. Cory, and D. C. Huang. 1998. Bim: a novel member of the Bcl-2 family that promotes apoptosis. *EMBO J* 17: 384-395.
294. Yoon, M. K., J. H. Ha, M. S. Lee, and S. W. Chi. 2015. Structure and apoptotic function of p73. *BMB Rep* 48: 81-90.
295. Jourdan, M., M. Ferlin, E. Legouffe, M. Horvathova, J. Liautard, J. F. Rossi, J. Wijdenes, J. Brochier, and B. Klein. 1998. The myeloma cell antigen syndecan-1 is lost by apoptotic myeloma cells. *Br J Haematol* 100: 637-646.
296. Simonetti, G., A. Carette, K. Silva, H. Wang, N. S. De Silva, N. Heise, C. W. Siebel, M. J. Shlomchik, and U. Klein. 2013. IRF4 controls the positioning of mature B cells in the lymphoid microenvironments by regulating NOTCH2 expression and activity. *J Exp Med* 210: 2887-2902.
297. Aslam, M. A., M. F. Alemdehy, E. M. Kwesi-Maliepaard, F. I. Muhaimin, M. Caganova, I. N. Pardieck, T. van den Brand, T. van Welsem, I. de Rink, J. Y. Song, E. de Wit, R. Arens, H. Jacobs, and F. van Leeuwen. 2021. Histone methyltransferase DOT1L controls state-specific identity during B cell differentiation. *EMBO Rep* 22: e51184.

298. Li, R., P. Cauchy, S. Ramamoorthy, S. Boller, L. Chavez, and R. Grosschedl. 2018. Dynamic EBF1 occupancy directs sequential epigenetic and transcriptional events in B-cell programming. *Genes Dev* 32: 96-111.
299. Trojer, P., and D. Reinberg. 2006. Histone lysine demethylases and their impact on epigenetics. *Cell* 125: 213-217.
300. Klemm, S. L., Z. Shipony, and W. J. Greenleaf. 2019. Chromatin accessibility and the regulatory epigenome. *Nat Rev Genet* 20: 207-220.
301. O'Connor, B. P., V. S. Raman, L. D. Erickson, W. J. Cook, L. K. Weaver, C. Ahonen, L. L. Lin, G. T. Mantchev, R. J. Bram, and R. J. Noelle. 2004. BCMA is essential for the survival of long-lived bone marrow plasma cells. *J Exp Med* 199: 91-98.
302. Peperzak, V., I. Vikstrom, J. Walker, S. P. Glaser, M. LePage, C. M. Coquery, L. D. Erickson, K. Fairfax, F. Mackay, A. Strasser, S. L. Nutt, and D. M. Tarlinton. 2013. Mcl-1 is essential for the survival of plasma cells. *Nat Immunol* 14: 290-297.
303. Joyner, C. J., A. M. Ley, D. C. Nguyen, M. Ali, A. Corrado, C. Tipton, C. D. Scharer, T. Mi, M. C. Woodruff, J. Hom, J. M. Boss, M. Duan, G. Gibson, D. Roberts, J. Andrews, S. Lonial, I. Sanz, and F. E.-H. Lee. 2021. Maturation of Human Long-lived Plasma Cells Results in Resistance to Apoptosis by Transcriptional and Epigenetic Regulation. *bioRxiv*: 2021.2005.2022.445269.
304. Ripperger, T. J., and D. Bhattacharya. 2021. Transcriptional and Metabolic Control of Memory B Cells and Plasma Cells. *Annu Rev Immunol* 39: 345-368.
305. Marchetti, P., Q. Fovez, N. Germain, R. Khamari, and J. Kluza. 2020. Mitochondrial spare respiratory capacity: Mechanisms, regulation, and significance in non-transformed and cancer cells. *FASEB J* 34: 13106-13124.
306. Wang, L., and A. Shilatifard. 2019. UTX Mutations in Human Cancer. *Cancer Cell* 35: 168-176.
307. Kim, K. H., and C. W. Roberts. 2016. Targeting EZH2 in cancer. *Nat Med* 22: 128-134.
308. Das, P., and J. H. Taube. 2020. Regulating Methylation at H3K27: A Trick or Treat for Cancer Cell Plasticity. *Cancers (Basel)* 12.
309. Wu, Q., Y. Tian, J. Zhang, X. Tong, H. Huang, S. Li, H. Zhao, Y. Tang, C. Yuan, K. Wang, Z. Fang, L. Gao, X. Hu, F. Li, Z. Qin, S. Yao, T. Chen, H. Chen, G. Zhang, W. Liu, Y. Sun, L. Chen, K. K. Wong, K. Ge, L. Chen, and H. Ji. 2018. In vivo CRISPR screening unveils histone demethylase UTX as an important epigenetic regulator in lung tumorigenesis. *Proc Natl Acad Sci U S A* 115: E3978-E3986.
310. Morera, L., M. Lubbert, and M. Jung. 2016. Targeting histone methyltransferases and demethylases in clinical trials for cancer therapy. *Clin Epigenetics* 8: 57.
311. Dobin, A., C. A. Davis, F. Schlesinger, J. Drenkow, C. Zaleski, S. Jha, P. Batut, M. Chaisson, and T. R. Gingeras. 2013. STAR: ultrafast universal RNA-seq aligner. *Bioinformatics* 29: 15-21.
312. Lawrence, M., W. Huber, H. Pages, P. Aboyoun, M. Carlson, R. Gentleman, M. T. Morgan, and V. J. Carey. 2013. Software for computing and annotating genomic ranges. *PLoS Comput Biol* 9: e1003118.
313. Robinson, M. D., D. J. McCarthy, and G. K. Smyth. 2010. edgeR: a Bioconductor package for differential expression analysis of digital gene expression data. *Bioinformatics* 26: 139-140.
314. Langmead, B., C. Trapnell, M. Pop, and S. L. Salzberg. 2009. Ultrafast and memory-efficient alignment of short DNA sequences to the human genome. *Genome Biol* 10: R25.

315. Zhang, Y., T. Liu, C. A. Meyer, J. Eeckhoutte, D. S. Johnson, B. E. Bernstein, C. Nusbaum, R. M. Myers, M. Brown, W. Li, and X. S. Liu. 2008. Model-based analysis of ChIP-Seq (MACS). *Genome Biol* 9: R137.
316. Heinz, S., C. Benner, N. Spann, E. Bertolino, Y. C. Lin, P. Laslo, J. X. Cheng, C. Murre, H. Singh, and C. K. Glass. 2010. Simple combinations of lineage-determining transcription factors prime cis-regulatory elements required for macrophage and B cell identities. *Mol Cell* 38: 576-589.
317. Love, M. I., W. Huber, and S. Anders. 2014. Moderated estimation of fold change and dispersion for RNA-seq data with DESeq2. *Genome Biol* 15: 550.
318. Lohsen, S., P. Majumder, C. D. Scharer, B. G. Barwick, J. W. Austin, W. M. Zinzow-Kramer, and J. M. Boss. 2014. Common distal elements orchestrate CIITA isoform-specific expression in multiple cell types. *Genes Immun* 15: 543-555.
319. Henikoff, S., J. G. Henikoff, H. S. Kaya-Okur, and K. Ahmad. 2020. Efficient chromatin accessibility mapping in situ by nucleosome-tethered tagmentation. *Elife* 9.
320. Buenrostro, J. D., B. Wu, U. M. Litzenburger, D. Ruff, M. L. Gonzales, M. P. Snyder, H. Y. Chang, and W. J. Greenleaf. 2015. Single-cell chromatin accessibility reveals principles of regulatory variation. *Nature* 523: 486-490.
321. De Silva, N. S., and U. Klein. 2015. Dynamics of B cells in germinal centres. *Nat Rev Immunol* 15: 137-148.
322. Shane, H. L., and K. D. Klonowski. 2014. Every breath you take: the impact of environment on resident memory CD8 T cells in the lung. *Front Immunol* 5: 320.
323. Slutter, B., L. L. Pewe, S. M. Kaech, and J. T. Harty. 2013. Lung airway-surveilling CXCR3(hi) memory CD8(+) T cells are critical for protection against influenza A virus. *Immunity* 39: 939-948.
324. Bear, J. E., and F. B. Gertler. 2009. Ena/VASP: towards resolving a pointed controversy at the barbed end. *J Cell Sci* 122: 1947-1953.
325. Chen, D., Y. Wang, G. K. Manakkat Vijay, S. Fu, C. W. Nash, D. Xu, D. He, N. Salomonis, H. Singh, and H. Xu. 2021. Coupled analysis of transcriptome and BCR mutations reveals role of OXPPOS in affinity maturation. *Nat Immunol* 22: 904-913.
326. Jiang, Y., and A. Melnick. 2015. The epigenetic basis of diffuse large B-cell lymphoma. *Semin Hematol* 52: 86-96.
327. Ghosh, S., and R. S. Klein. 2017. Sex Drives Dimorphic Immune Responses to Viral Infections. *J Immunol* 198: 1782-1790.
328. Klein, S. L., and K. L. Flanagan. 2016. Sex differences in immune responses. *Nat Rev Immunol* 16: 626-638.
329. Youness, A., C. H. Miquel, and J. C. Guery. 2021. Escape from X Chromosome Inactivation and the Female Predominance in Autoimmune Diseases. *Int J Mol Sci* 22.
330. Mousavi, M. J., M. Mahmoudi, and S. Ghotloo. 2020. Escape from X chromosome inactivation and female bias of autoimmune diseases. *Mol Med* 26: 127.
331. He, M., and L. S. Westerberg. 2019. Congenital Defects in Actin Dynamics of Germinal Center B Cells. *Front Immunol* 10: 296.
332. Morin, R. D., N. A. Johnson, T. M. Severson, A. J. Mungall, J. An, R. Goya, J. E. Paul, M. Boyle, B. W. Woolcock, F. Kuchenbauer, D. Yap, R. K. Humphries, O. L. Griffith, S. Shah, H. Zhu, M. Kimbara, P. Shashkin, J. F. Charlot, M. Tcherpakov, R. Corbett, A. Tam, R. Varhol, D. Smailus, M. Moksa, Y. Zhao, A. Delaney, H. Qian, I. Birol, J. Schein, R. Moore, R. Holt, D. E. Horsman, J. M. Connors, S. Jones, S. Aparicio, M.

- Hirst, R. D. Gascoyne, and M. A. Marra. 2010. Somatic mutations altering EZH2 (Tyr641) in follicular and diffuse large B-cell lymphomas of germinal-center origin. *Nat Genet* 42: 181-185.
333. Sneeringer, C. J., M. P. Scott, K. W. Kuntz, S. K. Knutson, R. M. Pollock, V. M. Richon, and R. A. Copeland. 2010. Coordinated activities of wild-type plus mutant EZH2 drive tumor-associated hypertrimethylation of lysine 27 on histone H3 (H3K27) in human B-cell lymphomas. *Proc Natl Acad Sci U S A* 107: 20980-20985.
334. Yap, D. B., J. Chu, T. Berg, M. Schapira, S. W. Cheng, A. Moradian, R. D. Morin, A. J. Mungall, B. Meissner, M. Boyle, V. E. Marquez, M. A. Marra, R. D. Gascoyne, R. K. Humphries, C. H. Arrowsmith, G. B. Morin, and S. A. Aparicio. 2011. Somatic mutations at EZH2 Y641 act dominantly through a mechanism of selectively altered PRC2 catalytic activity, to increase H3K27 trimethylation. *Blood* 117: 2451-2459.
335. Creighton, M. P., A. W. Cheng, G. G. Welstead, T. Kooistra, B. W. Carey, E. J. Steine, J. Hanna, M. A. Lodato, G. M. Frampton, P. A. Sharp, L. A. Boyer, R. A. Young, and R. Jaenisch. 2010. Histone H3K27ac separates active from poised enhancers and predicts developmental state. *Proc Natl Acad Sci U S A* 107: 21931-21936.
336. Shi, Y. J., C. Matson, F. Lan, S. Iwase, T. Baba, and Y. Shi. 2005. Regulation of LSD1 histone demethylase activity by its associated factors. *Mol Cell* 19: 857-864.
337. Weinberg, D. N., S. Papillon-Cavanagh, H. Chen, Y. Yue, X. Chen, K. N. Rajagopalan, C. Horth, J. T. McGuire, X. Xu, H. Nikbakht, A. E. Lemiesz, D. M. Marchione, M. R. Marunde, M. J. Meiners, M. A. Cheek, M. C. Keogh, E. Bareke, A. Djedid, A. S. Harutyunyan, N. Jabado, B. A. Garcia, H. Li, C. D. Allis, J. Majewski, and C. Lu. 2019. The histone mark H3K36me2 recruits DNMT3A and shapes the intergenic DNA methylation landscape. *Nature* 573: 281-286.